UNIVERSITÀ
DEGLI STUDI
DI PADOVA

Administrative unit: **University of Padova**

Department: Land, Environment, Agriculture and Forestry (TESAF)

PhD Program: Land, Environment, Resources and Health (LERH)

Batch: XXVI

THESIS TITLE

Parameters Optimisation of Agricultural Machinery for Soil Compaction Mitigation and Crop Yield Enhancement

PhD Program Coordinator: Prof. Marco Borga

Supervisor: Prof. Luigi Sartori

PhD candidate: Kaihua Liu

Table of contents

Part of the information reported in this dissertation has been published in scientific journals:

Liu, K.; Benetti, M.; Sozzi, M.; Gasparini, F.; Sartori, L. Soil Compaction under Different Traction Resistance Conditions—A Case Study in North Italy. Agriculture 2022, 12, 1954. IF:3.6

Liu, K.; Kayad, A.; Sozzi, M.; Sartori, L.; Marinello, F. Headland and Field Edge Performance Assessment Using Yield Maps and Sentinel-2 Images. Sustainability 2023, 15, 4516. IF:3.9

Liu, K.; M.; Sozzi, M.; Marinello, F; Sartori, L. “Combining simulations and field experiments: Effects of Subsoiling Angle and Tillage Depth on Soil Structure and Energy Requirements”, (Accepted), IF:13.6

Abstract

In this research, an exploration is undertaken into the intricate interplay between soil compaction, machinery performance, and tillage practices, revealing their profound implications for agricultural sustainability and productivity. Three fundamental objectives guide this investigation.

Firstly, the impact of varying levels of traction resistance during agricultural operations is scrutinized. In-depth analysis transcends static weight measurements, incorporating dynamic factors such as traction, rolling resistance, and subsoiler parameters. This comprehensive approach not only elucidates soil compaction dynamics but also identifies opportunities for energy consumption reduction, soil health enhancement, and the fostering of agricultural sustainability.

Secondly, the significance of field variability is unveiled. The research exposes the non-uniformity of crop yield within a field, particularly in headlands and field edges. These findings, correlated with specific soil properties, underscore the pivotal role of strategic machine traffic planning in optimizing yields and mitigating losses.

Lastly, the intricate realm of subsoiler tillage is investigated, emphasizing the substantial influence of subsoiler parameters on soil compaction mitigation and fuel efficiency. This holistic understanding of tillage dynamics equips farmers with insights to make informed decisions, thus improving operational efficiency and cost reduction.

In conclusion, this doctoral research represents a significant advancement in comprehending soil compaction, machinery performance, and tillage practices. Its practical implications extend to both agricultural practitioners and professionals, offering pathways to enhance productivity, reduce environmental impact, and cultivate a sustainable future for agriculture. As we navigate the evolving landscape of modern agriculture, the harnessing of these insights is deemed imperative to maximize agricultural potential while minimizing the ecological footprint.

1. Introduction

1.1 Background and Context:

1.1.1 The Growing Challenge of Soil Compaction in Modern Agriculture

Soil compaction has emerged as a significant concern over the last few decades, primarily attributable to the global increase in the size and weight of agricultural machinery (DeArmond et al., 2019; Mossadeghi-Björklund et al., 2016; Obour et al., 2018; Silva et al., 2018., e.g.). This ongoing study further substantiates that soil compaction is associated with heightened soil bulk density, amplified soil cone index, and increased soil shear strength (Blanco-Canqui et al., 2010; Schjønning and Lamandé, 2018; Tekeste et al., 2008). Additionally, soil compaction impedes root exploration, diminishes crop yields, and escalates energy requirements across all agricultural operations.

The transformation of the agricultural landscape can be attributed to the continuous development of agricultural machinery. These machines, which traverse fields multiple times during crop growth, have significantly contributed to the recurring issue of soil compaction.

Rewinding over a century, pioneering researchers such as Wollny in 1898 recognized the favorable implications of sound soil structure. Their studies underscored the need to explore the intricate relationships among soil structure, plant growth, and crop yields (Wollny, 1898). The predominant focus during this historical era rested on enhancing crop productivity, with environmental concerns occupying a limited role.

In modern times, soil compaction has become even more pronounced within the agricultural system, largely attributed to the increasing size and weight of agricultural machinery. Notably, the wheel load of combine harvesters surged by approximately 65% between 1989 and 2009 (Schjønning et al., 2015b). Consequently, the mechanical stress inflicted by modern agricultural machinery upon cultivated land frequently exceeds the soil strength thresholds of many fields, corroborating earlier observations (Horn and Fleige, 2003; Zink et al., 2010). For instance, the analysis of a typical Danish combine harvester's front axle wheel load between 1958 and 2009 revealed a consistent linear increase, escalating from approximately 1.5 Mg to approximately 9 Mg—an annual rise of approximately 0.14 Mg $^{-1}$ (Schjønning et al., 2015b) as shown in the Figure 1.1.1.

Soil compaction in the agricultural realm predominantly stems from the pressure exerted by the walking devices of agricultural machinery. Notably, tire-induced compaction stands out as a prominent contributor, with the dynamics of traction imposing substantial force on the soil during interactions between the tire and soil. This compaction mechanism entails the

transmission of force to the subsoil through the forced movement of soil particles subjected to external stress. Consequently, the soil compaction process intricately hinges on soil stress propagation, leading to damage in both the topsoil and subsoil. Significantly, certain studies underscore the disproportionately severe consequences of topsoil compaction on crop root growth compared to subsoil compaction (Botta et al., 2006).

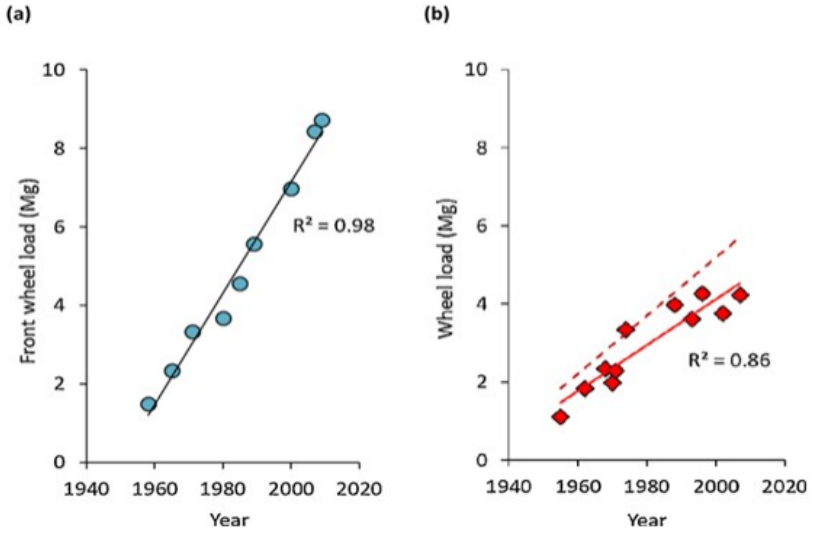

Figure 1.1.1 Historical evolution of a) front wheel loads of combine harvesters and b) rear wheel loads of tractors

Examining the historical evolution of agricultural machinery, we scrutinize a) the front wheel loads of combine harvesters (Schjønning et al., 2015b) and b) the rear wheel loads of tractors (Keller et al., 2019). These figures provide insight into the progressive increase in equipment weight. Notably, picture (b) demonstrates that wheel loads surged from 1.5 Mg to 4.2 Mg between 1950 and 2010. Furthermore, the dashed line within picture (b) signifies a 25% augmentation in the load of the rear furrow wheel during conventional ploughing (Joachim Brunotte et al., 2012). These calculations of wheel loads derived from tractor weights reveal a weight distribution of 40% on the front axle and 60% on the rear axle, aligning with the assumptions presented in the imagery (Keller et al., 2019; Pichlmaier and Honzek, 2011).

1.1.2 The Factors Influencing Soil Compaction

1.1.2.1 Soil moisture and soil type

Soil compaction is a multifaceted phenomenon influenced by various factors, encompassing physical and chemical properties, tire parameters, and specific working conditions. However, within this intricate interplay, two primary determinants wield significant influence: soil moisture content and soil type. A comprehensive understanding of their respective roles is paramount for a nuanced comprehension of soil compaction dynamics.

Soil moisture content stands as a prominent variable in the equation of soil compaction.

The quantity of water residing within the soil matrix exerts a profound influence on its susceptibility to compaction. Extensive research has illuminated the substantial impact of varying soil moisture content under specific loads on soil compaction (Munkholm and Schjønning, 2004). For instance, under moist conditions, discernible disparities in soil bulk density and porosity manifest at depths ranging from 12 to 17 cm. However, when exploring deeper, at approximately 32 to 37 cm and subject to a contact stress of 160 kPa on the soil surface, only marginal alterations in soil aggregate structure become apparent (Gysi Taenikon, M A Fluehler, n.d.). In stark contrast, under dry conditions, negligible deviations in soil physical properties are observed at depths of 0 to 30 cm when exposed to equivalent contact stress. Other research shows that the soil bulk density will correspondingly increase by 5.1% to 7.4% under the same compaction conditions for every 4% increase in soil moisture content (Bulinski and Sergiel, 2014).

Simultaneously, soil type emerges as a fundamental determinant of compaction susceptibility. Robust evidence supports the assertion that soils characterized by higher clay content tend to exhibit a heightened predisposition to compaction (Keller et al., 2007b; Keller and Lamandé, 2010; Stettler et al., 2014). This heightened susceptibility predominantly arises from the distinctive attributes of clay particles. Characterized by minuscule dimensions and a remarkable surface area relative to their size, clay particles enable dense packing. The application of pressure by agricultural machinery further compels these particles into tighter arrangements, diminishing the interparticle pore spaces.

1.1.2.2 Tire parameters

Tires serve as the primary source of propulsion for agricultural machinery, making their parameters a critical determinant of operational efficiency. The interaction with the soil is crucial in considering the impact of soil compaction. Extensive research has delved into the tire-related factors influencing soil compaction, particularly regarding tire type, section width, and air pressure. The parameters of agricultural tires wield substantial influence over the intricacies of soil compaction dynamics. Notably, the dimensions and configuration of the tire-soil interface profoundly impact stress distribution at the interface, subsequently dictating stress propagation within the soil profile. Consequently, meticulous consideration of tire size, shape, and tread pattern is fundamental when selecting tires for agricultural machinery.

In addition to tire size and shape, tire inflation pressure assumes significance in soil compaction (Schjønning et al., 2008). The recommended inflation pressure for a tire is the pressure at which optimal stress distribution uniformly spans the wheel's width. Deviations from this optimal inflation range, either through overinflation or underinflation, can

precipitate increased soil compaction. It is imperative to acknowledge that the influence of tire parameters on soil compaction exhibits variability contingent upon the specific soil type and prevailing conditions. Therefore, a judicious approach entails conducting field tests to ascertain the ideal tire parameters tailored to a given soil type and its unique condition.

In summation, the meticulous selection of appropriate tire parameters for agricultural machinery holds profound importance in curtailing soil compaction and safeguarding soil health. The tire-soil contact area, predominantly delineating the impact of diverse tire parameters, profoundly influences soil compaction dynamics. Studies substantiate that tire parameters wield a notable influence on surface soil compaction; radial tires demonstrate the capacity to mitigate surface soil compaction when compared to bias tires under equivalent conditions. Furthermore, it is underscored that subsoil compaction remains largely contingent upon tire type and air pressure (Bulinski and Sergiel, 2014).

1.1.2.3 Machine weight and number of passes

The weight of the load and the number of passes are factors that affect soil compaction. Soil compaction will become more severe with the increased weight and number of passed. For example, a tractor will cause permanent damage to the soil only when entering the uncompacted field the first time. The tractor entering the field multiple times will cause more severe soil compaction. Some research shows that the first three times have the most significant compaction effect on the topsoil and subsoil (Abebe et al., 1989; Arvidsson, 2001). Although small tractors have less weight than middle or large tractors, the compaction caused by multiple operations at the same position is no less than larger ones. Conventional farming uses rotary and other machines to tillage the topsoil. It resulted in the rotary machine destroying the soil structure during the tillage. To provide a good seedbed condition for seeds, soil tillage on the hard soil surface will cause excessive smashing of the soil, destroying the soil aggregate structure and reducing the internal strength of the soil. As a result, the soil becomes more susceptible to external forces, which lead to more severe soil compaction during the next year's field operation.

1.1.3 The Factors Influenced by Soil Compaction

1.1.3.1 Impact on soil physical and chemical properties

The soil bulk density will increase after the compaction as one of the sensitive and test-easy parameters of soil physical properties. So it makes the soil bulk density one of the most important soil physical factors used during the soil compaction measurement.

Soil compaction can destroy or over-squeeze soil aggregates to form a damaged layer of soil structure during the first time compaction(Ankeny et al., 1990; Badalikova and Hrub\`y,

2006; Cambi et al., 2016; Patel and Singh, 1981; Radford et al., 2000). After the compaction, the soil particles inside the damage layer are rearranged under external force, decreasing soil volume and soil bulk density increase (Chaudhary et al., 1991). For example, the agricultural machinery equipment with a load of 17.4Mg has a significant impact on soil bulk density after six times passes. The compaction also affects the soil nutrient cycle (Kuht et al., 2004). Soil compaction can significantly increase soil nitrogen loss because soil compaction increases N_2O gas emissions in the soil. As a result, soil compaction slows down the soil nitrogen cycle and reduces crop yields(Gregorich et al., 2014). It also affects the internal composition, accelerates the soil runoff, and causes severe soil water erosion. The main reason is that it slows down soil water infiltration rate (Mossadeghi-Björklund et al., 2016), causing the water flow formed during rainfall to take away the surface soil (Larsen et al., 2004).

The formation of the hardpan

Different agricultural machinery forms the hardpan (or the soil pan) during field operations in different depths. The hardpan has a core block structure, sticky texture, poor air condition, and water permeability, limiting root growth(Salem et al., 2015; Tuzzin de Moraes et al., 2016). The hardpan formation needs to simultaneously meet the following points: external force compaction, soil cohesion, and soil moisture downward. The hardpan layer will cause the soil bulk density increase, soil porosity decrease and root growth block (Schneider et al., 2017). Therefore, there are a few ways to loosen the soil through tillage machines such as rotary tiller, subsoilers and ploughs. However, the same tillage equipment is used all year round to plough or tillage the field. The bottom of the tillage and plough tools will squeeze and compact the bottom. As a result, the soil at the bottom of the cultivated layer cannot be loosened for a long time. Finally, the hardpan is formed. In addition, frequent soil cultivation for an extended period leads to the destruction of the soil structure. As a result, the strength of the soil becomes more fragile and causes more compaction. However, when the long-term cultivated layer is irrigated, the cohesive soil particles are brought to the bottom area of the tillage layer during the downward movement of the water. As a result, the infiltration rate of soil moisture decreases due to the soil compaction on the bottom of the tillage layer. This phenomenon causes more and more soil particles to accumulate in the tillage layer's bottom area, gradually forming the hardpan. Macroscopically, soil compaction is embodied in the vicious circle of compaction to tillage and re-compaction. Microscopically, it is embodied in soil compaction, which destroys soil structure and decreases soil compressive strength, making the soil more susceptible to external forces, leading to more compaction.

Soil compaction exerts a profound influence on soil physical and chemical properties, with soil bulk density emerging as a highly sensitive and readily measurable parameter

(Ankeny et al., 1990; Cambi et al., 2016; Patel and Singh, 1981; Radford et al., 2000). Soil bulk density is pivotal in soil compaction assessments due to its responsiveness to compaction-induced changes.

Initially, soil compaction can disrupt or excessively compress soil aggregates, forming a damaged layer within the soil structure during the initial compaction process. Subsequently, under external forces, soil particles within this damaged layer undergo rearrangement, reducing soil volume and increasing soil bulk density (Chaudhary et al., 1991).

For instance, after undergoing six passes, agricultural machinery bearing a 17.4 Mg load can significantly impact soil bulk density. This compaction-induced transformation extends beyond physical alterations, significantly affecting the soil's nutrient cycle (Kuht et al., 2004). Notably, soil compaction intensifies soil nitrogen loss by elevating N_2O gas emissions, impeding the soil nitrogen cycle, and contributing to diminished crop yields (Gregorich et al., 2014). Additionally, it disrupts the soil's internal composition, accelerates surface runoff, and fosters severe soil erosion, chiefly by reducing soil water infiltration rates (Mossadeghi-Björklund et al., 2016). These changes result in surface soil detachment and transport during rainfall (Larsen et al., 2004).

The hardpan formation represents another critical facet of soil compaction's adverse impact. Different agricultural machinery can induce the development of a hardpan (or soil pan) at varying depths during field operations, resulting in a compacted, block-like structure, reduced air permeability, and impaired water retention capacity. Consequently, root growth is hindered (Salem et al., 2015; Tuzzin de Moraes et al., 2016). The formation of a hardpan hinges on specific conditions, including the application of external compaction forces, soil cohesion, and downward soil moisture movement. This hardpan layer manifests as a decline in soil bulk density, reduced soil porosity, and root growth hindrance.

Efforts to ameliorate hardpan formation typically involve using soil tillage machinery such as rotary tillers, subsoilers, and ploughs. However, the repeated use of the same tillage equipment over time can exacerbate the situation. The lower parts of these tools inadvertently compress the soil's bottom layer during tillage, rendering it resistant to loosening. This perpetual compression eventually gives rise to the hardpan. Furthermore, prolonged and recurrent soil cultivation disrupts soil structure, rendering it increasingly fragile and prone to compaction. In addition, when the bottom layer of the cultivated soil is irrigated, cohesive soil particles migrate downward with the infiltrating water, reducing soil moisture infiltration rates and causing further accumulation of soil particles at the tillage layer's bottom. Over time, this process culminates in hardpan formation.

On a macroscopic scale, soil compaction manifests as a vicious cycle of compaction,

tillage, and re-compaction. Microscopically, it disrupts soil structure and diminishes soil compressive strength, rendering the soil more susceptible to external forces, thereby exacerbating the compaction phenomenon.

1.1.3.2 Impact on Crops

Soil compaction exerts a detrimental influence on crop germination rates and seedling growth compared to conventional seed-sowing conditions, as established in prior research (Dürr and Aubertot, 2000). Upon compaction, the soil bulk density surrounding the seeds escalates from 1.3 to 1.8 g.cm-3. Consequently, compacted soil delays the emergence of crops, elevates seedling mortality rates, and reduces plant height relative to uncompacted soil conditions (Jordan et al., 2003).

The efficacy of root systems in nutrient uptake and crop growth throughout the crop cycle is paramount. Soil compaction significantly affects root penetration capacity(Gerard et al., 1982; Hamza and Anderson, 2005; Kirby and Bengough, 2002), leading to restricted root growth and diminished root penetration ability. This, in turn, results in reduced root length and dry matter weight (Kristoffersen and Riley, 2005).

Some scholars have noted that crops endowed with robust root systems exhibit greater penetrating power and are less susceptible to soil compaction. Cultivating such crops can serve as a strategy to alleviate soil compaction (Rosolem et al., 2002). These crops feature root systems with diameters significantly larger than the pores between soil particles. As these root systems expand, they increase the soil bulk density in their vicinity, thereby enhancing the soil's physical and chemical properties and its microbial ecosystem (Dexter, 1987; Gliński and Lipiec, 2000).

Field operations involving large agricultural machinery can result in the permanent compaction of subsoil. For instance, experimental evidence demonstrates that tire-induced soil compaction can reduce wheat root density in soil layers ranging from 0 to 60 cm in depth by 17% (Cid et al., 2014). Compaction from a 14.5 Mg load also significantly impedes root system growth below the 20 cm depth in loam soil with 5% organic matter content (Bouwman and Arts, 2000).

Soil mechanical resistance primarily governs soil root elongation (Bengough et al., 2006; Materechera et al., 1992), impacting plant growth through various mechanisms (Colombi and Keller, 2019). Compaction elevates the mechanical resistance encountered by root growth, diminishing root elongation and limiting rooting depth and resource accessibility, especially water in the subsoil (Colombi et al., 2018). Moreover, compaction curtails the accessibility of nutrients absorbed by particle surfaces. Nutrient availability relies on soil accumulation; only about 10-20% of potential nutrient adsorption and exchange sites are accessible (Horn et al.,

2019). Furthermore, it's crucial to distinguish between resource accessibility and availability. Roots might not reach out to resources, signifying accessibility issues, while resource scarcity represents availability constraints. Generally, greater soil compaction results in a wider disparity between resource accessibility and availability, making compaction predominantly a resource accessibility issue (Colombi and Keller, 2019; Keller et al., 2019).

Furthermore, compaction reduces soil's gas transmission capacity (Haas et al., 2016; Horn et al., 1995; Simojoki et al., 2008; Uteau et al., 2013), leading to suboptimal soil aeration and exceptionally low oxygen concentrations in soil air, particularly under high oxygen demand and moist soil conditions (Stepniewski et al., 1994).

1.1.3.3 Impact on Biodiversity

Soil compaction can decrease the soil microbial diversity. Although the soil physical properties will change when the soil strength is in the range of 75-3800kPa, the biological indicators in the soil will not be affected (Shestak and Busse, 2005). However, excessive compaction can significantly affect the soil microbial biomass. For example, when soil compaction reduces the soil porosity from 13% to 36%, it significantly reduces the content of soil microbial biomass carbon, biomass nitrogen and phosphorus content. And when the soil bulk density reaches 1.7g.cm$^{-3,}$ it can seriously affect the soil microbial diversity and soil carbon sequestration effect (Beylich et al., 2010). In addition, research shows that almost any soil disturbance or changes in soil stress will affect the activity of soil enzymes (Buck et al., 2000).

As the soil animal communities live in large soil pores. Their living conditions are severely restricted depending on the soil macroporosity amount and distribution affected by soil compaction. Soil nematodes play a critical role in soil organic matter decomposition. Research shows that the number of plant nematodes increased, and the number of bacterial-eating nematodes, fungus-eating nematodes and omnivorous-predator nematodes decreased in the areas with severe soil compaction (Bouwman and Arts, 2000). Soil compaction will also affect the number of earthworms in the soil. The number of earthworms in the soil shows a downward trend as the degree of soil compaction increases (Kretzschmar, 1991; Radford et al., 2001).

1.1.3.4 Impact on Agricultural Economic Benefits

Although compaction is a well-recognised problem, and despite numerous studies on the impacts of traffic-induced compaction on soil properties and functions, it remains challenging to quantify compaction's economic and ecological costs. There is little doubt of soil compaction's economic and ecological damage to society (Graves et al., 2015). However, the reliable estimation of the cost of soil compaction remains elusive, especially the actual sum of

direct numbers. Nearly 30 years ago, it was reported that around 33 Mha areas were affected by soil compaction in Europe based on a worldwide semi-quantitative assessment of soil degradation (Oldeman et al., 1990). The area is one-third of all the arable land in Europe. Soil compaction causes tremendous costs to land users and society (Graves et al., 2015). However, there is limited quantitative information on the costs of soil compaction at the national and continental scale (Alaoui et al., 2018; Brus and Van Den Akker, 2018).

First, there is limited information on the extent and severity of soil compaction at national scales. Most soil compaction research considers scales from the soil pore to the soil profile and experimental plot scale, while larger scales are seldom addressed. According to previous research, soil compaction is estimated to affect between 25 and 45% (central estimate: 35%) of agricultural land (Brus and Van Den Akker, 2018; Graves et al., 2015; Keller et al., 2019; Oldeman et al., 1990; Schjønning et al., 2015a). Second, a large part of the cost of soil degradation is related to off-site impacts, which makes it challenging to link costs to sources (Graves et al., 2015). For example, soil compaction may increase flooding incidence and severity, trigger soil erosion, decline water quality through increased nutrient and pesticide leaching and increase greenhouse gas emissions (Alaoui et al., 2018; Ball, 2013; Horn et al., 1995; Jarvis, 2007; Lipiec et al., 1995; Rogger et al., 2017). Third, some of the costs may be difficult to value the off-site costs (Graves et al., 2015; Robinson et al., 2012). The weight of agricultural machinery has been steadily increasing during these years. For example, wheel loads of combine harvesters have increased by approximately 65% between 1989 and 2009 (Schjønning et al., 2015a). Consequently, the mechanical stresses exerted by today's machinery may exceed the strength of many arable soils (Horn and Fleige, 2003; Schjønning et al., 2015a; Zink et al., 2010). Most of the information I got about the yield reduction because of the compaction is based on data from field experiments. The yield decline immediately occurred after the soil compaction. However, the yield recovered relatively quickly within two years. After a few years, typically, only a slight yield reduction of a few percentages remains. However, some research mentioned that this reduction is quasi-permanent because of the subsoil compaction (Håkansson and Reeder, 1994). For example, another research shows that the data from a series of long-term field experiments in Northern Europe and North America with a one-time compaction event with a wheel load of 5 Mg indicate a quasi-permanent yield loss of 2.5% (Håkansson and Reeder, 1994).

1.1.3.5 Impact on Productivity Loss

Some research found that the agronomic productivity loss is due to soil compaction. Soil compaction affects plant growth in various ways (Colombi and Keller, 2019). One research assumed that compaction causes 4–5% yield losses on arable land and slightly less on

grassland (Graves et al., 2015). The yield loss cost per hectare of compaction is associated with the area affected by compaction of approximately 48.2 € ha-1 yr-1, based on the total agricultural area of approximately 19.4 € ha^{-1} yr^{-1}. Another research assumed yield losses due to compaction of 8% for soils with>40% clay and 4% for soils with 15–25% clay, and that yield losses for lighter soils are negligible (Eriksson et al., 1974). Long-term (decadal) experiments would also be needed in such systems to see the full effects because soil structure evolution is slow (Horn, 2004). In summary, estimating the impact of soil compaction on crop productivity is not easy because we typically do not have a reference situation with non-compacted soil. Therefore, compaction-induced crop productivity losses in field experiments are likely to underestimate the true productivity losses caused by compaction.

1.1.4 The measurement of the soil compaction

The mechanical resistance is typically expressed as penetration resistance. Measurements of the soil cone penetration resistance can be used to quantify the mechanical energetics of bioturbation by plant roots (Ruiz et al., 2015). For a given soil texture, penetration resistance is a function of soil bulk density, hydration status, or soil matric potential (Busscher, 1990; Vaz et al., 2011). The penetration resistance(Q) was estimated using the Busscher (1990) equation:

$$Q = a\rho^{b}\psi^{c}$$

Where ρ is the bulk density, ψ the matric potential, and a, b and c coefficients, root elongation in the soil is controlled mainly by the soil mechanical resistance (Bengough et al., 2006; Materechera et al., 1992). The accuracy of the stress reading while measuring the stress is essential for soil compaction research. The simple question is whether transducers provide accurate estimates of the soil stress. Stress in the soil can be measured either by transducers (housings containing load cells or pressure sensors) or fluid inclusions. Transducers can be used in the vertical direction only (Blunden et al., 1994; Keller and Arvidsson, 2004; Kirby et al., 1997; Lamandé et al., 2007), or in six directions (stress state transducer) as in the studies (Abu-Hamdeh and Reeder, 2003; Bailey et al., 1988; Bakker et al., 1995; Horn et al., 2003; Pytka and Dabrowski, 2001; Way et al., 1995; Wiermann et al., 1999). Soil stress measurements using fluid inclusions are performed using Bolling probes (Arvidsson and Andersson, 1997; Berli et al., 2003; Bolling, 1987; Gysi et al., 2000). The stress estimate provided by a transducer is influenced by the mechanical properties of the transducer comparison with the surrounding soil (Berli et al., 2006; Bolling, 1987; Kirby, 1999a, 1999b). The size and shape of the housing are other factors affecting the measurements. Kirby analysed the stress fields around transducers using finite element modelling. The transducers

used here might overestimate soil stresses as they have a greater stiffness than the soil (Kirby, 1999a, 1999b). Stress was measured by a load cell (DS Europe Series BC 302) with a diameter of 17.5 mm.

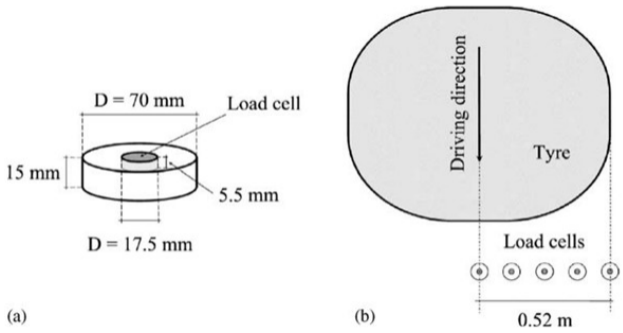

(a) Stress sensor for measurements in the topsoil. (b) Sketch of stress measurements in the topsoil (plane view).

Figure 1.1.2 The load cell transducer used in the stress measurement

Theoretical considerations on soil stress measurements using fluid inclusions showed that pressure measured in an incompressible liquid inclusion embedded in the soil depends on the Poisson ratio of the soil and exceeds the actual mean stress in the soil by 40% for a Poisson ratio of 0.3 (Berli et al., 2006). However, the dimensions and shape of the sensors used for the stress measurements in the subsoil presented in this study differed from those of the sensors, with a smaller width and the width/height ratio used here (Keller, 2005). Other researchers also used sensors with a smaller width/height ratio than those used by Keller and reported that the stress measurements overestimated Fwheel by 21% on average (Schjønning et al., 2006). Therefore, it suggests that the sensors used in the present study may have overestimated the actual soil stress.

1.1.5 Soil Compaction Analysis Model

The strategies to prevent soil compaction rely on soil compaction models. Soil compaction models can calculate stress propagation and soil damage in soil profiles for specific mechanical loads of agricultural machinery in specific soil conditions (such as soil texture and soil moisture status). The simulation models also can help farmers plan and make decisions for specific traffic situations in the field.

Soil compaction models are divided into analytical and finite element models (FEM) by research published before (Défossez et al., 2003). Some models of soil compaction analysis have been developed in the last decade (Keller et al., 2007b; O'Sullivan et al., 1999; Van Den Akker, 2004) as there are some studies focused on getting a better understanding of the soil compaction processes(Arvidsson et al., 2001; Défossez et al., 2003; Lamandé et al., 2007). As the FEM specifically developed for agricultural purposes(Gysi et al., 2000; Richards, 1992) has been used to simulate soil compaction due to agricultural field traffic in recent

studies(Berli et al., 2003; Cui et al., 2007; Gysi, 2001; Gysi et al., 2000; Peth et al., 2006; Poodt et al., 2003).

In soil science research, discrete element models (DEM) have been applied (Zhang and Li, 2006). The DEM provides a promising method for a better understanding soil deformation and stress transmission at different scales(Delenne et al., 2004; Walton, 1983; Zhang and Li, 2006). In addition, DEM has been used to simulate soil compaction due to agricultural field traffic(Jia et al., 2021). Analytical soil compaction models are based on previous studies' work to calculate stress propagation in soil(Boussinesq, 1885; Frölich, 1934; Söhne, 1953). The structure of soil compaction models can be divided into three parts: (i) the upper model boundary condition (the contact area and the stresses at the soil surface); (ii) the propagation of stresses through soil, and (iii) the stress-strain behaviour of soil (Keller and Lamandé, 2010).

1.1.5.1 Contact area between tire and soil

An ellipse can describe the contact area between tire and soil(Febo et al., 2000; Upadhyaya and Wulfsohn, 1990). The distribution of vertical stress at the tyre–soil interface has been described as power-law functions(Johnson and Burt, 1990; Sohne, 1958; Söhne, 1953), polynomials(Smith et al., 2000), and a combination of power-law and a decay function(Keller, 2005; Schjønning et al., 2008). Modelling shows that the stress distribution at the tyre–soil interface is highly non-uniform and largely influences soil stresses(Keller, 2005; Keller et al., 2007a; Keller and Arvidsson, 2004; Schjønning et al., 2008). A few factors could influence the surface stress and contact area as the upper model boundary condition (the contact area and the stresses at the soil surface). For example, the tyre properties and loading characteristics could influence the upper model boundary condition's surface stress and contact area. Tyre construction (radial or cross-ply construction; properties of the belt and tread; lug dimensions and pattern), tyre dimensions (tyre diameter, width and aspect ratio), and tyre loading (tyre inflation pressure, wheel load) influence the contact area (Febo et al., 2000; Sharma and Pandey, 1996)and the magnitude and distribution of stresses at the tyre–soil interface(Gysi, 2001; Jun et al., 2004; Keller, 2005; Lamandé and Schjønning, 2008; Schjønning et al., 2008; Way and Kishimoto, 2004).

Recently, models have been developed to estimate the upper model boundary condition (i.e. estimation of contact area and the magnitude and distribution of contact stress) from tyre properties and loading characteristics(Keller, 2005; Schjønning et al., 2008). In these models, the periphery of the contact area is calculated by a super-ellipse (Hallonborg, 1996), the stress distribution in the driving direction is described by a power-law function, and an exponential function describes the stress distribution across the tyre (Keller, 2005; Schjønning et al., 2008).

The stress at the tyre–soil interface, s(x,y), can then be described as (Schjønning et al., 2008):

$$\sigma(x,y)=\begin{cases} F_{\text{wheel}}\, C(\alpha,\beta,a,b,n) f(x,y) g(x,y) & (x,y)\in\Omega \\ 0 & (x,y)\notin\Omega \end{cases}$$

with:

$$\Omega=\left\{\left|\frac{x}{a}\right|^{n}+\left|\frac{y}{b}\right|^{n}\le 1\right\}$$

$$f(x,y)=\left[1-\left|\frac{x}{l_x(y)}\right|^{\alpha}\right]$$

$$g(x,y)=\left[\left(1-\left|\frac{y}{w_y(x)}\right|\right)\left(\frac{1}{g_{\max}}\right)\exp\left(-\beta\left(1-\left|\frac{y}{w_y(x)}\right|\right)\right)\right]$$

Where $g_{\max}$ is the maximum value of g in the range $\left(0<y<w_y(x)\right)$ expressed in terms of expressed in terms of β :

$$g_{\max}=\begin{cases} \exp(-\beta) & \beta\le 1 \\ \exp(-1)/\beta & \beta>1 \end{cases}$$

F_{wheel} is the wheel load,

$C(\alpha,\beta,a,b,n)$ is a function of the parameters

α,β,a,b,n defining an integration constant ensuring that when integrating

$\sigma(x,y)$ over the contact area,

Ω the total load is F_{wheel} , Ω denotes the boundary and interior of the super-ellipse,

a and b are half the width of the minor and major axes,

n is the 'squareness' of the super-ellipse,

α is a shape parameter for the stress distribution in the driving direction,

β is a shape parameter for the stress distribution perpendicular to the driving direction.

Furthermore, $l_x(y)$ is the half-length of footprint at y in the x-direction and $w_y(x)$ the half-width at x in the y-direction.

The f function elucidates the stress distribution pattern in the driving direction, specifically portraying the relative stress as a function of the relative contact area half-length. Conversely, the g function delineates the stress distribution characteristics orthogonal to the driving direction, traversing the wheel's surface. The size of the contact area increases with increasing wheel load and decreasing tyre inflation pressure (Diserens, 2009; Lamandé and Schjønning, 2008; Schjønning et al., 2008). The change in contact area with changing tyre loading is different for radial, cross-ply and twin tyres (Diserens, 2009). The magnitude of the vertical contact stress generally increases with increasing tyre inflation pressure (Arvidsson

and Ristic, 1996; Keller, 2005; Raper et al., 1995; Schjønning et al., 2008) and with increasing wheel load.

Tire deflection depends on the stiffness of the tire relative to the soil. The soil strength changes the contact area between the soil and tire and the size or distribution of the stress at the tire-soil interface. The contact area mainly depends on the tire's flexibility on hard surfaces such as roads or hard soils (Diserens, 2009). Tire deformation on (soft) soil is a function of soil deformation behaviour and tire flexibility. Generally, the contact area increases at a given tire at inflation pressure as the soil softens(Sohne, 1958; Wulfsohn and Upadhyaya, 1992).

1.1.5.2 Stress Propagation and stress-strain Behaviour

As the stress calculation method in the soil analytical models, stress at any depth Z can be calculated. The contact area is divided into i small elements with an area A_i and normal stress σ_i carrying the load $P_i = \sigma_i A_i$ treated as a point load. Disregarding horizontal stresses in the contact area, vertical stress σ_z was then calculated as (Söhne, 1953):

$$\sigma_z = \sum_{i=0}^{i=n} (\sigma_z)_i = \sum_{i=0}^{i=n} \frac{vP_i}{2\pi z_i^2} \cos^{v+2} \theta_i$$

The concentration factor is the concentration factor, the angle between the normal load vector and the position vector from the point load to the desired point (Frölich, 1934). When v =3, the model satisfies the elastic theory of Joseph Boussinesq (Boussinesq, 1885).

Hence, the soil stress state becomes a function of the concentration factor v for a given loading condition. Frölich assumed that depending on the soil properties, the stress propagation would be focused on the centre line of the load, which he expressed v. He further stated that his concentration factor model is empirical and has to be validated in (engineering) practice, yet little is known about the effects of soil properties on this concentration factor.

Research from 1953 suggested that v increases with increasing soil moisture content and proposed values of 4, 5 and 6 for hard, firm and soft soil, respectively (Söhne, 1953).

Subsequently, other researchers from Denmark measured an increase in vertical stress attenuation between 0.3 and 0.9 m depth, corresponding to a decrease in v undisturbed Stagnic Luvisol when the soil water content decreased (Lamandé and Schjønning, 2011a). He also estimated a concentration factor between 5.5 and 6.5 for wet loam soil with a poorly developed structure by comparing soil stress calculation with the abovementioned equation and two-dimensional stress measurements (Lamandé et al., 2007).

As for the stress calculation and determination of the concentration factor evaluation, some researchers use the root mean square error (RMSE) and bias to evaluate the stress

calculation.

$$\mathrm{RMSE} = \sqrt{\frac{1}{n}\sum_{i=1}^{n}(\hat{\sigma}_z - \sigma_z)^2}$$

$$\mathrm{bias} = \frac{1}{n}\sum_{i=1}^{n}(\hat{\sigma}_z - \sigma_z)$$

Where n is the number of observations, $\hat{\sigma}_z$ is the predicted vertical stress and σ_z is the measured vertical stress.

1.1.6 Evaluation of the soil compaction

1.1.6.1 Natural way (freeze-thaw, alternate dry and wet)

The annual freeze-thaw cycle is one of the processes affecting soil compaction and can alter the physical properties of soil and its structure each winter in some areas. Furthermore, the freeze-thaw cycle can naturally alleviate compaction due to the expansion of water in the pore space and contraction during freezing and thawing. In the earlier research, some papers discussed soil penetration resistance and bulk density reduction in agricultural soils during winter because of frequent freeze-thaw cycles (Henry, 2007; Unger, 1991). Several studies have also indicated that repeated freeze-thaw cycles could loosen the soil structure and alleviate soil compaction. It could also improve the soil's physical and hydraulic properties(Edwards, 2013; Fouli et al., 2013; Sahin et al., 2008). For example, some researchers found that the freeze-thaw cycle alleviated soil compaction up to a depth of 30 cm in clay loam soil in Montana. The topsoils (5–12 cm) experience more than one freeze-thaw cycle yearly (Jabro et al., 2014). Most freeze-thaw cycles influence the surface or the properties and structure of the topsoil. However, the compaction also happens in the subsoil or under the hardpan. The freeze-thaw cycle may not reach that depth. For example, research mentioned that the annual freeze-thaw cycle did not alleviate the soil compaction at the bottom of the plough furrow in Nicollet silty clay loam soil in Minnesota (Voorhees, 1983). Although some researchers mentioned the effect of the freeze-thaw to reduce the soil compaction, the impact of the freeze-thaw on soil compaction recovery is not very useful in some areas. A report tells about this situation in some areas of Canada where only the top 2 to 3 inches experience more than one freeze-thaw cycle per year, which is necessary to break up compaction. The compacted soil below the top few inches will typically see one freeze and one thaw (Anken and Holpp, 2011).

1.1.6.2 Artificial methods

(1) agronomic method

Choose the right time to enter the ground. Soil compaction is the most serious when the soil moisture content of the 7-15cm soil layer is close or reaches the field water holding capacity. Therefore, it is recommended to avoid entering the field when the soil moisture content is high. Instead, try to choose the driest time to finish the field operation. Cooperating with other soil compaction mitigation measures is also recommended to protect the soil if possible and necessary.

Enter in the field as less as possible during the crop round.

(2) Adjust and optimise the structure of the machine

During the agricultural machinery design, reduce the axle load and ground pressure as much as possible. Improve the driving system of the existing machinery, such as changing two to four-wheel drive, increasing the number of tires, and increasing the ground contact area.

For example, changing the tractors' tires into the crawler will reduce the soil compaction because the ground area of the crawler type is much larger than standard tires. Therefore, more contact areas have less compaction. However, the crawler also has disadvantages: lower walking speed and larger power requirement than the traditional tires. Another method to reduce soil compaction is changing high-pressure tires to low-pressure tires. The low-pressure tires can increase the tire-soil contact area, reduce the tire-soil contact surface stress, and reduce the topsoil compaction.

(3) Mechanised reduction of soil compaction

Soil compaction is a common problem during agricultural production. Hence, mechanised measures must be taken to quickly solve the soil compaction problems.

Surface soil operations can alleviate the compactness of the surface soil. In addition, the surface operation reduces the soil's sensitivity to compaction, increases the amount of surface residues, and prevents the formation of surface crusts. Deep soil loosening technology can break the hardpan formed by ploughs, rotary tillers and other land preparation machines at the same depth for a long time. After the deep loosening breaks the hardpan, the soil seepage rate will increase by 5-10 times, and the soil porosity will be significantly improved. Combined with the soil compaction evaluation system, different mechanised soil loosening measures for different farming measures can better loosen the soil in all directions, make the soil characteristics of the plough layer more uniform, and solve the problem of soil compaction.

(4) controlled traffic farming system(CTF)

According to the previous research, most arable land in Europe is managed in a conventional tillage system. The 74% of all arable land in Europe (EU-27) is conventionally tilled, while only 4% is under no-till, and the remaining 22% is managed with reduced-tillage

(Keller et al., 2019). The alternative solution to soil compaction is controlled traffic farming (CTF), which protects most of the field's cropped area by restricting all traffic to permanent traffic lanes. CTF aims to separate machinery driving areas from crop fields, establishing permanent tractor lanes between the planted fields (Antille et al., 2016, 2015; Bluett et al., 2019; Tullberg et al., 2007). Researchers focusing on soil compaction actively endorse CTF to mitigate the adverse impacts of wheel traffic on soil physical quality (Bluett et al., 2019). CTF can reduce the negative effects of compaction, prevent soil structure destruction (Blanco-Canqui et al., 2010), save energy consumption (Sartori et al., 2005), lower operating costs, and enhance crop yields through suitable seedbed conditions (McPhee et al., 2015).

1.2 Statement of the Problem:

The central problem addressed by this research revolves around the pervasive issue of soil compaction and its far-reaching implications for agricultural productivity and environmental sustainability. Soil compaction arises from the relentless use of heavy machinery in modern agriculture, exerting immense pressure on soil particles, diminishing its natural structure and quality. Specifically, this research scrutinises the following facets of the soil compaction problem:

1.2.1 Agricultural Productivity Impact.

Soil compaction is known to be detrimental to crop productivity. The compression of soil particles leads to reduced pore space, impeding root growth and restricting the movement of water and nutrients within the soil. Consequently, crops face challenges in accessing essential resources, resulting in decreased yields. Understanding the extent and variability of these impacts is crucial for devising effective mitigation strategies.

1.2.2 Environmental Consequences

Beyond the scope of agricultural productivity, soil compaction has profound environmental repercussions. Compacted soil increases surface runoff and erosion, contributing to soil degradation and water pollution. Furthermore, the altered soil structure can lead to diminished soil microbial activity, affecting nutrient cycling and carbon sequestration. These environmental ramifications underscore the urgency of addressing soil compaction in sustainable agricultural practices.

1.2.3 Knowledge Gaps

Despite the importance of soil compaction and tillage operations in agricultural

production, there are still significant knowledge gaps in our understanding of the effects of tractive efficiency on soil stress, bulk density, moisture, and cone index under different traction resistance conditions. While some research has been conducted in this area, the existing literature is limited and does not comprehensively understand the complex interactions between soil properties, tillage operations, and tractive efficiency (Arvidsson et al., 2011; Khafizov et al., 2020; Md-Tahir et al., 2019; Nurmiev et al., 2018; Schjonning et al., 2022; Serrano et al., 2009). Furthermore, there is a lack of information on the optimal tillage operations and soil management practices that can minimize soil compaction and improve soil health under different traction resistance conditions (ten Damme et al., 2021a). The existing literature on soil compaction and tillage operations has mainly focused on conventional tillage practices, and there is a need for more research on conservation tillage practices and their effects on soil compaction and soil health. Therefore, this study aims to address these knowledge gaps by conducting a field experiment to quantify the effects of tractive efficiency on soil stress, bulk density, moisture, and cone index under different traction resistance conditions and to identify the optimal tillage operations and soil management practices that can minimize soil compaction and improve soil health.

Previous research has investigated the impact of various factors, such as edge-feeding of insects and weeds, competition for resources with adjacent obstacles, and machine traffic management, on crop yield in headlands and field edges (Kayad et al., 2016; Kross et al., 2015; Peigné et al., 2013; Xue and Su, 2017). However, a significant knowledge gap exists in analysing vegetation indices (VIs) specifically related to soil compaction in headlands and field edges. While previous studies have investigated the impact of soil compaction on crop yield, there is a lack of research on using VIs to assess this impact. The importance of this research lies in its potential to improve the sustainability and profitability of farming practices. By identifying the factors that contribute to yield losses in headlands and field edges and developing effective strategies for mitigating these effects, farmers can improve their crop yields and reduce their environmental impact. This research also highlights the need for further investigation into the complex interplay between soil structure, crop yield, and environmental factors and provides decision-makers with valuable insights to improve yields and increase profitability.

Subsoiling is an important tillage practice that improves soil structure and productivity. However, further research is still needed to fully understand the effects of subsoiling angle and tillage depth on soil structure and machinery performance in different soil types and tillage conditions. While previous studies have investigated the effects of subsoiling on soil structure and machinery performance, there are still knowledge gaps in the specific effects of

subsoiling on soil structure and machinery performance in certain soil types or tillage conditions(Azevedo et al., 2022; Celik and Raper, 2012; Li et al., 2018; Pulido-Moncada et al., 2021; Zhang et al., 2022). Therefore, this study aims to contribute to the knowledge base surrounding subsoiler tillage and provide valuable insights for optimizing tillage practices in agriculture. By identifying the knowledge gaps in this research, we can better understand the current study's limitations and the potential for future research to expand our understanding of subsoiling practices.

1.3 Research Questions:

Research Question 1: How does transit on varying soil conditions, including no-tillage soil, different numbers of passes, and the permanent traffic lane, each characterized by distinct levels of traction resistance, influence soil compaction, and what are the resulting implications for soil structure and crop productivity?

Research Question 2: What are the key performance differences between machinery operating in headland and field edge areas, and how do these differences contribute to variations in soil compaction and crop yield?

Research Question 3: What is the influence of subsoiling angle, tillage depth, and tractive efficiency on soil structure, energy requirements, and crop productivity, and how can these parameters be optimised to mitigate soil compaction and enhance agricultural sustainability?

1.4 Research Objectives:

Clearly state the primary objectives of your research based on the three published papers.

Describe what you aim to achieve through your investigation. The primary objectives of this research, derived from the findings presented in three published papers, are as follows:

Objective 1: To assess the tire pressure distribution during soil compaction under varying levels of traction resistance, employing a dual approach of simulation calculations and field tests, with a focus on understanding its impact on soil compaction, soil structure, and crop productivity.

Objective 2: To assess the difference between headland, field edges and field centre

using VIs data and yield map data. Provide actionable recommendations for the efficient management of machinery practices and the reduction of soil compaction..

Objective 3: To investigate the influence of subsoilers parameters such as tillage depth, subsoiling angle, slip rate and traction efficiency on soil structure and energy requirements.

2. Soil Compaction under Different Traction Resistance Conditions

Abstract:

Tractive efficiency is essential in tillage operations to optimise traction performance. In this field experiment, the tractor performance was measured under different traction resistance conditions. This study quantified the soil stress, soil bulk density, soil moisture, soil cone index, soil surface disturbance, rolling resistance and slip rate under different numbers of passes and traction conditions. The actual power used under different soil and traction conditions was collected. Fuel consumption and savings were calculated between uncompacted soil, compacted soil and the permanent traffic lane. The results show that soil stress increases in each location as traction and the number of passes increase. Soil's physical properties increase, such as the soil bulk density, soil cone index and soil surface disturbance. Additionally, the slip rate increases with traction in each soil condition as uncompacted soil, compacted soil and the permanent traffic lane. The results show that the permanent traffic lane has a lower slip rate under different traction conditions than the uncompacted and compacted soil. Furthermore, the permanent traffic lane has less energy consumption with the same traction resistance. The permanent traffic lane saved 25.50%, 29.23% and 42.34% fuel compared to the uncompacted field in 7.85, 14.71 and 24.52 kN traction condi-tions, respectively. Our results confirm that dynamic factors such as traction and rolling resistance should be considered in soil compaction research rather than static weight only. In practice, the controlled traffic farming (CTF) system or driving the tractor more frequently on the permanent traffic lane should be considered to improve working efficiency and reduce energy consumption.

2.1 Introduction

Soil compaction has become an increasingly severe problem in the past few decades, with the size and weight of agricultural machines increasing worldwide (Keller et al., 2019). Researchers in different countries have studied the negative effects caused by soil compaction (DeArmond et al., 2019; Mossadeghi-Björklund et al., 2016; Obour et al., 2018; Silva et al.,

2018). The previous study shows that soil compaction could increase soil bulk density, soil cone index and soil shear strength (Blanco-Canqui et al., 2010; Schjønning and Lamandé, 2018; Tekeste et al., 2008). In addition, soil compaction causes the impeding of root exploration, reduced crop yield and increased energy requirements in all field operations (Antille et al., 2016; Bluett et al., 2019; Colombi et al., 2018; Keller, 2018; Tullberg, 2010).

Soil compaction is defined by the Environmental Assessment of Soil for Monitoring (ENVASSO) as "The densification and distortion of soil by which total and air-filled porosity are reduced, causing a deterioration or loss of one or more soil functions" (Huber et al., 2008). It can destroy or over-squeeze soil aggregates to form a damaged layer of soil structure during the first pass (Ankeny et al., 1990; Cambi et al., 2016; Patel and Singh, 1981; Radford et al., 2000). After the compaction, the soil particles inside the damaged layer are rearranged under external force, decreasing soil volume and increasing soil bulk density (Chaudhary et al., 1991; Kirby, 1991).

As for soil compaction measurement, different methods may have different advantages and disadvantages. The load cell (de Lima and Keller, 2021; Lamandé et al., 2015) measures the soil stress generally in the vertical direction of the target position but provides only one stress component. Stress-state transducer (Harris and Bakker, 1994; Nichols et al., 1987) contains load cells in six different directions. However, ensuring good probe contact with the soil can be difficult due to the complex probe geometry of the sensor. The fluid-filled flexible pressure probe (Berli et al., 2006; Bolling, 1987; R. L. Raper and F. J. Arriaga, 2007) is directly related to the mean normal stress, which is simple and quick to install and has good probe contact with the soil. However, the pressure reading is still a function of the Poisson's ratio of the soil, which may change during the compaction process.

The risk of soil compaction can be reduced by (I) avoiding entering the field in wet soil conditions (Braunack and Johnston, 2014; He et al., 2017; Munkholm and Schjønning, 2004; Obour et al., 2018), (II) using tyres with a larger contact area and low inflation pressure (Arvidsson and Keller, 2007; Lamandé and Schjønning, 2011a; ten Damme et al., 2020) and (III) introducing the controlled traffic farming (CTF) system (Antille et al., 2016; Chamen, 2015; McHugh et al., 2009; R. L. Raper and D. W. Reeves, 2007; Taylor, 1983; Tullberg et al., 2007).

Tyre inflation pressure and wheel load are also well-known key drivers of compaction. Many researchers work on the soil stress distribution underneath the soil caused by different properties of soil, tyre and machine weight conditions (De Pue and Cornelis, 2019; Keller, 2005; Keller et al., 2016; Lamandé and Schjønning, 2018, 2011a). However, most of them focused on static wheel load rather than dynamic wheel load, which is the actual weight that

compacts the soil. Dynamic wheel loads are higher than static wheel loads. For example, the wheel load could increase by 25% of the static wheel load during plough (J Brunotte et al., 2012). The extra weight is caused by the traction required to carry out the plough operation and the weight redistribution from the front to the tractor's rear axle. The increase in rear wheel load during conventional tillage given in the guidelines of the German Engineers' Association (VDI, 2014) is even higher (up to 45%), which causes much more compaction than the static wheel load.

Drawbar pull, travel reduction (slip) and rolling resistance are the three main criteria describing off-road vehicles' traction behaviour. The lugs on tractor wheels tend to penetrate deep into the soil layer in terms of working on the soft ground that characterises almost all agricultural operations (Lamandé and Schjønning, 2011b; Nadykto et al., 2015; Way and Kishimoto, 2004). The tractor lugs compress soil horizontally, opposite to the tractor movement when they are dug into the soil. As a result, the speed at which the tractor moves decreases. This loss of relative speed of the tractor is estimated as the slip coefficient (Bulgakov et al., 2020; Ekinci et al., 2015; Nadykto et al., 2015; Zoz and Grisso, 2003b). Maximum traction can go into slippage, increasing the soil structure damage (Battiato and Diserens, 2017; Bulgakov et al., 2020; Czarnecki et al., 2019; Grosch, 1996; Nadykto et al., 2015).

Controlled traffic farming (CTF) is a mechanisation system in which all machinery has the same (or modular) working and track width so that field traffic can be confined to the least possible area of permanent traffic lanes (G.D. Vermeulen, J.N. Tullberg, 2010; Hussein et al., 2021). The CTF is one of the solutions for reducing soil compaction, ensuring that the tractor travels on the traffic lane, which has a more solid soil structure than conventional agriculture. In addition, the permanence of the non-pavement surface facilitates the maintenance of softer soil conditions, thus reducing resistance and energy requirements during field operation (Anken and Holpp, 2011; Antille et al., 2016; N.V. Halpin, 2012). The reduced energy consumption of CTF systems is also attributable to the lower rolling resistance and slippage of tyres on permanent traffic lanes (Antille et al., 2016; Bulgakov et al., 2020; Schreiber and Kutzbach, 2008). Tractor slip rate and traction efficiency are critical parameters for farm operations. Although many studies have demonstrated that the CTF system has lower slippage and higher traction efficiency than conventional agriculture, these two parameters have been less studied in conventional fields under different compaction times and traction resistance conditions. The effect of different levels of soil compaction on the tractor's working efficiency under conventional farming is unclear. Most of the previous research was conducted to increase traction resistance by increasing the weight of the load (Arvidsson et al.,

2011; Khafizov et al., 2020; Md-Tahir et al., 2019; Nurmiev et al., 2018; Schjonning et al., 2022; Serrano et al., 2009; ten Damme et al., 2021a). However, this research approach cannot focus on the effect of traction resistance on soil compaction because of the machine's added weight. Thus, in this experiment, the method of increasing the traction resistance without adding weight was implemented.

The aim of our study was to test the effects of different traction conditions on soil bulk density, soil moisture, soil cone index, soil surface disturbance, slip rate and tractor working efficiency. In this experiment, a method to increase the traction force is proposed. A method was set to increase the traction force independently rather than increasing the weight simultaneously, as in the previous research (ten Damme et al., 2021a). First, we tried to determine if the wheel slippage rate would be less under more wheel passes in this experiment. Then, we focused on whether the soil structure damage would be more significant at higher traction forces and a greater number of wheel passes.

2.2 Materials and Methods

The field experiment lasted from March to May 2022. The experiment field used for this study is located at the experimental farm of Padova University (Veneto, Italy). The area of the field is 1.87 hectares. The slope of the field is less than 1°, measured by Google Earth Pro (Https://www.google.it/earth/about/versions/, n.d.). Temperatures rise from January (min average: −1.5 °C) to July (max average: 27.2 °C). The sub-humid climate receives about 850 mm of rainfall annually, with the highest average rainfall in June (100 mm) and October (90 mm). The lowest averages happen in winter (50–60 mm). Soil moisture was 23.01%, 23.54% and 27.01% at 20 cm, 40 cm and 60 cm depth when the experiment started. No rainfall occurred during the experiment. The soil texture of the experiment field is clay loam (Piccoli et al., 2020). The sand–silt–clay content of the soils used for testing was 33.8%, 37.0% and 29.2%, respectively. The organic matter content of the topsoil (0–30 cm) was 1.81%, referring to another field also located at the experimental farm of Padova University (Piccoli et al., 2020) (straight line distance not exceeding 200 m between two fields). The field was deep ploughing (0–50 cm) after the 2021 crop season, which has a partly bare surface. There were no other field management practices until the start of the field experiment.

The field experiment was preceded in the field as shown in Figure 2.2.1. First, slip rates and rolling resistance under different traction and soil conditions were performed in the left part of the field. Then, the field's right area was set into small plots located after the 40 m long area for the stable driving speed of the tractors (3.3 km/h) during the test, as shown in Figure 2.2.1b. The blue box area is the place where we collected the data. The 6 m area

between each plot was designed for the tractors turning after each round. The detailed data collection procedure for the experiments is listed below.

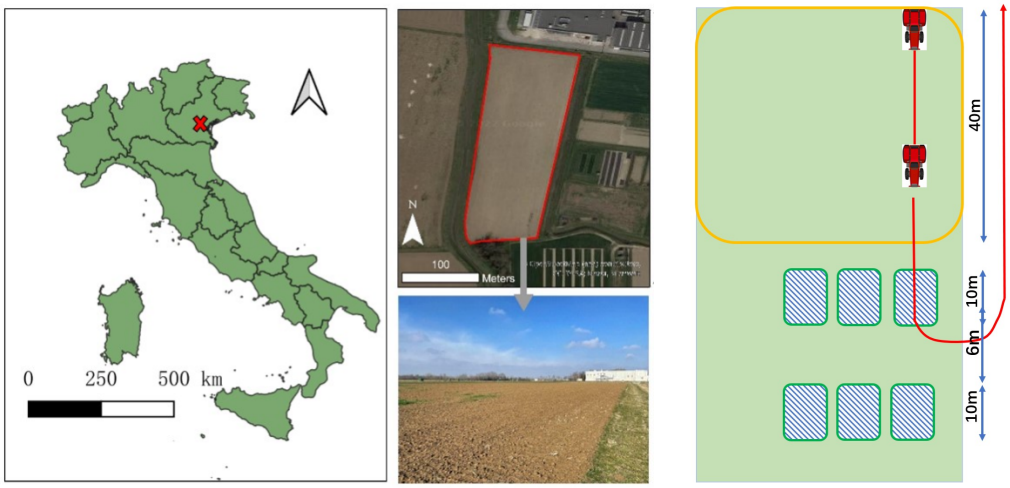

(a) (b)

Figure 2.2.1 Experiment field in Legnaro, North Italy (a), and the experimental procedure (b).

Two tractors were used in the experiment. The front tractor was used to compact the soil in different traction conditions and number of passes. The rear tractor was designed to use the hydrostatic transmission system to adjust the braking force.

The front tractor was a Fiat 680 (CNH Industrial N.V., Amsterdam, The Netherlands), as shown in Figure 2.2.2. The machine's weight was increased by adding additional counterweights to the back of the front tractor to increase the soil pressure on the tyre and soil contact surfaces for better stress detection and analysis.

(a) (b) (c)

Figure 2.2.2 Two tractors used in the field experiment (a), counterweight attached in the back of the front tractor (b) and dynamometer between the tractors (c).

A tractor prototype three-wheeler was used at the back, equipped with a hydrostatic gearbox, which made it possible to change the traction resistance during the experiment. As a rear tractor, the high responsiveness of the hydrostatic gearbox was used to regulate the

forward speed and braking capacity to generate different amounts of traction.

Table 2.2.1 Technical data of the tractors used in the experiment.

Name	Unit	Model
Tractor Model		Fiat 680
Total mass	kg	4310
Front axle	kg	780
Rear axle	kg	3530
Rear tyre	Kleber traker	420/85R30
Front tyre	Vredestein multirill	7.50-16
Front tyre inflation pressure	bar	1.7
Rear tyre inflation pressure	bar	1.45

The actual speed was recorded from the GPS. The real-time kinematic positioning (RTK) system from Trimble was equipped on the front tractor, which was used to record the track with high accuracy during the experiment. For theoretical speeds, the sensor was placed on the tractor power take-off unit (PTO) to detect the number of revolutions. We calculated the theoretical speed of the tractor by detecting the PTO rpm and measuring the tractor's fixed gear ratio.

Mean Normal Stress

Normal stresses underneath the soil were measured using the Bolling probe (Berli et al., 2006; Bolling, 1987) in the field experiment. The probe is deformable and cylindrical, and could sense the mean radial stress experienced. For the installation of the Bolling probe, the drill and reamer were inserted into the soil at a specific angle on the side of the probes by using a special steel frame which could ensure the angle consistency during the installation of the drill, reamer and Bolling probe. After the completion of reaming, the probe was inserted into the soil and tested for good contact with the soil to ensure accurate data collection.

In this experiment, the mean normal stress of the soil was measured in the vertical direction and also in the lateral direction. The soil mean normal stress in the vertical direction can be applied to the depth of the subsoil (0–100 cm) (Olsen, 1994). However, the lateral compaction affects shallower soil (ten Damme et al., 2020), also verified by the simulation results. Considering the amount of pressure that can occur at different positions, three Bolling probes were used in the vertical direction (0–60 cm) and two in the lateral position (0–40 cm) in this measurement.

Three probes were installed in the centre of the track at 20, 40 and 60 cm depth to measure the soil mean normal stress in the vertical direction. Two probes were installed in the track edge at 20 and 40 cm depth to measure the soil mean normal stress in the lateral direction. There were five groups overall: 20 cm depth in vertical (20 V), 40 cm depth in vertical (40 V), 60 cm depth in vertical (60 V), 20 cm depth in lateral (20 L) and 40 cm depth in lateral (40 L). The width between the centre and the lateral is 25 cm. The stress data under

different depths were collected after each time compaction (9 times in total). The probes were inserted into the soil from the edge side of the wheel rut, as shown in Figure 2.2.3.

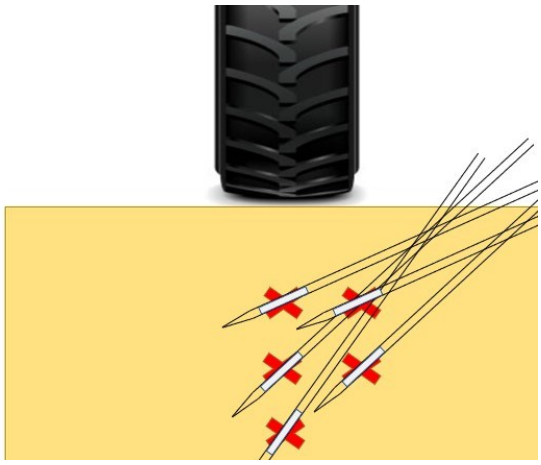

Figure 2.2.3 Installation position of Bolling probe to measure the mean normal stress in vertical (3 probes) and lateral (2 probes) directions. The three probes in the vertical direction and the two probes in the lateral direction were staggered during the installation, with 25 cm between two groups.

The mean normal stress (σ_m) was calculated (Berli et al., 2006; Bolling, 1987) to compare the results of different traction conditions and number of passes. The following is the calculation formula of the mean normal stress.

$$\sigma_m = \frac{1+v}{3(1-v)} p_i$$

where p_i measures stress from the Bolling probe, and v is the Poisson ratio in the soil matrix. The value of the Poisson ratio was considered within 0.2–0.45 (de Lima and Keller, 2019; Défossez et al., 2003; Keller et al., 2016; Kirby, 1999a; Naderi-Boldaji et al., 2014). We set the Poisson ratio as 0.3 in our study, considering the results of other studies (Berli et al., 2006; de Lima and Keller, 2019).

The mean normal stress collected from the Bolling probe was compared with the simulation results produced by Terranimo (Lassen et al., 2013; Stettler et al., 2014). Terranimo is a computer model that predicts the risk of soil compaction by farm machinery (Keller and Arvidsson, 2016; Schjønning et al., 2016). It includes two inputs (machinery and soil) and two outputs (stresses in the tyre–soil interface and stresses transmitted to the soil profile). An example of the simulation results of the soil stress of the rear tyre is shown in Figure 2.2.4. The simulation results and the data collected during the field experiment are given in Section 3. It is worth noting that the soil depths on the y-axis are negative numbers generated automatically by the system. However, in analysing this graph, we default to this problem, as in the graphs in other studies, there is no negative sign in the process of indicating depth (Keller et al., 2002; ten Damme et al., 2021a, 2020).

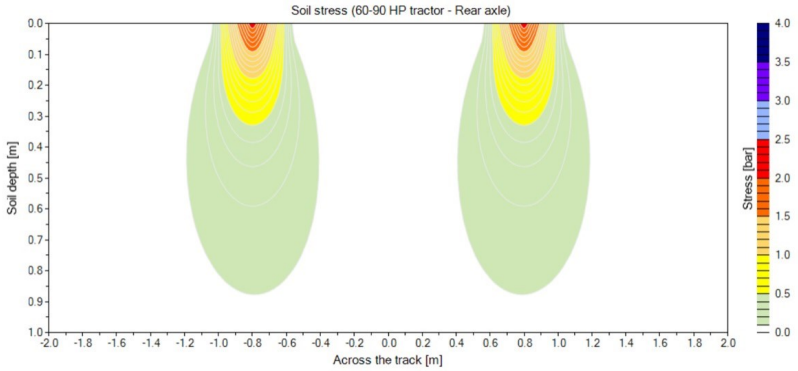

Figure 2.2.4. Soil stress simulation results of the rear tyre using Terranimo.

Soil Bulk Density and Soil Moisture

The soil bulk density and soil moisture were collected and calculated through the experiment of uncompacted field conditions (0 pass) and each traction condition after 1, 4 and 9 passes. Soil bulk density was collected by the soil sampler (Eijkelkamp, EM Giesbek, The Netherlands). Three groups of soil samples were collected in the vertical direction at 20, 40 and 60 cm depth. Two groups of soil samples were taken on the lateral side of the tyre at 20 and 40 cm depth as shown in Figure 2.2.5. There are five groups in total: 20 cm depth in vertical (20 V), 40 cm depth in vertical (40 V), 60 cm depth in vertical (60 V), 20 cm depth in lateral (20 L) and 40 cm depth in lateral (40 L), which are the same as for the soil cone index. Each point was repeated three times. In total, 240 soil samples were collected in the experiment.

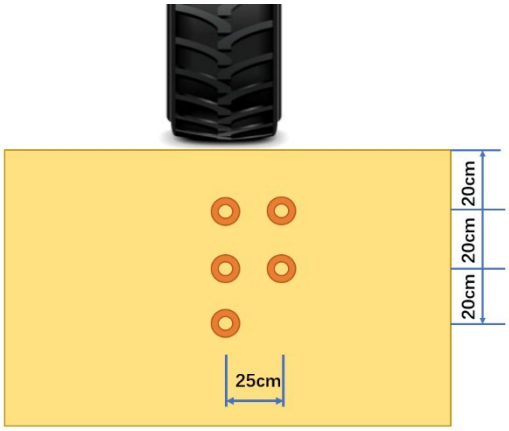

Figure 2.2.5 The locations of the soil sample collection to measure the soil bulk density in vertical (3 locations) and lateral (2 locations) directions.

Soil Cone Index

Penetration resistance of the soil under different treatments was measured with a penetrometer named Penetrologger (Eijkelkamp, Geesbek, The Netherlands). The probe has a 2 cm^2 needle with a 30° cone (standard ASAE S3133 FEB04). Each data group contains a 0–70 cm depth soil cone index collected from the centre line to 50 cm width lateral (5 cm each,

11 points in 50 cm width), as shown in Figure 2.2.6. In order to measure the soil cone index from 0 to 70 cm, a hydraulic system was used during the data collection. The penetrometer was mounted on a designed iron frame fixed to the hydraulic piston. The iron frame allows the penetrometer to change the location of measurement horizontally. The hydraulic piston driven by the tractor allows the uniform insertion speed during the measurement. The soil cone index was recorded in every centimetre of each insert. Each data group was collected before the first pass, and after 1, 4 and 9 passes. Each point in each condition was repeated three times.

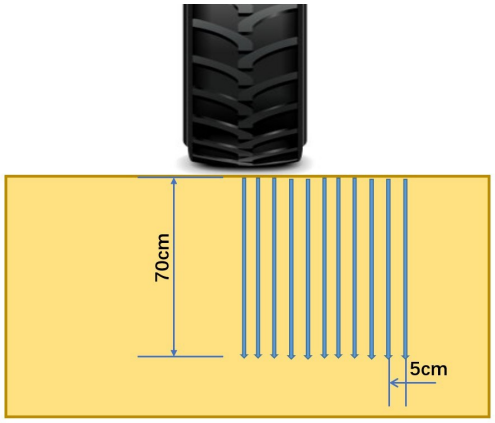

Figure 2.2.6 Soil cone index measurement using the penetrometer at 0–70 cm depth vertical and 5 cm each horizontal.

The soil cone index measurements were used to analyse the following method (Jabro et al., 2021; Tekeste et al., 2008). The four parts of the results were collected and calculated as (1) the range of the nose zone, (2) the depth of the max cone index, (3) the max cone index and (4) the average cone index from 0 to 40 cm. The nose zone in the soil cone index profile was assumed to be the peak in the profile, which starts and ends with the same soil cone index value, as shown in Figure 2.2.7.

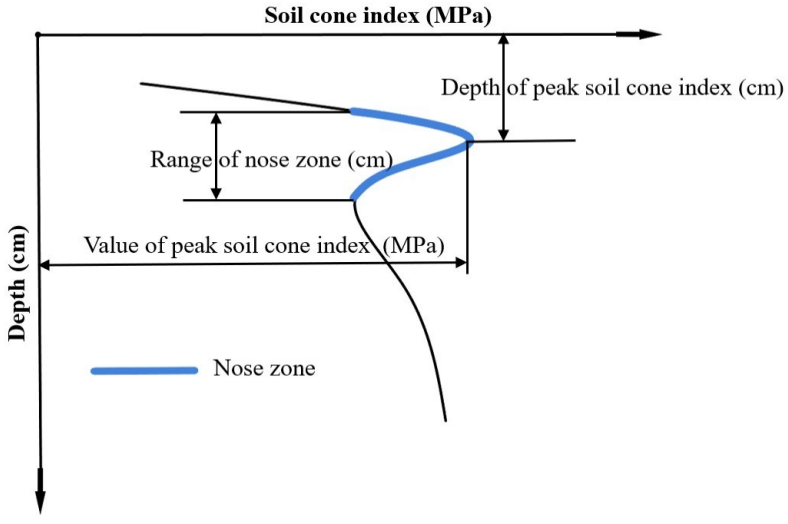

Figure 2.2.7 Schematic view of cone index (CI)-related traits.2.4. Profile Meter after the Compaction

The soil deformation was measured during the experiment to study the soil surface deformation in different traction conditions and number of passes. A steel flame combined

with a laser rangefinder (Disto Pro, Leica Geosystems AG, Balagah, Switzerland) measured the distance between the flame and the soil surface horizontally every 2 cm, as shown in Figure 2.2.8. Data were collected before the first pass, and after 1, 4 and 9 passes. The data collection was repeated three times.

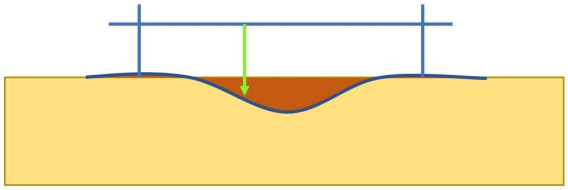

Figure 2.2.8 Profile meter measurement using a laser rangefinder to calculate the value difference between the compacted and undisturbed soil surface.

Slip Rate

Wheel slip is more likely to cause soil compaction than additional wheel loading, especially for heavier tractors (DAVIES et al., 1973). When the tractor's rear wheel slip rate increases, the maximum shear contact stress rises sharply (Battiato et al., 2015). This test aimed to assess if and how traction performance varied with the number of passes the tractor made. The slip was calculated as:

$$S = \frac{(d_2 - d_1/4)}{d_2} * 100$$

The d_1 is the actual distance after four turns of rear wheels. d_2 is the theoretical moving distance during the four-wheel turns, and *S* represents the slip rate.

Rolling resistance was calculated first by pulling the unload front tractor, simulating nine passes on a predetermined track and using the dynamometer.

In addition, the slippage of the tractor used in the experiment in different traction conditions was tested and measured: 0, 800, 1500 and 2500 kg, which were 0, 7845, 14,710 and 24,517 N, respectively. Using the data collected by the dynamometer, the traction loads were obtained for the traction in four levels. The coefficient of adhesion (ka) was then calculated using the collected rolling resistance and the adherent weight of the machine on the driving axle (Bodria et al., 2013).

$$k_a = c_a/G_a$$

where c_a is the rolling resistance, and G_a is the loading weight.

The machine's inherent losses were subtracted from the power generated by the engine to calculate the actual power used for productive work. The 7 kW and 4 kW power losses were considered while calculating the actual power used for the work because of the transmission and hydraulic system based on the previous study (Bodria et al., 2013). To

estimate the power used during the tractor moving, the formula for the determination of the rolling power (P_r) expressed in kW is as follows:

$$P_r = R_r * Va * 10^{-3}$$

where R_r is torque (N), and Vais the rolling speed (m/s). The same formula was used to estimate the useful power (Pu) for each level of traction, considering the previously calculated traction loads. Based on the power used and the type of use, the specific diesel fuel consumption of 260 g/kWh was considered according to data in the literature (Bodria et al., 2013). Through the relationship between specific consumption and useful power, the fuel consumption in kg/h has been estimated for each level of traction.

The fuel consumption in different traction and soil conditions was calculated. In addition, the diesel saving was calculated to assess diesel fuel consumption in varied soil conditions such as uncompacted soil, compacted soil and field edges (permanent traffic lanes). Finally, the combustion of one litre of diesel fuel produces 2.67 kg of CO_2 (Institute for European Environmental Policy et al., 2012), and the carbon dioxide emissions were estimated in the various simulations. In the experiment, we assume that the density of diesel fuel is 0.85 kg/dm^3.

Statistics

In each type of result, the arithmetic mean value of mean normal stress, soil bulk density, soil moisture, soil cone index and soil disturbance were calculated for each position (centre 20, 40 and 60 cm depth, lateral 20 and 40 cm) with a different number of passes and traction conditions as 0, 7.85, 14.71 and 24.52 kN. The three resulting values for each position of each treatment were considered replicates. Statistical analyses of results were undertaken with SPSS (IBM Corp. Released 2019. IBM SPSS Statistics for Windows, Version 26.0. Armonk, n.d.). The analysis of variance (ANOVA) was used to compare means with a probability level of 5%.

2.3 Results

Stress under the Soil Using the Bolling Probe Sensor

In this study, a method to incorporate traction and rolling resistance into soil pressure simulations compared with the collected results was implemented. As discussed in the slip rate test section, the rolling resistance calculated is 273 (±4.79) kg as 2677 (±46.97) N of the tractor in the experiment. Then, 0 kg, 800 kg, 1500 kg and 2500 kg, which were 0, 7845, 14,710 and 24,517 N, were considered as the extra traction compared to the rolling resistance

of the tractor. Therefore, these two parts consist of the net traction, which was considered the additional horizontal pressure with the weight of the tractor. In Terranimo, a slightly higher additional stress was calculated for the rear axle in each simulation. For example, an additional 1000 kg was considered in the simulated rear wheel pressure conditions by simulating 100 investigated tractors at a support load of 3000 kg, which means the total weight to input into the model during the simulation is 4000 kg rather than the actual weight (3000 kg) (Stettler et al., 2014). The weight was overestimated to avoid underestimating the load and taking into account the additional load transfer effect due to the rolling resistance of the trailer (Stettler et al., 2014). However, previous studies have not tested the true value of rolling resistance in field tests. In our current study, the tractor gravity, rolling resistance in the vertical direction and traction resistance in the horizontal direction were considered. The values were put into the Terranimo system in different traction conditions to calculate the sum of squares in both directions.

The traction force (σ) was calculated by calculating the arithmetic sum of squares of the vertical load (W) and the net traction (NT), as shown in Figure 2.3.1. The vertical load of the rear tyre was settled during the experiment. The net traction changed between four traction conditions. The net traction was considered located in the rear tyres only because of the two-wheel drive system of the Fiat 680. The traction force (σ) in different conditions was input into the Terranimo system, and the simulation results were obtained at different locations and depths. After the traction force was calculated, we compared the soil stress data collected from the field experiment with the simulation results, as shown in Figure 2.3.2.

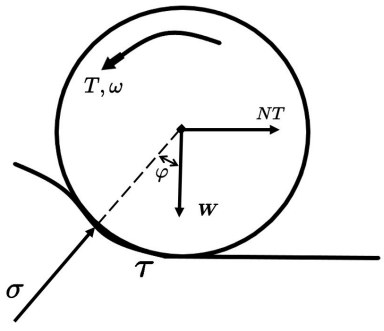

Figure 2.3.1Schematic of soil–tyre interaction. Total driving torque on the wheel (T), angular velocity of the wheel (ω), net traction (NT), angle between normal stress and the vertical (φ), vertical load (W), normal stress (σ) and shear stress (τ).

Simulated results and collected data are shown in Figure 2.3.2. There are five groups of bars: 20 cm depth in vertical (20 V), 40 cm depth in vertical (40 V), 60 cm depth in vertical (60 V), 20 cm depth in lateral (20 L) and 40 cm depth in lateral (40 L). The result of each bar was made by the average value of one to nine passes in each depth and position. The simulated results have a higher value than the collected data in each depth and direction. The

error bars are made by the standard deviation of each position of collected results. The simulation soil stress increases as the traction increases, and the collected data show the same trend in most positions. However, the vertical 60 cm in 0 kg traction shows a higher value than the 800 kg and 1500 kg. The result of the simulation grows uniformly with the increasing traction. The collected results in the vertical 60 cm, lateral 20 cm and lateral 40 cm directions show that the increasing trend with the increasing traction is not distinct compared to the collected results for vertical 20 cm and 40 cm. The subsoil spatial variability could cause this irregular variation in these positions. Furthermore, the data acquisition was likely unsatisfactory in the low-value condition. The probe may have had insufficient contact with the soil in low-pressure conditions compared to high-pressure locations.

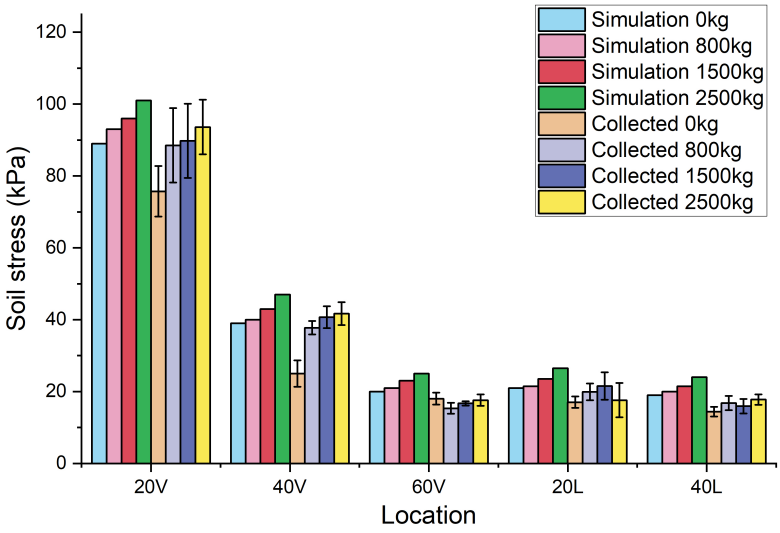

Figure 2.3.2 Simulated and collected soil stress comparison.

Soil Bulk Density and Soil Moisture

As shown in Figure 2.3.3, the 60 cm depth had the highest soil moisture in the five positions among the four kinds of traction conditions. In general, the soil moisture slightly increases after compaction. The ANOVA test showed no significant difference in the soil moisture based on the different traction conditions, number of passes and position, except for the moisture in lateral 20 cm in the 1500 kg traction condition. However, there is a slight difference in different traction conditions and the soil moisture in the experiment. The mean difference in soil moisture content is within 1.5%, considering random errors in the data collection process. Studying this experiment with other parameters is recommended for more in-depth analyses and conclusions.

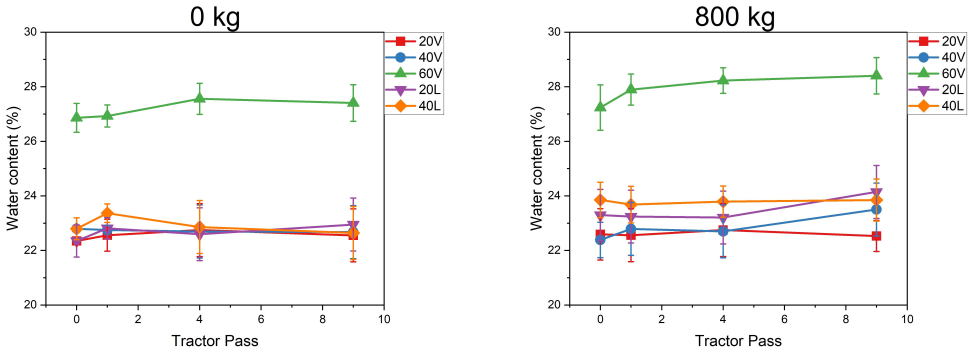

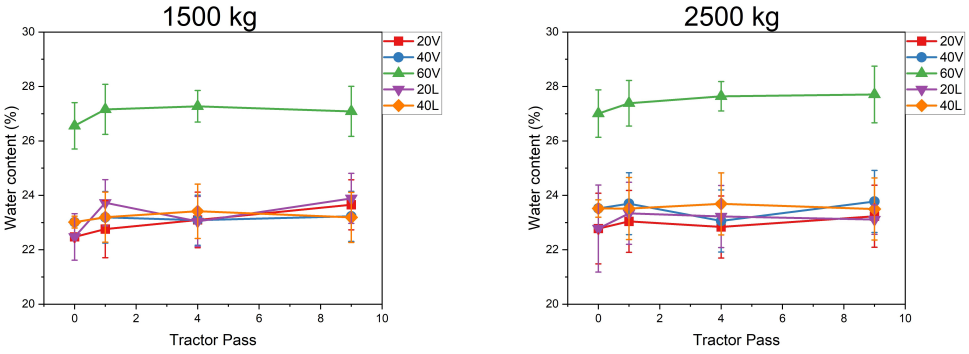

Figure 2.3.3 Soil moisture content in different traction conditions.

The soil bulk density data in different traction conditions and the number of passes are shown in Figure 2.3.4. The results indicate that the soil bulk density increases as the number of passes increases. However, there is no significant difference between different traction conditions of the bulk density, except for 2500 kg traction compared to the other three. Bulk density in vertical and lateral 20 cm positions increased with the number of passes and reached a similar value of 1.41 (±0.028) g/cm^3. As for the 40 cm depth, the bulk density in vertical and lateral directions reached the same range as 1.47 (±0.020) g/cm^3 after nine passes in 0 kg, 800 kg and 1500 kg conditions. However, the vertical 40 cm (1.50 ± 0.067 g/cm^3) shows a higher bulk density value than the lateral 40 cm (1.43 ± 0.060 g/cm^3). The soil bulk density in the vertical 60 cm condition increased with the number of passes in the four traction conditions. After nine passes in four traction conditions, the average bulk density at 60 cm depth is 1.53 ± 0.005 g/cm^3.

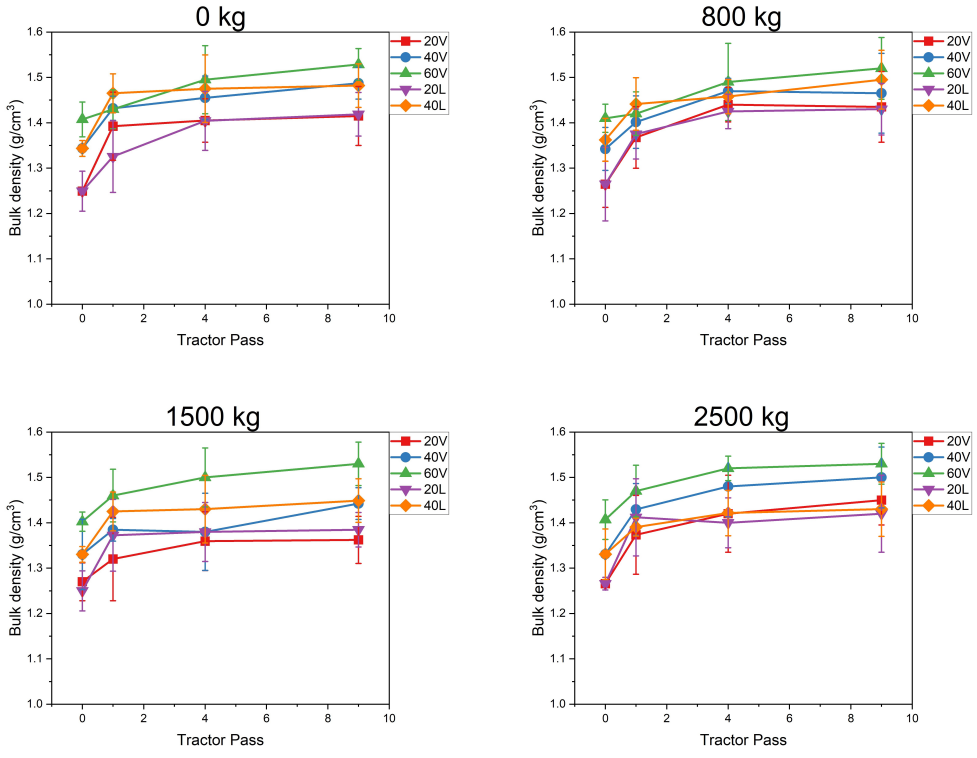

Figure 2.3.4 Soil bulk density in different traction conditions.

Soil Cone Index

The soil cone index data before the first pass and after one, four and nine passes are shown in Figure 2.3.5. The first figure is the average of 0–50 cm data (11 points in total), and the other three are the 0–10 cm data (three points in total in the centre of the rear tyre). All four traction conditions maintained a similar trend for the soil cone index before the first pass. However, one location below 40 cm had a lower soil cone index than the other three (here, we used the word "location" because the four areas were not compacted yet). As for the soil cone index after one, four and nine passes, the peak value increased with traction. It is worth mentioning that the compaction caused the subsidence of the soil surface, so the value begins below the 0 cm depth. However, the peak value of the soil cone index does not show a significant difference under different traction conditions located around 10 to 30 cm depth. The result shows that the main change in the soil cone index happened in the 0–40 cm area because the field's hardpan exists at 40–45 cm depth. Hardpans (plough pans) are formed by years of deep ploughing at the same depth, which stop the compaction at a deeper depth (Mohawesh et al., 2008).

Figure 2.3.5 Soil cone index with different numbers of passes in different traction conditions.

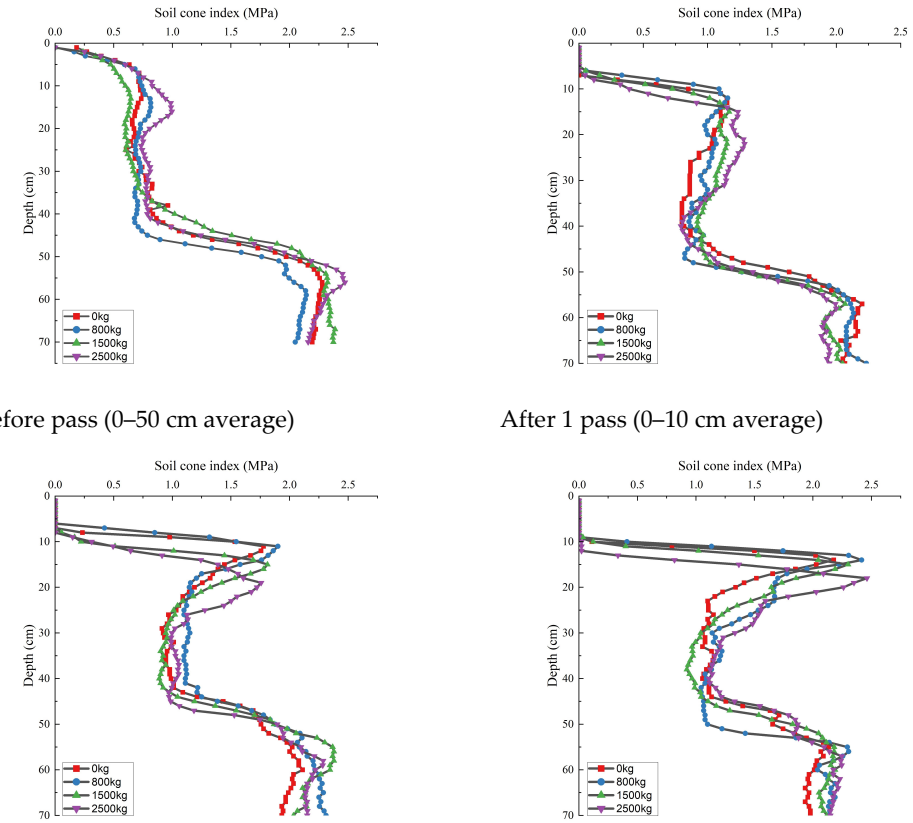

Before pass (0–50 cm average)

After 1 pass (0–10 cm average)

After 4 passes (0–10 cm average)

After 9 passes (0–10 cm average)

The soil cone index data of the different traction conditions with zero, one, four and nine passes are shown in Figure 2.3.6. In general, each figure shows that the soil cone index

increased after compaction in each traction condition. The peak soil cone index increased with the number of passes. However, the soil cone index with different traction conditions and the same number of passes did not show a significant difference. The main change in the soil cone index happened at a depth from 0 to 40, which is the upper part of the hardpan. The soil cone index before the first pass shows a slight difference within four fields. For example, the field with 2500 kg traction conditions shows a higher soil cone index between 10 and 20 cm depth than the other fields.

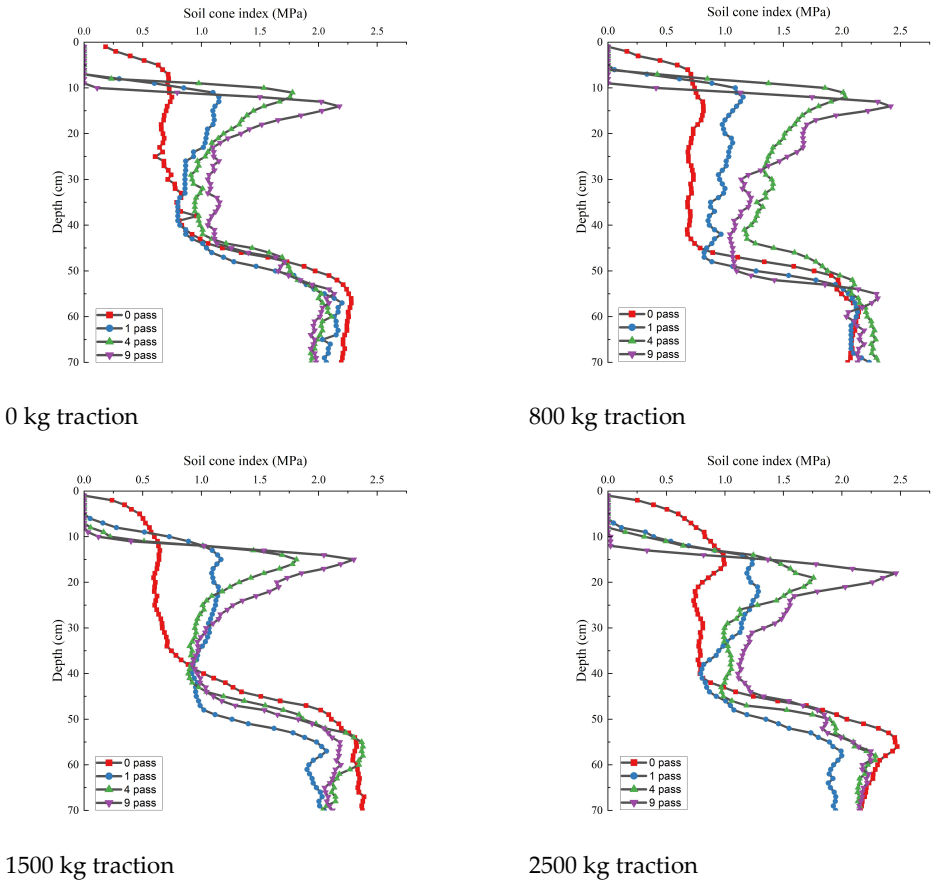

Figure 2.3.6 Soil cone index in different traction conditions with different numbers of passes.

Table 2.3.1 shows the soil cone index results focused on the nose zone area. Soil cone index results in different traction conditions and the number of passes were compared between each group. Lowercase letters (abc) indicate the comparison under different pass conditions within the same traction group (vertical). Capital letters indicate the comparison under different traction conditions within the same pass condition (horizontal).

Table 2.3.1 Cone index analysis of the nose zone.

Range of the nose zone (cm)

pass	0kg	800kg	1500kg	2500kg
1	17.07bB	20.17aA	17.07cB	16.23bB
4	19.93aA	19.2aA	18.1bA	19.1aA
9	20.33aAB	18.57aBC	21.17aA	17.5bC

Depth of the max cone index (cm)

pass	0kg	800kg	1500kg	2500kg
1	12.5bC	12.1bC	15.03aB	22.17aA
4	11.33bC	11.3bC	15.07aB	19.07bA
9	14.17aB	14.1aB	15.07aB	18.03bA

Max cone index (MPa)

pass	0kg	800kg	1500kg	2500kg
1	1.15cA	1.15cA	1.17cA	1.29cA
4	1.78bA	1.9bA	1.81bA	1.75bA
9	2.17aC	2.42aA	2.3aB	2.46aA

Average cone index (MPa)

pass	0kg	800kg	1500kg	2500kg
1	0.765cB	0.839cA	0.838bA	0.824cA
4	0.931bB	1.042bA	0.899bB	0.92bB
9	0.979aC	1.124aA	1.010bBC	1.075aAB

The range of the nose zone did not change significantly with increasing passes at 0 and 800 kg traction in most situations. However, the range increases with the number of passes when the traction is under 1500 and 2500 kg conditions. For different traction conditions and the same number of passes, the range of soil cone index did not differ significantly for most of the traction conditions between one and four passes. After nine passes, there is a significant difference in the range of soil cone index between traction conditions.

For the depth of max soil cone index, the depth of max soil cone index increases with the number of passes, increasing with 0 and 800 kg traction conditions. However, under 1500 kg traction conditions, it did not change significantly with one, four and nine passes. Moreover, under 2500 kg traction conditions, the depth of the max soil cone index reduced as the number of passes increased. For different traction conditions and the same number of passes, the depth of the max soil cone index increased with the traction increasing significantly.

For the max soil cone index, the value increased with the number of passes increasing in each traction condition. No significant difference in max cone index was found for the different traction conditions at one and four passes. After nine passes, a significant difference was found at different tractions. However, the 800 kg traction had a higher max cone index than

the 1500 kg traction condition.

For the average soil cone index from 0 to 40 cm, the average soil cone index increases significantly as the number of passes increases in all four traction conditions. The results after one and four passes show the soil cone index increasing significantly with the traction increase. However, the 800 kg traction condition had the highest average soil cone index value after nine passes rather than the highest traction condition, 2500 kg, as expected.

Profile Meter after the Compaction

The soil profiles for different traction forces are shown in Figure 2.3.7. The results show that the soil profile increases with the number of passes for all traction conditions. Although the soil profile shows a higher value after four and nine passes in higher traction conditions, there were no statistically significant differences in the soil profile value for each traction condition.

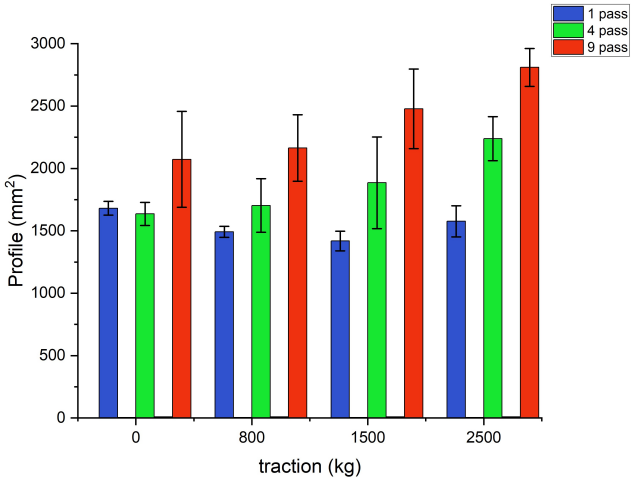

Slip Rate

In this section, the slip rates under different soil conditions and traction conditions were analysed. The specific results are listed below.

The slip rate (%) under repeated wheeling in different traction conditions is shown in Table 2.3.1 The results show that no slip rate exists in the first pass at 0 kg. The first pass in three traction conditions had the maximum slip rate compared to the conditions of two to nine passes. No significant difference in slip rate was found between two and nine passes in all four traction conditions.

Table 2.3.1 Slip rate (%) under repeated wheeling.

Pass	Traction (kg)			
	0	800	1500	2500
1	0.00	7.95	15.77	40.11
2	1.29	6.54	14.42	30.79
3	1.15	5.86	14.42	29.78
4	1.52	5.70	14.64	29.83
5	1.37	7.05	14.81	27.75
6	1.40	6.20	14.81	29.78
7	1.22	5.92	14.64	28.99
8	1.89	5.30	14.42	28.71
9	1.66	6.37	14.47	29.50

Rolling resistance data were collected after the number of passes, as shown in Figure 2.3.8. Trendlines were made using the method of single exponential decay. The results indicate that the first pass of the tractor has the highest rolling resistance. The rolling resistance gradually decreases to a stable area as the number of passes increases in the same traffic lane.

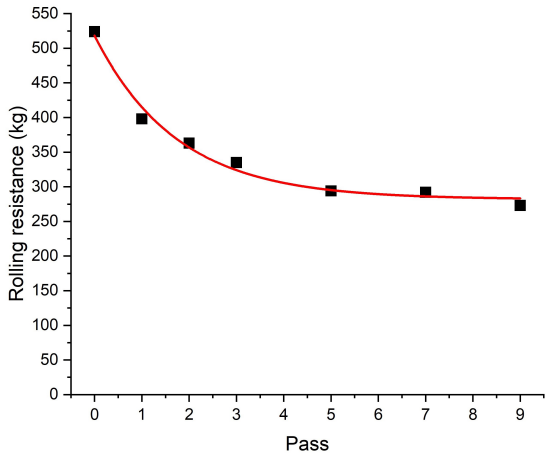

Figure 2.3.8 Rolling resistance collected after the number of passes.

Here is the slippage rate in different traffic and traction conditions. Three kinds of traffic conditions were chosen as the original field, which is an uncompacted field (zero passes), the trafficked field after nine compactions (nine passes) and the permanent traffic lane, which is located on the edge of the field used for transporting the machine during the farming operation. Trendlines were made using the method of single exponential decay. The results show that the slip rate increased with the traction in all three soil conditions. After nine passes, the permanent traffic lane has a lower slip rate than the zero-pass field in all traction conditions. The slip rate in the uncompacted field rises significantly with the increasing traction compared to the nine-pass field and the permanent traffic lane. Compared to Figures

2.3.9 and 2.3.10, the hard traffic lane has lower rolling resistance and slip rate, saving more energy and working efficiency than conventional agriculture.

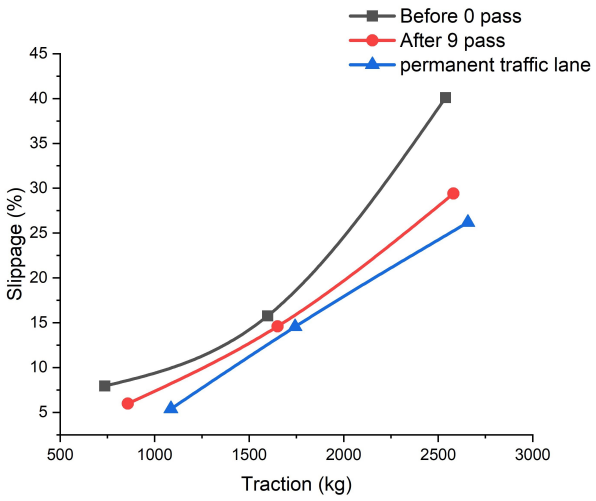

Figure 2.3.9 Slippage rate in different traffic conditions.

Fuel consumption

Table 2.3.2 shows the fuel consumption with different traction levels and the number of passes. The calculation of power used in Table 2.3.2 considers the net tractive effort, slip rate and energy loss in the transmission and hydraulic system. Fuel consumption is calculated by the power used. Fuel savings in each pass situation were calculated by comparing with fuel savings with zero passes in each traction condition.

Table 2.3.2 Fuel consumption with different traction levels and number of passes.

	Power used (kW)			Fuel consumption (kg/h)			Fuel savings (%)		
Pass	800	1500	2500	800	1500	2500	800	1500	2500
0	13.86	25.92	56.13	3.60	6.74	14.59	0.00	0.00	0.00
1	13.91	26.62	45.85	3.62	6.92	11.92	-0.37	-2.68	18.31
2	12.36	26.14	44.08	3.21	6.80	11.46	10.82	-0.86	21.48
3	12.93	22.91	43.81	3.36	5.96	11.39	6.73	11.63	21.95
4	11.61	23.56	41.42	3.02	6.13	10.77	16.22	9.11	26.21
5	13.16	23.21	44.30	3.42	6.04	11.52	5.01	10.45	21.09
6	13.39	22.85	42.68	3.48	5.94	11.10	3.39	11.86	23.96
7	12.48	22.39	43.81	3.25	5.82	11.39	9.93	13.61	21.96
8	13.23	24.19	43.73	3.44	6.29	11.37	4.53	6.68	22.09
9	11.72	22.30	44.23	3.05	5.80	11.50	15.40	13.98	21.20
Permanente lane	10.32	18.34	32.37	2.68	4.77	8.42	25.50	29.23	42.34

As the number of passes increases, the power loss due to rolling resistance and slip decreases, and the useful power available for traction increases. As the number of passes increases, the machine uses less power for all traction levels to produce the same work. On the uncompacted field (the field without pass) and compacted field (the field after 9 pass) all traction levels require more power than the permanent traffic lane.

From an environmental point of view, fuel savings are relative to reducing CO_2 emissions into

the atmosphere. As the number of passes increases, the machine produces less CO_2 for all traction levels for the same work. All traction levels produce more CO_2 on the uncompacted field (the field without pass) and compacted field (the field after 9 pass) than the permanent traffic lane.

2.4 Discussion

Effect of Traction

The stress in the soil was calculated by vertical load, horizontal load and radial normal stress at each collection point. Horizontal stress (shear stress) on the soil surface can be calculated from the given traction (Keller et al., 2007b) as one part of the stress which creates the soil compaction. Our results show that the stress underneath the soil, soil bulk density, soil cone index and soil disturbance increased with the increasing traction in our field experiment. Higher traction had higher soil stress at different soil depths and locations were found in both collected and simulation results. A similar result was also found in previous research (ten Damme et al., 2021b). Higher pressure underneath the soil causes more compaction and increases the soil bulk density and soil cone index in each depth (Keller et al., 2014, 2007b; Keller and Arvidsson, 2016).

Many researchers have found that higher traction has more compaction (Battiato and Diserens, 2017; Bulgakov et al., 2020; ten Damme et al., 2021a, 2021b). Moreover, the static pressure distribution of the compaction procedures was studied. However, the shear stress distribution caused by the traction was not considered in soil compaction research but probably contributes significantly to soil structure deterioration (Schjønning et al., 2020). Furthermore, many factors can influence the distribution of shear force in the soil under different soil conditions with different parameters. For example, tractor tyre size, pressure, the weight of the tractor, four or rear-wheel drive of the tractor, the distance between the front and rear wheels of the tractor and how the PTO is hooked up to the working part all affect the shear force caused by the traction (Battiato, 2014). The method of increasing the traction resistance without adding weight was implemented in the field experiment. The results confirm that higher traction increases the soil compaction (Battiato, 2014; Schreiber and Kutzbach, 2008; ten Damme et al., 2021b; Zoz and Grisso, 2003a) by using the brake power from the rear tractor rather than adding the machine's weight during the test. However, the method of how the tractor is hooked up to the other, the equipment used to connect the two tractors and the stability of the tractor's operation all impact the experimental results, so further research is needed (Battiato, 2014).

Effect of Repeated Wheeling

Significant differences were found in soil bulk density, soil cone index and soil profile after repeated wheeling compared to the uncompacted field. The main change in the soil bulk density and soil profile occurs in the first pass compared to the next eight passes. The soil cone index changes mainly happened from 0 to 40 cm, with the number of passes increasing. Additionally, the sinking of the topsoil was observed during repeated wheeling. The trend of the changing values in soil bulk density, soil cone index and soil profile is similar in different traction conditions. Compared to the changing results, soil moisture and stress showed no significant differences in repeated wheeling.

Other studies have also observed that the first pass forms a harder soil surface in the form of wheel ruts (Way et al., 1995). It also causes maximum near-surface deformation (Pytka et al., 2006). As for the topsoil's sinking, the soil layer's thickness decreased significantly from the first to the second passes, while no differences were found in the subsequent ten passes (Lamandé et al., 2015). Our experiments were carried out in a dry condition. This damage to the top layer of soil due to the first and second compaction further increases the contact area between the tyre and soil, reducing the pressure per unit area caused by the tyre on the soil. Specifically, the increased contact area minimises the soil pressure per unit area. However, as the number of passes increases, the soil pressure increases due to a tighter soil structure. This phenomenon has also been observed in previous studies (Horn et al., 1998; ten Damme et al., 2021b).

Effect of Slippage

The experimental results show that the slipping rate increases with the traction increasing in different soil conditions. The tractor had a lower slip rate in compacted soil where the nine passes had been completed. Furthermore, the permanent traffic lane has an even lower slip rate than the compacted field. The experimental results show that the permanent traffic lane has the lowest slip rate and highest working efficiency compared to the uncompacted and compacted fields. The limited slip rate and high working efficiency save more energy and produce less CO_2, guaranteeing economic and ecological benefits. Similar results were obtained in the previous study (DAVIES et al., 1973; Tijink, 1994). Higher slip causes higher soil compaction (BASHFORD, 1995; DAVIES et al., 1973; Raghavan et al., 1977), which has a significant impact on soil erosion (Battiato et al., 2015) and causes great damage to soil fertility (Nadykto et al., 2015).

Fuel economy on the permanent traffic lane may have several practical implications. First, lower fuel consumption reduces operating expenses. Economic savings can be easily obtained by multiplying the litres of fuel per hour by the price per litre purchased. According

to our tests, a higher traction load has higher energy savings and efficiency, which was also obtained by the previous study (Battiato and Diserens, 2013). Therefore, farms can use fuels in different ways. One of these is the possibility of higher quality operations with the same power used, such as better preparation of seedbeds or other tillage operations. Another example is in performing split fertilisation to improve the uptake of inputs by plants. Other possibilities include using the saved fuel for other operations such as irrigation, or the option of using the power saved by the machine to increase work capacity and time.

One strategy to reduce power loss due to skidding and rolling is to ensure traffic in the permanent traffic lane. This is one of the advantages of using a CTF system to organise the viability of field machinery (Chamen, 2015; Kingwell and Fuchsbichler, 2011; Latsch and Anken, 2019). For this reason, in the CTF system, the permanent traffic lane reduces the slippage within limits compared to the conventional tillage field for the same load and working resistance (Antille et al., 2016). Furthermore, the field experiment made it possible to evaluate and quantify the machine's slip rate and rolling effects in terms of power loss and associated fuel consumption under various transport conditions. Therefore, farmers should be advised in agricultural operations to consider controlled traffic farming (CTF) systems to improve efficiency and reduce energy consumption. Despite the difficulties of changing from conventional agriculture to CTF (Bluett et al., 2019; Chamen, 2015), planned driving trajectories for tractors rather than random movements can increase efficiency and reduce operating costs.

2.5 Conclusions

Tractor performance was measured under different traction resistance conditions in this field experiment. The study quantified the soil stress, soil bulk density, soil moisture, soil cone index, soil surface disturbance, rolling resistance and slip rate under different numbers of passes and soil and traction conditions. The actual power used under different traction conditions was collected in uncompacted soil, compacted soil and the permanent traffic lane. Fuel consumption and savings were calculated between uncompacted soil, compacted soil and the permanent traffic lane.

The results show that soil stress increases in each location as traction and the number of passes increase. Soil's physical properties increase, such as the soil bulk density, soil moisture, soil cone index and soil surface disturbance, with the increasing traction and number of passes. However, no significant difference was found between different traction conditions for the different number of passes. The slip rate increases with traction in each soil condition as uncompacted soil, compacted soil and the permanent traffic lane. The results show that the

permanent traffic lane has a lower slip rate under different traction conditions than the uncompacted and compacted soil.

Furthermore, the permanent traffic lane has less energy consumption with the same traction resistance. The permanent traffic lane saved 25.50%, 29.23% and 42.34% fuel compared to the uncompacted field in 7.85, 14.71 and 24.52 kN traction conditions, respectively. Our results show that the traffic lane not only could reduce the negative effect of the soil compaction caused by the random traffic, but also could increase the working efficiency and save energy. Moreover, the dynamic factors such as traction and rolling resistance should be considered in soil compaction research rather than static weight only. In practice, the controlled traffic farming (CTF) system or driving the tractor more frequently on the permanent traffic lane should be considered to improve working efficiency and reduce energy consumption.

3. Headland and Field Edge Performance Assessment

Abstract

Headland and field edges have higher traffic frequency compared to the field centre, which causes more compaction. Most repeat compaction is located at the field entrance area and headland during the machinery turning and materials transporting within fertilisation, herbicide, and harvest, which could cause soil structure destruction and yield reduction. In this study, the differences between headland, field edges and field centre were studied using yield maps and the vegetation indices (VIs) calculated by the Google earth engine (GEE). First, thirteen yield maps from years 2019 to 2022 were used to measure the yield difference between headland, field edges and field centre. After that, one hundred and eleven fields from north Italy were used to compare the vegetation indices differences (VIs) between headland, field edges and field centre area. Then, field size, sand and clay content were calculated and estimated from GEE. The yield map result showed that headland and field edges were 12.20% and 2.49% lower than the field centre. The VIs result showed that headland and field edges were 4.27% and 2.70% lower in NDVI, 4.17% and 2.67% lower in GNDVI, 5.87% and 3.59% lower in NDRE, respectively. The yield losses in headland and field edges increased with the clay content increasing and sand content decreasing.

3.1 Introduction

Headland and field edges are the areas close to the boundary within arable field margins where the farm equipment turns and moves during field operation (Boatman, 1994; Sparkes et al., 1998a; Wilcox et al., 2000). Many turns were made in headland areas during each field operation of planting, fertilising, and harvesting (Bochtis and Vougioukas, 2008; J. Jin and L. Tang, 2010). As a result, the field edges have a higher traffic frequency than the field centre (Duttmann et al., 2013; Rodrigues et al., 2015; Scott et al., 2005; Spekken and de Bruin, 2013; Sunoj et al., 2021). Also, most of the repeat compaction is localised at the headlands and field edges (Duttmann et al., 2014, 2013; Godwin and Miller, 2003). The repeat wheelings in the headland and field edges caused more soil compaction both in the topsoil and subsoil (Duttmann et al., 2014).

Soil compaction in the headland and field edges leads to physical and mechanical disturbance of soil structure and reduced root growth (Gaženja, 2019; Szatanik-Kloc et al., 2019). As a result, yields were often lower in the headland and field edges compared to the field centre (Boatman and Sotherton, 1988; Cook and Ingle, 1997; De Snoo, 1994; Kuemmel, 2003; Sparkes et al., 1998b; Speller et al., 1992; Sunoj et al., 2021; Wilcox et al., 2000). For

example, a five-year field experiment was conducted with sugar beet, wheat and barley. The headlands yield was 26% and 7% less than the field centre in sugar beet and cereals(Sparkes et al., 1998a). Similarly, a three-year study of barley and rye showed that soil compaction on the headland was 43.32–44.51% higher than the field interior during germination, as the soil compaction increased to 51.76-53.28% before the harvest. As a result, it reduced the yield of barley and rye by 36.16% and 35.48% for each crop (Barać et al., 2015). In addition, some studies mentioned the impact of headlands on crop performance (Kuemmel, 2003; Ward et al., 2020; Wilcox et al., 2000) and the negative yield effect of traffic-induced soil compaction (Arvidsson and Håkansson, 2014; Arvidsson and Keller, 2007). Although most of the research said that the headland and field edges have a lower yield than the field centre, some research didn't find a significant difference in the yield performance of the headland and field edges. For example, a 2-year field experiment on no-till Maize and soybean fields showed no significant difference in yield even though the soil bulk density increased due to compaction (Sivarajan et al., 2018). Similarly, another study found that the wheat yield in the centre part was 44% to 69% higher compared to the headland. However, the volume of the seed and 1,000 kernel weight in the field centre were lower than the field edges(Gaženja, 2019).

The previous research found spatial variability in the field between the headland, field edges, and field centre. Many studies discussed the spatial variability in crop performance (Ward et al., 2020; Wilcox et al., 2000). Yield sampling, yield monitoring and hand-collecting were used to study the yield spatial variability (Barać et al., 2015; Cook and Ingle, 1997; Gaženja, 2019; Sivarajan et al., 2018; Sparkes et al., 1998a). For example, the yield data were collected to determine the effects of proximity to the field edge on Maize and soybean yields by using a yield monitor equipped combine harvester (Barbour et al., 2007). Similarly, the field and farm-scale yield monitor data were used to estimate the yield difference between headland and non-headland from 4,145 fields across 63 farms in the US. The result showed that yields per hectare were 14% and 16% lower in the headland areas for grain and silage (Sunoj et al., 2021). While other researchers also concluded that the yield in the headland area has a 15.6% reduction compared to the field centre area(Cook and Ingle, 1997). However, yield increase was also recorded in headland areas (Boatman and Sotherton, 1988; Cook and Ingle, 1997).

Remote sensing and satellite data were used to study within-field variability and crop yield monitoring. Remote sensing technology avoids the laborious and the time limit compared to the previous method, such as surveys of the field or monitoring in the combined harvester, which were used in within-field spatial variabilities studies in the past. Previous studies focused on the within-field spatial variability based on remote sensing data (Campos

et al., 2019; Kayad et al., 2019, 2016). Besides, other studies have shown the linear connection between the vegetation indices and the crop yield (Al-Gaadi et al., 2016; Báez-González et al., 2002; Gao et al., 2018; Maestrini and Basso, 2018; Toscano et al., 2019). In general, there are two main strategies in yield monitoring studies. First is the yield prediction and estimation using biomass and the harvest index (Gao et al., 2018; Tucker et al., 1981; Yao et al., 2015). The second is crop growth monitor and yield prediction based on plant physiological models, remote sensing data, and meteorological data (Asrar et al., 1985; Campos et al., 2019; Patel et al., 2001; Yao et al., 2015). Vegetation indices have been developed to describe crop growth conditions and estimated yield, such as the Normalised Difference Vegetation Index (NDVI), Soil Adjusted Vegetation Index (SAVI), Green Normalized Difference Vegetation Index (GNDVI), and Normalised Difference red edge (NDRE) (Gitelson et al., 1996; Kayad et al., 2019; Panda et al., 2010; Tucker, 1979; WANG et al., 2007; Xue and Su, 2017).

Many researchers have already focused on using satellite data to estimate crop yield and got accurate results (Báez-González et al., 2002; Bu et al., 2017; Duttmann et al., 2013; Godwin and Miller, 2003; Sibley et al., 2014). The publicly accessible Sentinel-2, jointly initiated by the European Commission (EC) and the European Space Agency (ESA), represents an opportunity to implement high-resolution yield prediction models in high-resolution satellites (Drusch et al., 2012). Sentinel-2 systematically provides global acquisition of high-resolution (10 to 60 meters) multispectral images with high revisit frequency (5 days at the equator) and can be easily obtained and analysed through platforms such as Google Earth Engine (GEE). Sentinel-2 data has already been used to analyse the spatial variability (Cohrs et al., 2020; Drusch et al., 2012; Gao et al., 2018; Kayad et al., 2021, 2019; Toscano et al., 2019). So our idea was to use yield map and Sentinel-2 data to estimate the yield and VIs differences between headland, field edges and field centre rather than harvester yield only or hand-collecting results in the previous research.

The objective of this paper was to investigate the differences between headland, field edges and field centre using yield maps collected during harvest and the vegetation indices calculated by the GEE. The specific objectives of this study were to: I) Quantify the yield difference between the headland, field edges, and centre area of the field; II) Quantify the VIs difference between the headland, field edges, and field centre; III) Determine the impact of field size on vegetation indices difference between headland, field edges and field centre; IV) Determine the impact of clay and sand content on vegetation indices difference between headland, field edges and field centre.

3.2 Materials and Methods

All selected fields are located in North Italy between latitudes 44.586 to 46.129 and longitudes 7.595 to 13.149 (Figure 3.2.1). This area is the Mediterranean climatic zone with an average rainfall of 994 mm. The yield and vegetation indices (VIs) differences were studied in headland, field edges and field centre. First, thirteen yield maps were used to estimate the yield and VIs difference between the three areas as listed the detailed information in Table 3.2.1. Second, one hundred and eleven fields were selected to calculate the VIs difference between headland, field edges and field centre. And the last, the field size and the clay content were used to study the value differences between three areas in different field sizes and clay content conditions.

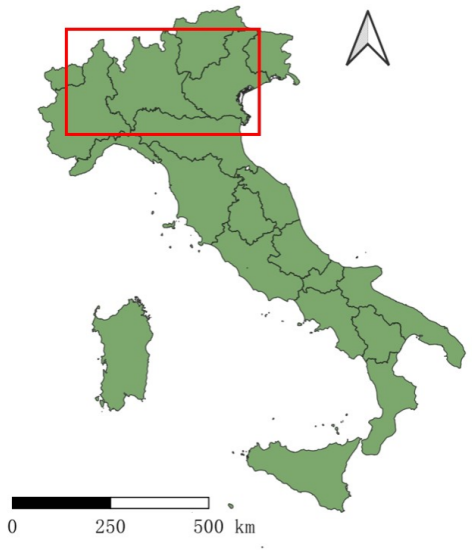

Figure 3.2.1 Study fields in the red rectangle area which located in Veneto, Lombardy, and Emilia-Romagna, North Italy

Yield maps for yield and VIs study

In total, thirteen yield maps were used in the study recorded from the CLAAS combine harvester (Lexion 8000) or forage harvester (Jaguar 900). A detailed description of years and crops was listed in Table 3.2.1 The yield monitoring system mounted on the combine harvester was used to record the yield, which could collect thousands of yield points each hectare. Outliers points were removed by removing points in ±3 standard deviations. Filtering was carried out to remove spatial outliers since the delay in data recording was already considered in the yield monitor calibration performed by the producer. According to this latter point, between 20% and 30% of points were removed, comparable with previously published studies (Vega et al., 2019). The yield map consisting of sparse points was interpolated to a raster using the kriging (“Kriging method in ArcGIS pro,” n.d.) method. Kriging, which used the ordinary method and the spherical semi-variogram model, was performed through ArcGIS

pro (version 2.7.0). Then the rasters were imported into the GEE. Yields performance and VIs difference were analysed in headland, field edges and field centre of each field. The specific methodology of the study is listed below.

Field selection for VIs study

Field were selected based on the following criteria. Maize is one of the most important crops in North Italy, with an average yield ranging between 8 and 10.6 t/ha over the last ten years (EUROSTAT 2019, 2019). The One soil ("A website for precision farming service Https://onesoil.ai/en/ (accessed 17.1.23)," n.d.) website was used to select fields which planted Maize for three years from 2016 to 2018 during the field selection process. The 2018 crop was then confirmed using EUCROPMAP 2018 (d'Andrimont, Raphaël; Verhegghen, Astrid; Lemoine, Guido; Kempeneers, Pieter; Meroni, Michele; van der Velde, Marijn European Commission, 2021; d'Andrimont et al., 2021). One soil website identifies the crops grown in different fields yearly. EUCROPMAP 2018 is a crop-type map based on Sentinel-1 and LUCAS Copernicus in-situ observations released in 2018. Each field was planted with the same crops in the three positions of the headland, field edges and field centre and was confirmed.

Fields were selected which have the regular rectangular shape. The regular rectangular shape field has more disciplined traffic conditions than the irregular one. Moreover, the regular rectangular shape maintains the study consistency among the selected fields.

Fields were selected while avoiding neighbour obstacles or influencing objects. The obstacles and objects around the field could affect crop performance in field boundaries. For example, the fields with neighbour trees, rivers, or irrigation canals were removed from the study. The trees on the edge of the fields may influence the satellite data collection by covering the field with the shade of trees. Additionally, rivers or irrigation canals around the field could cause yield spatial variability in cultivated crops due to the available water variability. The clean boundaries of each field ensure the comparability of selected fields.

Fields with different sizes ranged from 2.45 to 38.82 ha, with an average of 13.48 ha. In total, one hundred and eleven fields were selected in the study.

Field classification

Each field was divided into three zones using recent and archived Worldview satellite images in GEE. The field was defined in three parts: headland (red), field edges (blue) and field centre (green), as shown in Figure 3.2.2.

Headland: Two opposite edges where the machinery turns and starts a new track or boundary manoeuvres during the farming operation (red).

Field edges: Two opposite edges that the machinery precede the linear movement during the farming operation (blue).

Field Centre: Centre area of the field without the headland and field edge areas (green).

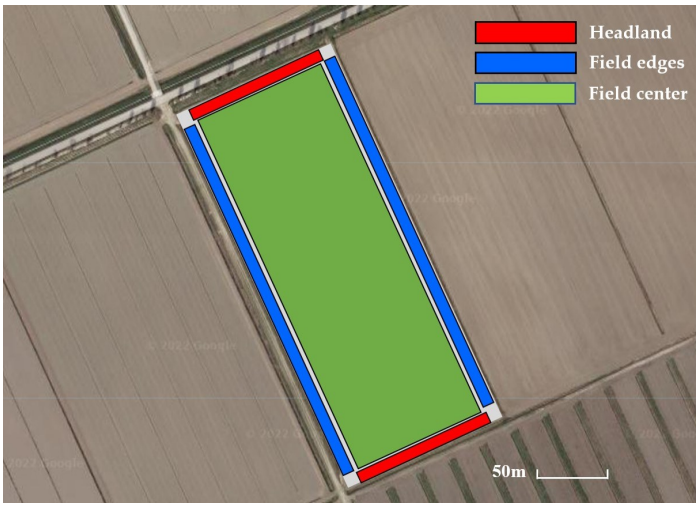

Figure 3.2.2. Example of a selected field

Figure 3.2.3 illustrates one sample field with three corresponding zones. Headland and field edges were presented as points of the Sentinel-2 pixels (10m×10m) (headland: red points; field edges: green points). The points were selected from pixels located precisely on the edge of the polygon, as shown in Figure 3.2.3. For example, some pixels are half inside the polygon, or others have a gap between the filed edges and themselves. The field centre area was presented by a 30m narrower polygon of the field edges, as the green area shown in Figure 3.2.3. The field centre value was automatically calculated by GEE, which used the mean of all pixels inside the field centre polygon.

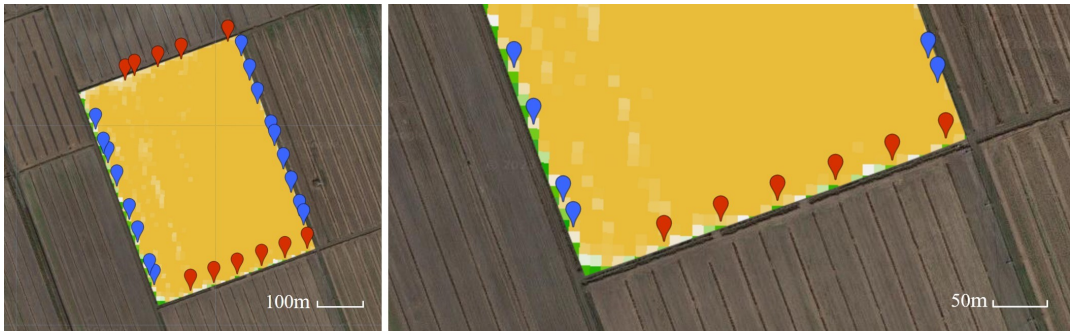

Figure 2.2.3 Headland points (red) and field edges points (blue) in the field, which background is a NDVI layer for selecting the points of headland and field edges in the field

Yield and VIs data collect

The yield in headland, field edges and field centre of each field were collected using the yield maps uploading.

Three VIs results from each area and each field were collected through the highest three dates each year from 2016 to 2018. Three indices that we used in this study were the normalised difference vegetation index (NDVI), green normalised difference vegetation index

(GNDVI) and normalised difference red-edge (NDRE), in equations 1 to 3. Three equations were applied through GEE on filtered Sentinel-2 satellite images, considering the time from 2016 to 2018 and corresponding zones. The applied filters on Sentinel-2 images include calendar images ranging from May to August. The period corresponds to the summer crop mid-season, which was reported as the most correlated Maize yield with vegetation indices from the study area (Kayad et al., 2021, 2019).

$$NDVI = \frac{NIR - R}{NIR + R} \quad (1)$$

$$GNDVI = \frac{NIR - G}{NIR + G} \quad (2)$$

$$NDRE = \frac{NIR - RE}{NIR + RE} \quad (3)$$

Where: NIR is the reflectance at the near-infrared band (band 8, 785-793nm), R is the reflectance at the red band (band 4, 650-850nm), G is the reflectance at the green band (band 3, 543-578nm), and RE is the reflectance at the red-edge band (band 5, 698-713nm) of the Sentinel-2 satellite images.

The temporal resolution was also influenced by the cloud cover (Bukowiecki et al., 2021). Therefore, deliberate attention was paid to the effect of cloud cover on data acquisition from VIs in the study (Bukowiecki et al., 2021). A cloud percentage filter of 10% maximum was applied to consider the clear satellite images for further analysis. In addition, a pixel-level cloud filter was applied, taking advantage of the Scene Classification Layer (SCL) provided by Copernicus. The applied filters led to three satellite images from each season with the maxim value within each growing season. Each VI was calculated from each field, corresponding zones, and all available images. Field size, clay content (Hengl, 2018) and sand content (Hengl, 2018) of each field were calculated through the GEE using the OpenLandMap which was calculated by the average of whole field area.

Statistics

Collected data were used to compare the headland and the field edges with the field centre. The field centre acted as the control for each field to evaluate the performance of headland and field edges. Each field yield map was input into the GEE, which used the same methodology as the VIs analysis. As for the VIs, the max three values in headland, field edges and field centre of each field and each year were used to analyse during the study. And then, value differences between headland(H), field edges(L) and field centre(C) were compared by using H/C, L/C, 1-H/C and 1-L/C. One-way ANOVA and t-test (5% significance level) were performed to assess the difference between the three zones from the study fields under the condition that each data group was verified as normally distributed. The Pearson test (0.05 significance level) was used to quantify the linear association with field size, clay content and

sand content in headland, field edges and field centre.

3.3 Results

Comparision between yield map and VIs results

In total, thirteen fields were used in the study collected from 2019 to 2022. There were seven silage Maize (Zea mays) fields, four triticale (Triticosecale) fields and two Maize (Zea mays) fields, separately. Field size ranged from 2.66 to 26.62 ha. The VIs (NDVI) map (left) and yield map(right) are shown in Figure 3.2.4 as an example. The red points represented the headland, and the blue points represented the field edges selected based on the methodology located at the field edges precisely. It is worth noting that only two points in the northern headland were accurately located on the edge of the field. The black polygon inside the field (shown in the right figure was the field centre. The grayscale image is the yield map imported into the GEE after the kriging.

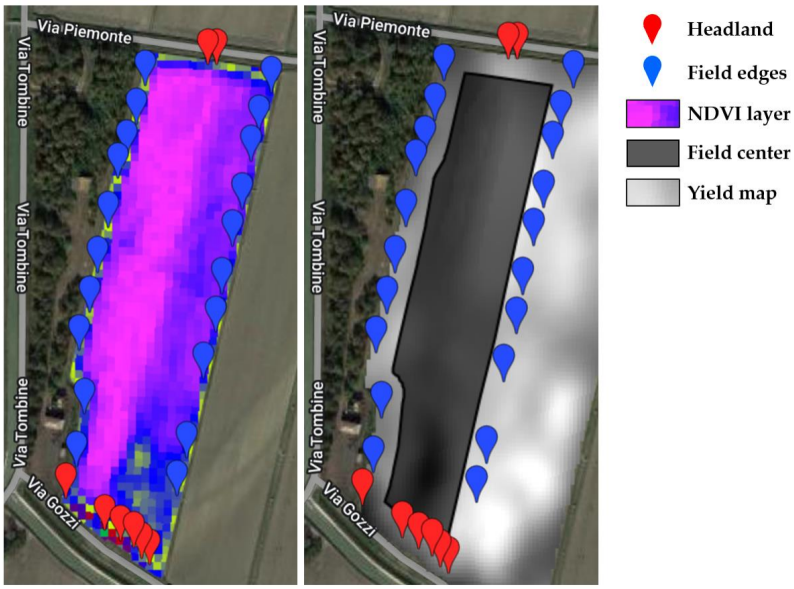

Figure 3.2.3 NDVI (left) map and yield map (right) image of one selected field

The yield map results of the selected fields are listed in Table 3.2.1. The specific year of the field, crop type, field size, the yield in each location and the difference between headland (H) with field centre (C) and field edges (L) with field centre (C) were listed. The result showed that the average yield was 12.20% and 2.49% lower in headland and field edges than in the field centre. Among all the fields, eleven fields showed a lower yield in headland and field edges than the field centre. Field numbers 5 and 9 had the highest yield in field edges rather than field centre. Among all the fields, nine fields showed significant differences among headland, field edges and field centre to each other. However, field numbers 5, 6 and 9 showed no significant difference between headland and field centre or field edges and field centre at 0.05 level.

Table 3.2.1 Yield difference between headland, field edges and field centre

Number	Year	Crop	Size (ha)	Yield (t/ha)			1-H/C	1-L/C
				H	L	C		
1	2019	Silage Maize	26.62	25.71c	34.14b	34.82a	26.17%	1.96%
2	2019	Silage Maize	25.41	26.60c	28.21b	28.63a	7.08%	1.44%
3	2019	Silage Maize	4.26	30.96c	31.45b	32.20a	3.84%	2.33%
4	2020	Silage Maize	9.38	19.51c	24.50b	25.47a	23.39%	1.85%
5	2021	Triticale	3.86	19.67b	20.75a	20.53a	4.22%	-1.08%
6	2021	Triticale	6.82	20.97a	20.12b	21.15a	0.84%	4.87%
7	2021	Triticale	2.66	20.91c	21.56b	21.78a	3.99%	0.98%
8	2021	Triticale	10.41	19.50c	22.97b	23.29a	16.30%	1.40%
9	2021	Silage Maize	26.62	42.31b	45.37a	45.24a	6.46%	-0.29%
10	2021	Silage Maize	13.85	38.10c	43.81b	47.39a	19.59%	7.55%
11	2021	Silage Maize	10.67	34.16c	41.86b	44.80a	23.75%	6.55%
12	2022	Maize	10.37	15.37c	16.51b	17.06a	9.89%	3.24%
13	2022	Maize	7.14	15.12c	17.12b	17.40a	13.10%	1.61%
Average							**12.20%**	**2.49%**

Lower letters (abc) indicate significant differences between headland(H), field edges(L) and field centre(C) of each field at 0.05 level.

The VIs results comparison within each group is shown in Table 3.3.1. The NDVI, GNDVI and NDRE results showed that headland and field edges had a lower value than the field centre in most fields. The value difference between headland and field centre (1-H/C) is higher than the difference between headland and field centre (1-L/C) in most fields. The average result among all the fields showed that headland and field edges were 12.97% and 5.89% lower than the field centre in NDVI, 10.55% and 5.11% in GNDVI, and 16.27% and 7.03% lower in NDRE.

Table 3.3.1 VIs results comparison within each field

Number	NDVI		GNDVI		NDRE	
	1-H/C	1-L/C	1-H/C	1-L/C	1-H/C	1-L/C
1	16.57%	2.30%	12.61%	2.15%	19.90%	4.39%
2	0.20%	2.14%	1.76%	3.74%	1.68%	2.86%
3	1.93%	2.07%	3.58%	1.82%	4.15%	2.63%
4	4.99%	1.19%	3.77%	1.32%	5.78%	1.99%
5	4.99%	2.20%	3.77%	1.96%	5.78%	2.86%
6	9.10%	3.80%	7.35%	3.65%	10.72%	4.95%
7	5.41%	0.62%	5.98%	0.84%	9.86%	1.71%
8	10.06%	0.34%	10.20%	0.23%	10.49%	-0.04%
9	11.90%	1.61%	9.97%	1.77%	14.80%	3.40%
10	7.60%	2.52%	3.69%	2.31%	13.02%	2.29%
11	11.68%	5.62%	10.66%	4.80%	15.92%	7.57%
12	25.01%	3.48%	24.69%	3.56%	31.29%	5.30%
13	30.91%	-1.40%	27.84%	-0.26%	36.05%	0.44%
Average	**10.80%**	**2.04%**	**9.68%**	**2.15%**	**13.80%**	**3.10%**

In both the VIs and the field results, smaller values were found at the headland and field

edges compared to field centre both in yield and VIs result. The VIs result showed the same trend and value differences as the yield data. However, the NDVI and GNDVI slightly underestimated the difference in values, and the NDRE slightly overestimated the difference, respectively.

Comparision of VIs between headland, field edges and field centre

The VIs in the headland, field edges and field centre are shown in Table 3.3.2 The result showed that headland has the lowest VIs and the field edges have lower VIs than the field centre in NDVI, GNDVI and NDRE. The mean value of NDVI and GNDVI showed a significant difference between the field centre with headland and field edges at 0.05 level. However, there was no significant difference between headland and field edges. As for the result of NDRE, the three positions all show significant differences compared with each other at 0.05 level.

Table 3.3.2 VIs value and differences between headland, field edges and field centre

Type	Headland(H)	Field edges(L)	Field center(c)	1-H/C	1-L/C
NDVI	0.673b	0.684b	0.703a	4.27%	2.70%
GNDVI	0.574b	0.583b	0.599a	4.17%	2.67%
NDRE	0.577c	0.591b	0.613a	5.87%	3.59%

Lower letters (abc) indicate significant differences between headland(H), field edges(L) and field centre(C) to each area in 0.05 level.

The comparison between the field centre with headland and field edges in NDVI, NDRE and GNDVI are shown in Figure 3.3.1. The red point represents the value of the headland and field centre, and the blue point represents the value of the field edges and field centre. Among all the 111 fields, 96/111(86.5%) of the headland and 93/111(83.8%) of field edges were lower than the field centre in NDVI. And 96/111(86.5%) of the headland and 94/111(84.7%) of field edges were lower than the field centre in GNDVI. As for the NDRE, 103/111(92.8%) and 97/111(87.4%) headland and field edges were lower than the field centre.

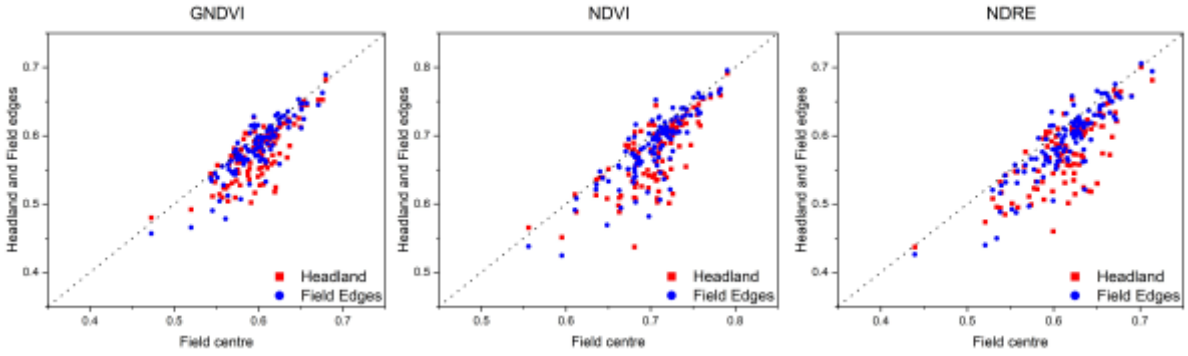

Figure 3.3.1 Comparison between headland, field edges and field centre in NDVI, NDRE and GNDVI

Determine the impact of field size on vegetation indices difference between three areas

Figure 3.3.2 shows the correlation between field size and VIs difference (%) of headland and field edges to field centre (H/C and L/C). The result showed that the H/C and L/C increased with the field size. The red point represents the value of the headland/ field centre. The blue point represents the field edges/ field centre. The red and blue lines are the trend lines, respectively.

The Headland/field centre trend line (red line) showed a steeper slope in all three VIs than the field edges/field centre (blue line). Although the trend could be found in figure 3.3.2 about the value differences between headland, field edges and field centre increased with field size. No significant correlations were found between headland, field edges and field centre in NDVI, GNDVI and NDRE. The p-value was higher than 0.05 and lower than 0.169 in the six comparisons of H/C and L/C in NDVI, GNDVI and NDRE

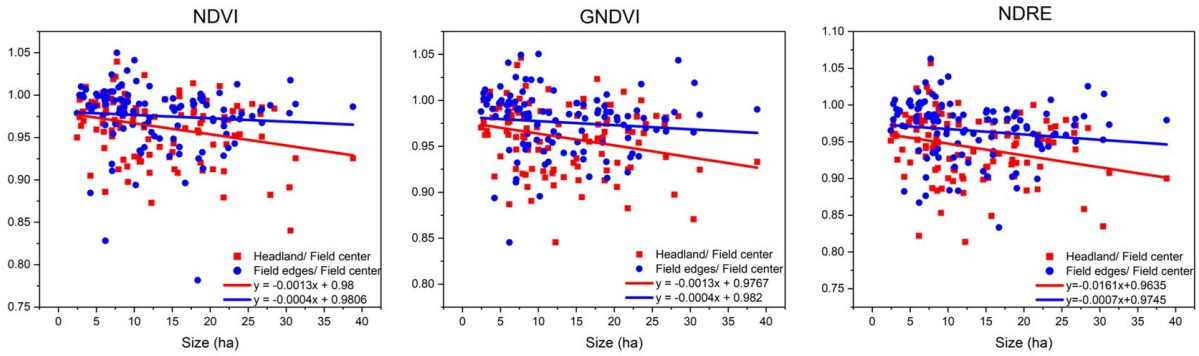

Figure 3.3.2. Comparison between headland, field edges and field centre in field size.

Determine the impact of soil texture on vegetation indices difference between three areas

Figure 3.3.3 shows the correlation between clay content and VIs difference (%) of headland (red point, H/C) and field edges (blue point, L/C) to field centre. The red points represents the value of the headland/ field centre. The blue point represents the field edges/ field centre. The red and blue lines are the trend lines, respectively. The field's clay content range was from 20.63% to 43.70%. The result showed that the value differences between headland, field edges with field centre increased as the clay content. And also, the value differences between headland to field centre and field edges were narrowed as clay content increased.

Significant correlations were found between headland, field edges and field centre in NDVI, GNDVI and NDRE. Except for the H/C in GNDVI and NDRE, which was 0.069 and 0.086, respectively, showed no significant correlations with the clay content of the field. The p-value was lower than 0.05 in most of the comparisons of H/C and L/C in NDVI, GNDVI and NDRE.

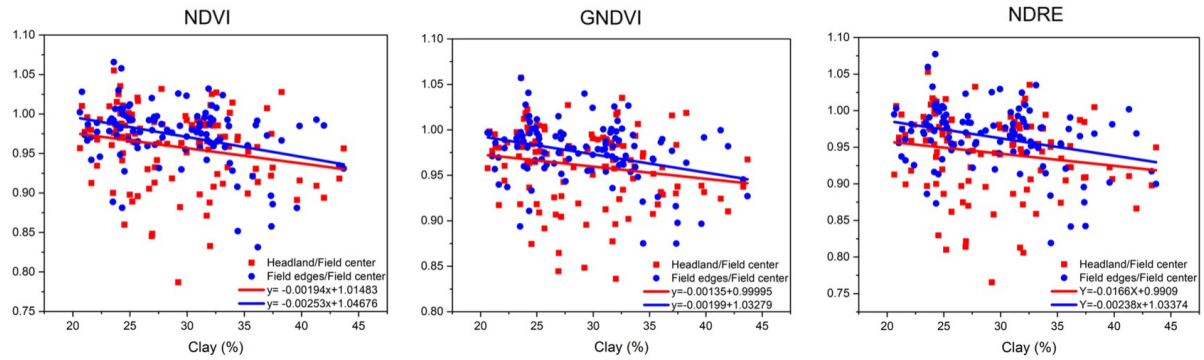

Figure 3.3.3 Comparison between headland, field edges and field centre in clay content.

Figure 3.3.4 shows the correlation between sand content and VIs difference (%) of headland (red point, H/C) and field edges (blue point, L/C) to field centre. The value differences between headland, field edges and field centre were calculated from the average of three years from 2016 to 2018. The red point represents the value of the headland/ field centre. The blue point represents the field edges/ field centre. The red and blue lines are the trend lines, respectively. The sample field's sand content range was from 16.81% to 48.62%. The result showed that the value differences between headland, field edges with field centre reduced as the sand content increased. And also, the value differences between headland and field edges became larger as the sand content increased. Significant correlations were found between headland, field edges and field centre in NDVI, GNDVI and NDRE. Except for the H/C in GNDVI (0.063) showed no significant correlations with the clay content of the field. The p-value was lower than 0.05 in all other comparisons of H/C and L/C in NDVI, GNDVI and NDRE.

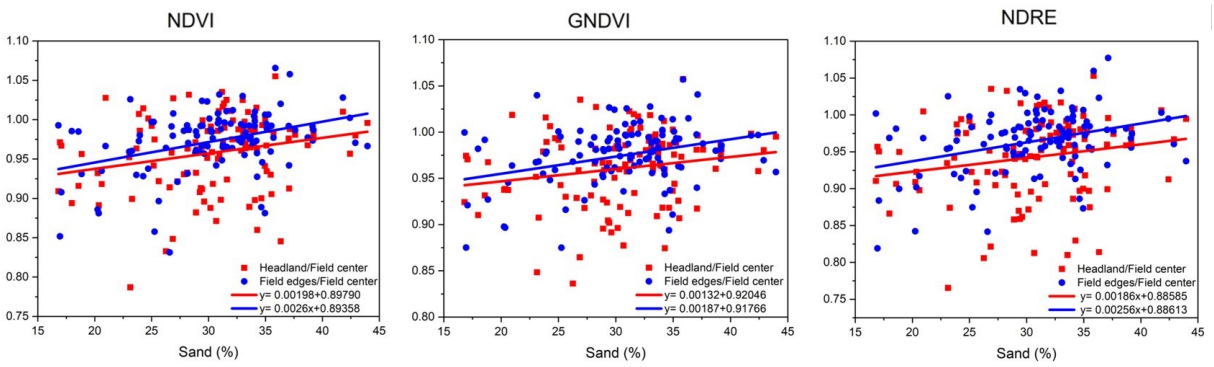

Figure 3.3.4 Comparison between headland, field edges and field centre in sand content.

3.4 Discussion

Yield and VIs difference between headland, field edges and field centre

In this study, yield and VIs results both showed significant differences between headland, field edges and field centre at 0.05 level. The yield map result showed that headland and field edges were 12.20% and 2.49% lower than the field centre in 13 field. The VIs result showed that headland and field edges were 4.27% and 2.70% lower in NDVI, 4.17% and 2.67% lower

in GNDVI, 5.87% and 3.59% lower in NDRE, respectively in 111 fields. The yield losses in headland and field edges increased with the field size and clay content increasing and sand content decreasing. Our study showed a similar result about the lower yield of the headland (turning area) compared to the field centre area (mid-field area, non-compacted area or non-headland) in the previous research (Cook and Ingle, 1997; Kuemmel, 2003; Sparkes et al., 1998b; Speller et al., 1992). In the previous research, significant variations in winter wheat yield were found between the headland and field centre (Wilcox et al., 2000). Headland yields were 14% (grain) and 16% (silage) lower than yields in the non-headland areas (Sunoj et al., 2021). The average yield headland and field edges for various crop types compared to field yields ranged from 7-45% for cereals, 10% for potatoes and 26% for sugar beet at different sampling widths (Chaney et al., 1999; De Snoo, 1994; Kuemmel, 2003; Sparkes et al., 1998a). A study estimated yield gain amounted to 4% at the field and farm levels, considering the percentage of headland and field edges in each field (Sunoj et al., 2021).

However, each field has its unique soil condition, climate characteristics of different regions, specific annual weather conditions and manual operation experience. For example, the traffic conditions will differ because of each field′s implement size, working widths and turning method. So the result of the sample field could vary among the study field we selected. That could be the reason that not all the fields had lower yields or VIs in headland and field edges. The headland and the field edges have more compaction during the field operations because of more traffic (K. Liu et al., 2022; ten Damme et al., 2021b), leading to considerable production losses (Kaczorowska–Dolowy et al., 2019; Li et al., 2007; Sivarajan et al., 2018). The headland and field edges should have a lower yield because of more machine traffic than the field centre if all the fields have the same working condition and agronomy. Besides the soil compaction, yield loss in the headland and field edges may also reflect soil erosion, planter and fertiliser efficiency, within-field variability, edge-feeding of weeds and pests（birds, rodents and deer), and competition for light, water, and nutrients resources with adjacent obstacles. Several reasons could influence the performance of the headland and field edges.

More soil compaction in headland and field edges: During each field operation, there is more traffic in the headland and field edges than in the field centre. Most repeat compaction is localised at the field entrance area and in the headlands (Duttmann et al., 2014, 2013; Godwin and Miller, 2003). The field edges have a higher traffic frequency than the field centre (Rodrigues et al., 2015; Scott et al., 2005). Traffic in the headland and field edges will cause more compaction both in the topsoil and subsoil [6], which destroys the soil structure, increase soil erosion (Fleige et al., 2000; Prasuhn, 2011; Rauws and Auzet, 1989; SANDERS and MOSIMANN, 2005) and causes yield reduction (Boguzas et al., 2001; Obour et al., 2018;

Ridge, 2001).

Planter and fertiliser efficiency: Skips and overlaps could happen in the headland during the seeding and fertilising. Skip could reduce the sown area and crop uniformity, which reduces the yield (K. Liu et al., 2022). The overlaps (doubling inputs) could negatively affect the crop due to reduced stand uniformity within the field. Overlaps could result in excessive plant densities, which could be favourable for disease development. And it also could have negative impacts on production applications, such as difficulty determining optimal spray timing for uneven maturity. Overlaps could also lead to lodging, making harvesting difficult (R19075P, 2020).

Edge-feeding of insects and weeds: A large number of weeds in the field could invade neighbouring crops and affect crops by competing for light, nutrients or water(Boatman, 1992; Marshall and Arnold, 1995), which would reduce the performance of the headland and field edges. However, the time collected VIs data was during the period when the crop had the highest index, which was a few months before the main crop product was harvested. So this reason may be less influential in this study.

Competition for light, water, and nutrient resources with adjacent obstacles: The obstacles and objects around the field could affect crop performance in field boundaries like neighbour trees, rivers, or irrigation canals. Trees that grow on the edge of fields may influence crop growth by shading the field. Additionally, rivers or irrigation canals around the field could cause yield spatial variability in cultivated crops due to the available water variability. As in this study, fields surrounded by trees and rivers have been avoided, as described in the methodology. So, the study removed this reason for the yield and VIs decreasing.

Methodology of the data collecting: The pixel size is 10×10m which was selected from the GEE. It is quite a large area if the field is not large size. The previous study even divided the headland area into three areas: field edge, turning and transition to study the performance difference between each other (Ward et al., 2020). So it could be possible to find a higher value difference between headland, field edges and field centre if the resolution was higher than 10×10m. Additionally, not all the pixels selected during this study were parallel-selected with the field boundaries, as shown in Figure 3.4.1. The purple nails were the data collection points, which means that the result underestimated the yield reduction in the headland and field edges because pixels were more distant from the field boundaries rather than located precisely on the field boundaries. So it means that if the resolution of the pixel was higher than 10×10m like this time, more yield losses or the lower VIs could be found in the future research study. And also that could be tested by comparison of parallel and non-parallel fields

in the further study.

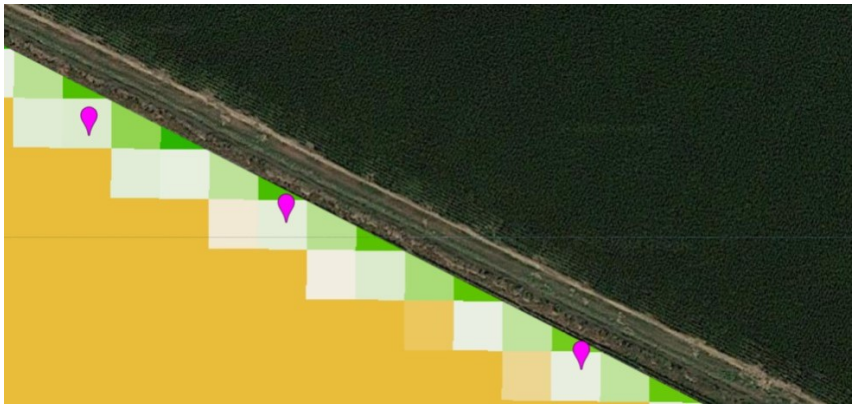

Figure 3.4.1 Pixels (10×10 m) in the field edges.

In general, researchers mentioned that the reduced headland yields was due to factors such as compaction by the trafficking of the agriculture machines, water and light competition from woods and hedgerows, weed ingress and destruction of animals (Speller et al., 1992). Although each of the reasons above could influence the yield in the headland, most research considered traffic and compaction are the predominant factors causing the headland yield reduction by many studies (Sparkes et al., 1998a; Speller et al., 1992; Welch et al., 2016; Wilcox et al., 2000).

Our study aimed to know how much yield has been lost in the headland and field edges based on the yield and VIs maps. Concerning the interpretation of the crop behaviour, deeper information might be achieved by implementing hyperspectral data (Lee et al., 2010). However, it is worth noting that such an approach would increase the effort for data analysis. Also, it might reduce the potential interest and applicability in farm practice. The farm could make a better strategy using the yield and VIs map result if it is convenient enough. Then, better decisions could be made by increasing potential production, planting other crops, or reducing fertility or other input. Such as assessing the economic benefits if the same amount of fertiliser needs to be put in the headland and field edges. If the crop performance of the headlands is affected by machine traffic, it may indicate that headland traffic management may need to be improved to protect the production capacity of these areas. As for the yield losses in headland and field edges, potential solutions include optimal path planning (Bochtis and Vougioukas, 2008) or controlled traffic farming (CTF) (McPhee et al., 2020; Tullberg et al., 2018, 2007), which could reduce the impact of compaction of the field. However, optimal path planning could be challenging to implement when the width of the equipment is different, such as planters, harvesters, and fertiliser application equipment (Sunoj et al., 2021).

Impact of field size and soil texture

The study result found that the VIs differences became larger between headland, field

edges to field centre with the field size increasing. The value differences were less in the smaller fields (less than 10ha), mainly between 95% and 102.5%. However, no significant correlations were found between headland, field edges and field centre in NDVI, GNDVI and NDRE.

The results showed that the value difference of headland to field edges and field edges to field centre increased with the clay content. Conversely, the difference was reduced with the sand content increasing. This phenomenon emphasised the effect of soil compaction on VIs reduced yield losses in areas of headland and field edges because of the effect of soil texture on soil compaction. The plastic limits (lower plastic limit and liquid limit) are important soil properties that can influence the soil's mechanical behaviour, which is highly related to the clay content (Keller and Dexter, 2012). The higher clay content field was considered more sensitive to soil compaction (Keller et al., 2019; Schjønning et al., 2015b). Some researchers assumed yield losses due to the soil compaction of 8% for soils with>40% clay and 4% for soils with 15–25% clay and that yield losses for lighter soils are negligible (Eriksson et al., 1974). Conversely, Sandy soils are often considered structurally inert because of their massive structure and the absence of shrink-swell properties [77] and caused less compaction by the machine traffic (Keller et al., 2007b; Keller and Håkansson, 2010).

3.5 Conclusions

In this study, the value differences between headland, field edges and field centre were studied using yield maps and the VIs result calculated by the GEE. The field size, clay content and sand content were considered in the study. The result showed that headland and field edges have lower yield or VIs than the field centre. The yield map result showed that headland and field edges were 12.20% and 2.49% lower than the field centre. VIs result showed that headland and field edges were 4.27% and 2.70% lower, 4.17% and 2.67% lower, 5.87% and 3.59% lower in NDVI, GNDVI and NDRE results, respectively. And also, the value differences between headland, field edges and field centre increase with the clay content increases. Conversely, the value differences between headland field edges and field centre decreased with the sand content in-creasing. However, no significant correlations were found between headland, field edges and field centre in field size. Soil organic content and crop type should be considered in the future study. Our study suggestsed that the decision maker of the farms pay more attention and plan better machine traffic to reduce the yield losses in headland and field edges.

4. Effects of Subsoiling Angle and Tillage Depth on Soil Structure and Energy

Requirements

Abstract

The study investigates the impact of subsoiling on soil structure and energy requirements, focusing on the angle of the subsoiler and the depth of tillage. Combines discrete element analysis and field experiments, various parameters related to soil structure and machinery performance were analysed. These parameters include simulation traction, energy and velocity of soil particles, soil cone index, soil surface flatness, fuel consumption, traction force, and slip rate during the field experiment. The resuly showed that the soil cone index reduction was influenced by both the subsoiling angle and tillage depth. Traction resistance increased with greater tillage depth and varies based on soil type and subsoiler angle. Furthermore, fuel consumption during the subsoiling is significantly affected by the chosen tillage depth and subsoiling angle. The analysis also reveals that slip rate was influenced by soil type, tillage depth, and subsoiler angle. However, no significant difference in soil surface flatness was observed across most tillage depths and working angles after the tillage operation. Significant correlations were observed between simulation traction with field experiment traction, simulation soil particle energy with simulation traction, and fuel consumption with field experiment traction, at a significance level of 0.05. By considering the angle of the subsoiler and the depth of tillage, practitioners can optimise soil structure, energy consumption, and machinery performance, thereby promoting sustainable and efficient agricultural practices.

4.1 Introduction

Soil compaction has become a challenge in agriculture in recent decades due to the increasing size and weight of agricultural machines worldwide (Keller et al., 2019). The negative effects of soil compaction have been widely studied in different countries and include increased soil bulk density, soil cone index and soil shear strength (Blanco-Canqui et al., 2010; DeArmond et al., 2019; Mossadeghi-Björklund et al., 2016; Obour et al., 2018; Schjønning and Lamandé, 2018; Silva et al., 2018; Tekeste et al., 2008). In addition, soil compaction could impede root exploration, reduce crop yield, and increase energy requirements for field operations (Celik and Raper, 2016, 2012; Obour et al., 2017; Wells et al., 2005). Tillage is one of the methods employed to mitigate the adverse impact of soil compaction. By compressing and disrupting soil aggregates essential for air and water movement and root growth, tillage helps to break down the compacted soil structure. However, it is essential to note that tilled soils are generally more vulnerable to compaction

compared to no-till soils. Additionally, addressing subsoil compaction through tillage poses significant challenges (Arvidsson, 2001; Etana et al., 2013; Hamlett et al., 1990; Schjønning et al., 2012).

Subsoiling is a widely accepted mechanical method to alleviate soil compaction and enhance crop growth (Abu-Hamdeh and Reeder, 2003; Celik and Raper, 2012; Sun et al., 2023). Conservation agriculture involves keeping a certain amount of crop residues on the surface to promote soil health and protect against erosion. In this context, subsoiling should not only reduce the density of the compacted soils but also avoid the inversion of soil layers and the creation of clods, which can limit the effectiveness of reduced tillage or no-till planters. In addition, research has shown that subsoiling can improve water-holding capacity and root penetration, reducing soil resistance and increasing rooting depth (Raper et al., 1998; Wells et al., 2005). However, excessive energy consumption during soil preparation is a critical issue that impacts farmers' income, making energy savings a crucial factor in subsoiling practices (Lu and Lu, 2017; Uzun et al., 2012).

The efficiency of subsoiling heavily depends on factors such as tillage depth, subsoiler design, and technique. Various subsoiler designs have been tested for various soil types and conditions to reduce energy consumption and improve tillage efficiency (ASAE Standards, 1999; Askari et al., 2016; Raper and Schwab, 2008; Song et al., 2022; Uzun et al., 2012; Zhang et al., 2022; Zheng et al., 2016). Considering these factors is vital in designing and implementing subsoiling practices to optimise benefits and minimise potential negative impacts on soil structure and yields. This approach aligns with sustainable agriculture principles, promoting soil health and productivity while mitigating environmental harm.

Subsoiling involves using shanks equipped with wings or curves to disrupt compacted soil profiles at varying depths. The choice of shank design and wing angle can significantly impact subsoiler performance, including draft force, soil disturbance, bulk density, penetration resistance, and soil aggregation (Aikins et al., 2021; Li et al., 2018). For example, some studies have investigated the effects of shank and wing design on subsoiler performance, showing that angled shanks reduce draft force, and forward-bent wings with bend angles of 10° show the best performance for deep soil loosening (Askari et al., 2019, 2016). However, the effects of operating angle and depth on subsoiler performance remain unclear.

Optimising tillage tool design can be resource-intensive and time-consuming, requiring repeated experimental evaluations (Ani et al., 2018; Chen et al., 2013). However, finite element modelling (FEM), computational fluid dynamics (CFD), and the discrete element method (DEM) have streamlined this process. DEM is advantageous as it models the discrete nature of soil particles, producing more realistic simulations of soil particle displacement and

forces based on Newton's Second Law of Motion and mechanical contact force models (Aikins et al., 2021; Hang et al., 2018; Li et al., 2016; Ucgul et al., 2014; Wang et al., 2020). By utilising the discrete element model, comprehensive insights can be gained regarding the impact of subsoiling tool design and operating parameters on subsoiler performance. This scientific approach enables a deeper understanding of the factors influencing subsoiling effectiveness, facilitating informed decision-making for optimal subsoiling practices.

This study study aims to comprehensively analyse the impact of working angle and depth on subsoiler performance by employing discrete element and field experiment methodologies. Multiple performance parameters, including subsoiler traction resistance, soil particle energy, and soil particle velocity, were evaluated using DEM. Additionally, field experiments were conducted to assess soil cone index before and after tillage, soil surface flatness, traction force, fuel consumption and slip rate. By integrating these approaches, a comprehensive understanding of the subsoiler's performance under different working conditions can be achieved.

4.2 Materials and Methods

Methodology of DEM simulation

The discrete element analysis in our study was conducted using the software EDEM 2018 (Altair Engineering, Troy, Michigan, USA) ("EDEM 2018," n.d.). Previous research studies (Di Renzo and Di Maio, 2004; D. Liu et al., 2022; Wang et al., 2017; Zheng et al., 2016) provided the basis for the simulation parameters, including the properties of the sand and clay soil, as well as the subsoiler. The sand and clay soil samples, with respective soil accumulation angles of 36.2° and 34.7°, were collected on the day of the field experiment. The contact between the soil and subsoiler employed the Hertz-Mindlin (no slip) contact model. Plastic deformation was accounted for using the Hysteretic Spring contact model, while normal cohesion utilised the Linear Cohesion contact model (Tamás et al., 2013; Ucgul et al., 2015, 2014). Table 4.2.1 presents the specific simulation parameters, including soil particle properties, material properties of the subsoiler, the interaction between the subsoiler and soil, and other relevant parameters. Careful selection of these parameters ensured an accurate representation of the soil and subsoiler behaviour during the analysis.

Table 4.2.1 Parameter of DEM simulation

Type	Parameter	Sand soil	Clay soil
Soil particle properties	Density ϱ/(kg/m3)	2550	2550
	Shear modulus G/Mpa	1	50
	Poisson's ratio v	0.25	0.3
	Soil particle radius r/mm	1	1
Material properties of the subsoiler	Density ϱ'/(kg/m3)	7865	7865
	Shear modulus G′/Pa	7.9×10^{10}	7.9×10^{10}
	Poisson's ratio v'	0.3	0.275
Interaction between subsoiler and soil	Coefficient of restitution between soil and soil, e1	0.6	0.3
	Coefficient of rolling friction between soil and soil, e2	0.17	0.1
	Coefficient of static friction between soil and soil, e3	0.35	0.45
	Coefficient of restitution between soil and subsoiler, f1	0.5	0.475
	Coefficient of rolling friction between soil and subsoiler, f2	0.1	0.1
	Coefficient of static friction between soil and subsoiler, f3	0.45	0.5
Other parameters	Number of soil particles, n	107774	
	Acceleration of gravity, G (m/s)	9.81	
	Rayleigh Time step (s)	0.0016267	
	Fixed Time step (s)	0.000325332	
	Simulation time, t (s)	2	
	Soil bin dimensions (length, width, height)/(mm)	2300×1000×600	
	Subsoiler time speed, v (m/s)	0.5	
	Tillage depth, h (mm)	250,350	

In the DEM (Discrete Element Method) experiment, the Alpego Skat S2 model subsoiler (ALPEGO S.p.a, Lonigo, Italy) was utilised, and it was accurately imported into the EDEM 2018 (EDEM, 2018) at a 1:1 scale. The subsoiler model comprised two wings, as depicted in Figure 4.2.1. A forward velocity of 0.5 m/s was maintained throughout the experiment to ensure simulation stability. The working depths of 25 cm and 35 cm were achieved by determining the depth at which the subsoiler blade effectively penetrated the soil. The angle of the subsoiler during the simulation was calculated and adjusted based on the angle of the wings relative to the horizontal plane. During the simulation, the subsoiler angle was varied in 5-degree increments ranging from 0 to 25 degrees. In addition, angles of 7.5° and 12.5° were also employed to analyse the reasons behind the optimal performance observed at 10° in sand soil. The right figure of Figure 4.2.1 illustrates the simulation process, with different colours denoting the speed of the soil particles.

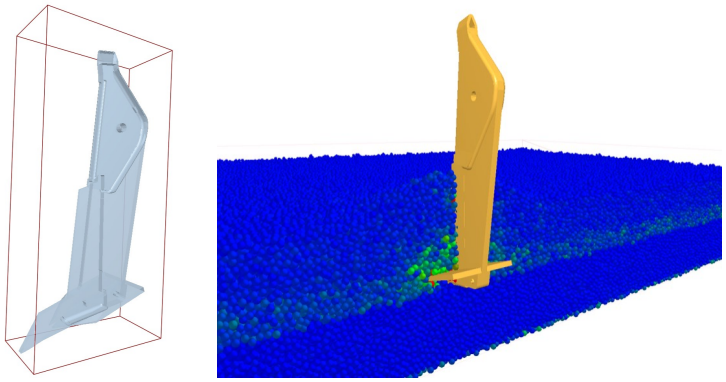

Figure 4.2.1 Subsoiler 3D model (left) and simulation example (right)

This study investigated the impact of manipulating the subsoiler's working angle and tillage depth on soil disturbance and energy requirements. Data was collected and analyzed from the simulation process, focusing on traction resistance, soil particle energy, and soil particle velocity. The simulation aimed to gain insights into the subsoiler's performance, similar to previous research methodologies (Aikins et al., 2021; Li et al., 2016; Zhou et al., 2016). By utilizing this approach, the study aimed to enhance our understanding of how different subsoiler working angles influence soil disturbance and energy requirements. The collected data served as a resource for investigating the relationship between subsoiler parameters and their impact on soil dynamics.

Methodology of field experiment

The field experiment was conducted both in sand and clay soil. Two different tillage depths, 25cm and 35cm, along with two angles of the subsoiler, 10 and 20 degrees, were tested in the field experiment. The angle between the subsoiler and the equipment frame was adjusted to achieve the desired subsoiling angles. To enhance flexibility, a low-disturbance anchor was attached to the cultivators. The study utilized a three-meter-wide Alpego "SKAT S2" subsoiler, equipped with seven anchors and a hydraulically adjustable cage roller. The subsoiler had a width of 42 cm between the tines, with approximately 80 cm spacing between the front and rear tines. Initially, the blade inclination was set at 10° to the ground and could be adjusted to 20° by adding shims under the anchor support, as depicted in Figure 4.2.2.

To standardise the working depth adjustment, the test involved extending the hydraulic cylinders and adjusting the rear roller while measuring the distance between the drum centre and the machine support surface. It is important to note that the right figure not only changes the angle of the lateral wings from 10 to 20 degrees compared to the left figure but also alters the angle of the anchor from 15 to 5 degrees and the height of the subsoiler from 568 to 632 mm. However, the same working depth was maintained under different angle conditions during the field experiment to maintain experiment accuracy.

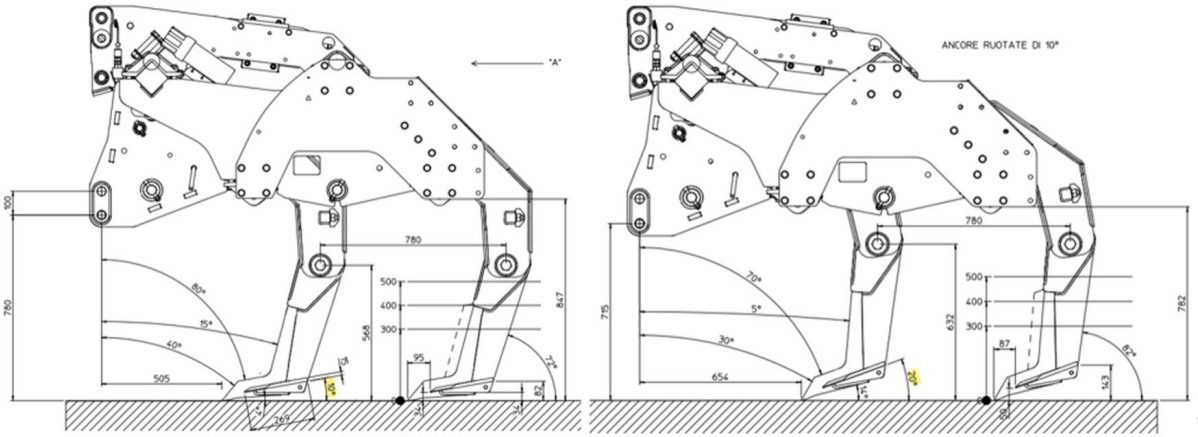

Figure 4.2.2 Subsoiler designed with two positions

The field experiment was conducted in Trecenta, Rovigo, Italy (45.031694, 11.465849). The experiment used two types of soil: pure sandy soil, which had previously been planted with corn and fertilised with liquid manure after harvest, and clay soil, with hard wheat as the previous crop. The residues on both fields were threshed and chopped by a combine harvester. The field experiment involved two working depths (25 and 35 cm) and two subsoiler wing angles (10° and 20°). Various parameters were measured during the tests, including soil cone index, soil surface flatness, traction, fuel consumption, and slip rate. Figure 4.2.3 illustrates the field experiment, where two tractors were utilised to measure traction. A dynamometer was placed at the rear of the front tractor for this purpose.

Figure 4.2.3 Two tractors (left) and the dynamometer (right) used in the field experiment

The soil cone index, which represents the soil penetration resistance, was measured using a Penetrologger (Eijkelkamp, Geesbek, The Netherlands). The Penetrologger was mounted on an iron frame attached to a hydraulic piston. Additional information can be found in the previous study (K. Liu et al., 2022). Measurements were taken from 0 to 70 cm depths with a lateral width of 50 cm, covering 5 cm increments (21 lines in 100 cm width). The measurements were repeated three times for each angle and working depth combination.

The soil surface flatness, also known as the soil surface profile, was measured simultaneously with the soil cone index using a penetrometer as a pin meter during the field experiment, following similar methodologies in previous studies (Miriti, 2013; Moreno et al.,

2008). To assess the soil surface flatness, the distance was calculated from the starting point, where the penetrometer was positioned in the frame parallel to the soil surface, to the last zero point, indicating the penetrometer has contacted the soil surface. The number of zero lengths encountered during the measurement was recorded. Subsequently, the standard deviation of the lengths within each group, consisting of 21 lines, was calculated. Finally, the differences in average standard deviation each group between different groups under varying angle and depth conditions were analysed.

The instantaneous fuel consumption data were directly collected from the onboard computer of the tractor, specifically a Fendt 826 with a power of 191 kW ("Fendt. Fendt 826 Vario," n.d.). The tractor maintained a constant speed of 6 km/h throughout the experiment. Traction measurements were obtained by connecting two tractors with a 6 m wire rope during the field experiment. A dynamometer (TZR 20 t, Yale Industrial Products GmbH, Wuppertal, Germany) was attached to the rear of the front tractor, and real-time traction data was transmitted to the monitor of the front tractor, as depicted in right of Figure 4.2.3.

The slip rate (slippage) was calculated for each working condition. The slip was calculated as:

$$S = \frac{(d_2 - d_1/4)}{d_2}$$

The d_1 is the actual distance after four turns of the rear wheel. d_2 is the theoretical moving distance during the four-wheel turns, and *S* represents the slip rate.

Statistical analysis

The analysis of the simulation results involved calculating the arithmetic mean values for traction resistance, total energy of soil particles, and average velocity across different subsoiler depths and angles. These variables served as counterparts to the field experiment measurements, which included soil cone index, soil surface flatness, fuel consumption, traction resistance, and slip rate. Rigorous statistical analysis was conducted using IBM SPSS Statistics software (IBM Corp. Released 2019. IBM SPSS Statistics for Windows, Version 26.0. Armonk, n.d.) to assess the significance of the findings. The ANOVA (Analysis of Variance) was used to compare the means at a significance level of 0.05. Additionally, Pearson linear correlation analysis was performed to evaluate the relationship between simulation and field experiment results at a significance level of 0.05.

4.3 Result

Simulation Results

The left side of Figure 4.3.1 provides information on the average horizontal force values experienced by the subsoiler in the sand soil simulation. These force values represent the resistance the subsoiler encounters in the opposite direction of movement. The results include measurements at different angles and depths and their corresponding standard deviations. The data reveals that the highest horizontal force values were observed at an angle of 25°. At a depth of 25 cm, the maximum horizontal force value recorded was 2961.4 N, while at a depth of 35cm, the maximum value was 4118.0 N. Conversely, the lowest horizontal force values were observed at an angle of 10°. At a depth of 25cm, the minimum horizontal force value measured was 1810.6 N; at a depth of 35cm, the minimum value was 2910.8 N. Considering the data from both depths, significant differences between 10 degrees and 20 degrees were observed, as well as 10 degrees and 25 degrees. While no significant differences were found among the other angles at the 0.05 level.

The right side of Figure 4.3.1 presents the vertical resistance experienced by the subsoiler during the sand soil simulation. This resistance represents the average traction resistance encountered by the subsoiler in the vertical direction. The table displays the vertical force values at various angles and depths. The data reveals that as the angle increases, the vertical force decreases. At 0 degrees, the vertical force reaches its highest value, measuring 1233.50 N at a depth of 25cm and 1858.33 N at a depth of 35cm. On the other hand, at an angle of 10 degrees, the vertical force is the lowest, with values of 542.93 N at a depth of 25cm and 1263.82 N at a depth of 35cm. Based on the data from both depths, a significant difference was observed between the angles of 0 degrees and 10 degrees. However, no significant differences were found among the other angle conditions at a significance level of 0.05.

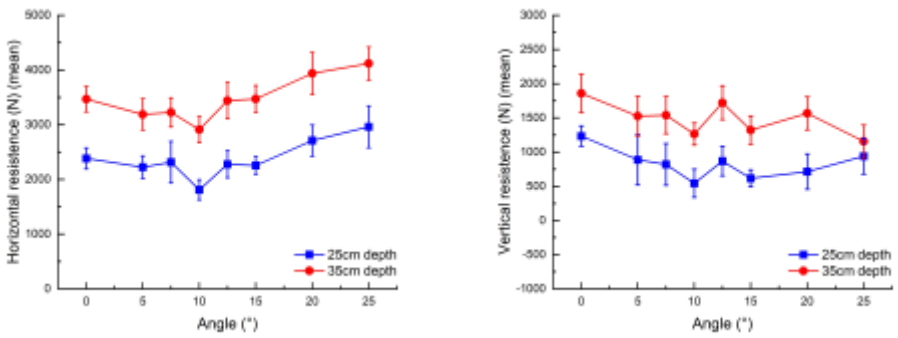

Figure 4.3.1 Traction resistance of the subsoiler in horizontal (left) and vertical (right) direction of the sand soil

The left side of Figure 4.3.2 illustrates the average horizontal force values encountered by the subsoiler, opposing its movement in clay soil. Among the tested angles, the subsoiler

demonstrated the highest horizontal force values at an angle of 25°. At a depth of 25 cm, the maximum force recorded was 4151.1 N, while at 35 cm, it was 4493.0 N. In contrast, the lowest horizontal force values were observed at 10° and 0° angles, measuring 3335.0 N at 25 cm depth and 3789.1 N at 35 cm depth. It can be noted that as the subsoiler angle increases, the horizontal force values generally exhibit an increasing trend. It is worth mentioning that the standard deviation of the horizontal resistance in the clay soil is generally higher compared to the results obtained from the sand simulation. Based on the data from both depths, significant differences were observed between the angle of 20 degrees and 25 degrees compared to the other angles, while no significant differences were found among the remaining angles at a significance level of 0.05.

On the right side of Figure 4.3.2, the average vertical resistance (N) experienced by the subsoiler is displayed, representing the traction resistance exerted in the vertical direction during the simulation. The data reveals a general trend where the vertical force increases as the angle of the subsoiler increases. At a depth of 25 cm, the highest vertical force value was observed at an angle of 20°, measuring 3148.1 N. Conversely, the lowest value was recorded at an angle of 0°, which was 1851.7 N. Similarly, at a depth of 35 cm, the highest vertical force value was observed at an angle of 20°, measuring 3690.3 N, while the lowest value was recorded at an angle of 5°, which was 2081.5 N. Similar to the findings in the sand soil simulation, the standard deviation of the vertical force values was generally large, indicating variability in the results. In descending order, the angle of 20 degrees demonstrated the highest level of significant difference among the four groups. This was followed by 25 degrees, 15 and 10 degrees, and 5 and 0 degrees, respectively. Each group exhibited a significant difference at a 0.05 level from one another.

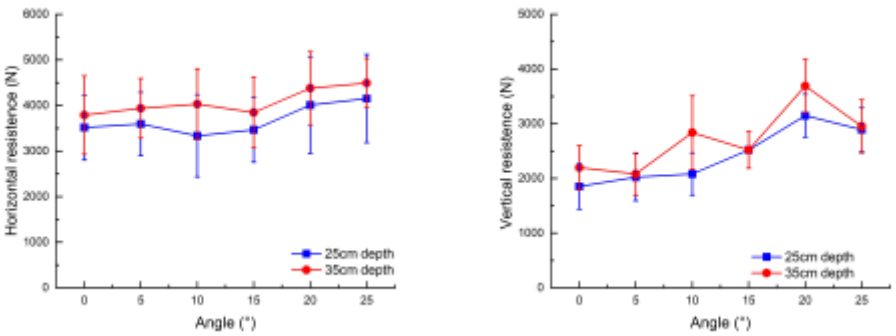

Figure 4.3.2 Traction resistance of the subsoiler in horizontal (left) and veritical (right) direction of the clay soil

The total traction resistance of the subsoiler is presented in Figure 4.3.3. At both depths (25 cm and 35 cm), the highest total force was observed at the 25 degree angle. At 25 cm depth, the force was 3106.74 N, while at 35cm depth, the force was 4277.29 N. The lowest total force was observed at the 10-degree angle for both depths. At 25cm depth, the force was

1890.24N, while at 35cm depth, the force was 3173.30N. Based on the data, the trend of the total force at 25 cm depth decreases as the angle increases from 0 to 10 degrees, then increases as the angle increases further to 25 degrees. The trend is similar at the 35cm depth, but the force values are generally higher. Considering the data from both depths, a significant difference was observed between the angle of 25 degrees and 10 degrees, while no significant differences were found among the other angles tested at 0.05 level.

The right of Figure 4.3.3 displays the total force exerted by the subsoiler in the clay soil simulation, representing the combined horizontal and vertical forces during the simulation. At a depth of 25cm, the highest total force value was observed at an angle of 20°, measuring 5098.5 N. In contrast, the lowest total force value was recorded at an angle of 10°, measuring 3931.5 N. Similarly, at a depth of 35cm, the highest total force value was observed at an angle of 20°, measuring 5726.4 N, while the lowest value was recorded at an angle of 0°, measuring 4381.2 N. The data indicates that increasing the subsoiler angle leads to an increase in the total force exerted. Considering the data from both depths, the angle of 20 and 25 degrees showed a significant difference compared to the other angle. However, other angles showed no significant difference between each other at 0.05 level.

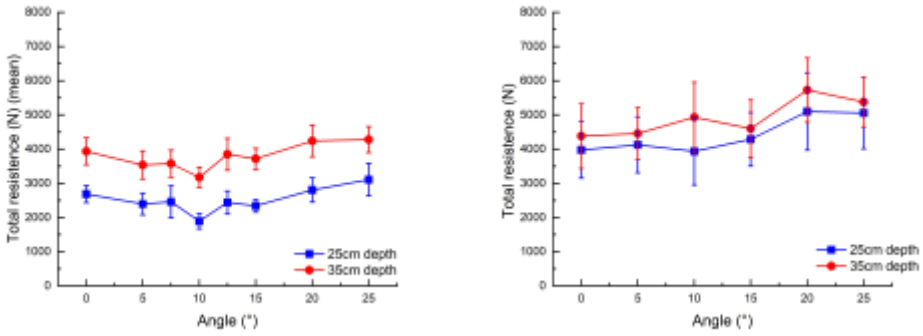

Figure 4.3.3 Total resistance of the subsoiler of the sand soil(left) and clay soil(right)

Figure 4.3.4 presents the total energy of soil particles in sand soil (left) and clay soil (right), the sum of the translational kinetic energy (J) and the rotational kinetic energy of soil particles. In sand soil the total energy ranged from 76.7 J to 84.5 J at the 25 cm depth,, with a standard deviation ranging from 15.9 J to 18.2 J. Similarly, for the 35 cm depth, the total energy ranged from 82.6 J to 90.4 J, with a standard deviation ranging from 16.8 J to 20.8 J. However, the results did not show a significant difference in the total energy values among the different angles at either depth level, with a significance level of 0.05. The simulation data also did not indicate a clear trend in the total energy required for tillage with increasing angle. Interestingly, the 10-degree angle was found to have the highest total energy among all angles for the 25cm depth, while it showed the lowest total energy among all angles for the 35cm depth.

The figure on the right side of Figure 4.3.4 presents the total energy of the subsoiler in the clay soil simulation. The figure provides the total energy values for different angles and depths and their corresponding standard deviation values. At a depth of 25cm, the highest total energy value was observed at an angle of 25°, measuring 126.4 J. In contrast, the lowest total energy value was recorded at an angle of 0°, measuring 93.0 J. Similarly, at a depth of 35 cm, the highest total energy value was observed at an angle of 20°, measuring 174.4 J, while the lowest value was recorded at an angle of 5°, measuring 112.5 J. The data suggests that the total energy values can vary depending on the angle and depth of the subsoiler. However, it is important to note that the standard deviation values indicate some degree of variability in the measurements. Considering the data from both depths, 20 degrees showed significant differences compared to 10, 0, and 5 degree angles at 0.05 level.

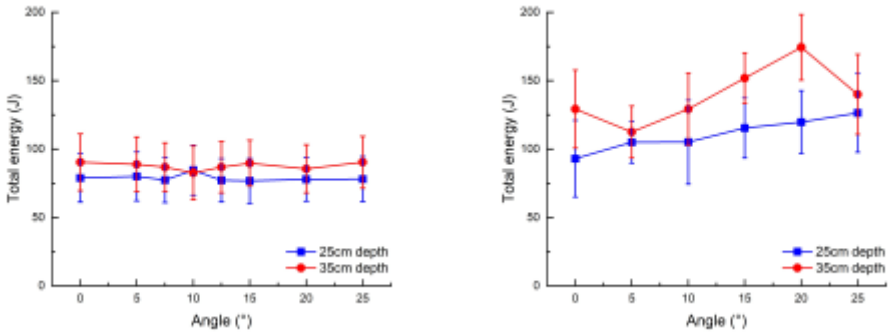

Figure 4.3.4 Soil particles total energy of the sand soil(left) and clay soil(right)

Figure 4.3.5 represents the average velocity in the horizontal (left) and vertical direction (right) the soil particle in sand soil simulation. For the horizontal velocit, the average velocity increased from 0.00169 m/s at 0 degrees to 0.00285 m/s at 25 degrees at a depth of 25 cm. Similarly, at a depth of 35 cm, the average velocity increased from 0.00216 m/s at 0 degrees to 0.00337 m/s at 25 degrees. The standard deviations of the average velocities varied from 3.21E-04 to 5.68E-04 m/s, indicating relatively small variations among the measurements. Taking into account the data from both depths, significant differences were found among the tested angles. Specifically, significant differences were observed between the angles of 0-12.5 degrees, 10-15 degrees, and 20-25 degrees. These three groups exhibited clear distinctions from one another at a significance level of 0.05. Overall, the data showed that increasing the angle of subsoiling generally leads to higher horizontal velocities of soil particles, particularly at greater depths.

The right figure of Figure 4.3.5 shows the average velocity of soil particle in the vertical direction. At both depths, the average velocity of soil particles increased as the angle of the subsoiler increased from 0 to 25 degrees. At an angle of 25 degrees, the highest average velocity of soil particles was 5.01E-04 m/s at 25cm depth and 6.05E-04 m/s at 35 cm depth.

The standard deviations were relatively high for all data points, indicating significant variability during the simulation. Considering the data from both depths, a significant difference was observed only between the 0 and 25 degrees angle. No significant differences were found among the other angles tested at a significance level of 0.05.

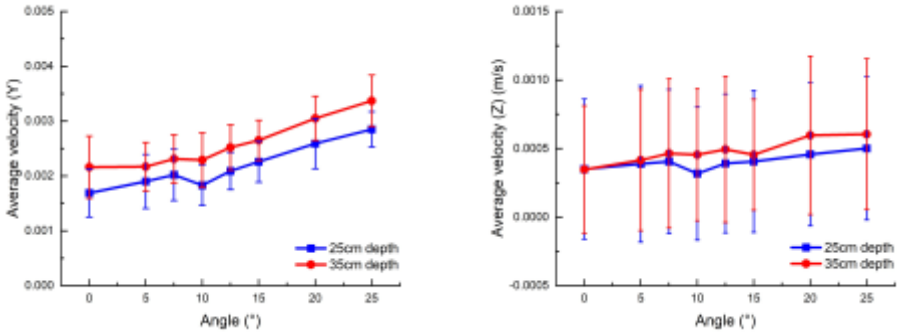

Figure 4.3.5 Average velocity in horizontal (left) and vertical direction (right) the sand soil particle

The average horizontal velocity of soil particles during the clay soil simulation is presented in the figure on the left side of Figure 4.3.6. At a depth of 25 cm, the highest average horizontal velocity was observed at an angle of 20°, measuring 0.00249 m/s. In contrast, the lowest average horizontal velocity was recorded at an angle of 0°, measuring 0.00176 m/s. Similarly, at a depth of 35cm, the highest average horizontal velocity was observed at an angle of 25°, measuring 0.00355 m/s, while the lowest value was recorded at an angle of 15°, measuring 0.00265 m/s. The data indicates that the average horizontal velocity of soil particles can vary depending on the angle and depth of the subsoiler. Under the conditions of 25cm and 35cm depths, no significant differences were observed among the various angles tested at a significance level of 0.05.

The average vertical velocity of soil particles during the clay soil simulation is presented in the figure on the right side of Figure 4.3.6. At a depth of 25 cm, the highest average vertical velocity was observed at an angle of 25°, measuring 0.00333 m/s. Conversely, the lowest average vertical velocity was recorded at an angle of 10°, measuring 0.00253 m/s. At a depth of 35cm, the highest average vertical velocity was observed at an angle of 15°, measuring 0.00404 m/s, while the lowest value was recorded at an angle of 10°, measuring 0.00311 m/s. However, no significant differences were observed among the various angles tested under 25cm and 35cm depths at a significance level of 0.05.

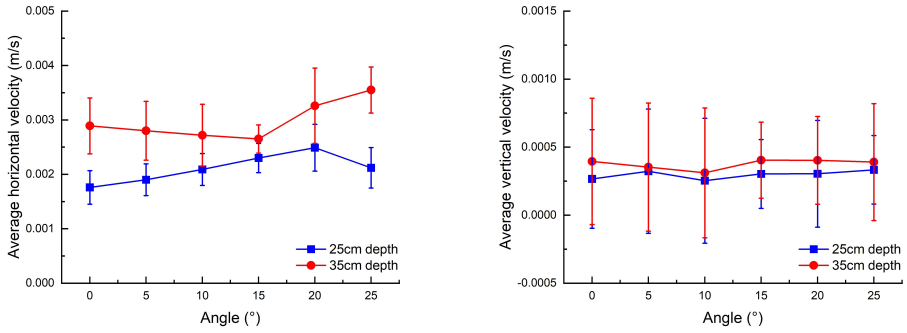

Figure 4.3.6 Average velocity in horizontal (left) and vertical direction (right) the clay soil particle

The results of the average total velocity of soil particle is displayed in Figure 4.3.7. The data in sand soil (left) shows that the average velocity increases from 0 to 25 degrees as the angle increases, with the highest velocity observed at 25 degrees. At a depth of 25vcm, the highest average velocity was observed at 25° (0.01132 m/s), while the lowest average velocity was observed at 10° (0.01012 m/s). The minimum value for the velocity at 25vcm depth was observed at an angle of 10° (0.01012 m/s). On the other hand, at a depth of 35cm, the highest average velocity was observed at an angle of 25° (0.01243 m/s), while the lowest average velocity was observed at an angle of 0° (0.000308 m/s), which was the minimum value for all measurements in the figure. No significant differences were found among the different angles tested when considering the combination of 25cm and 35cm depths at 0.05 level.

The average total velocity of soil particles in clay soil is presented in the figure on the right side of Figure 4.3.7. At a depth of 25 cm, the highest average total velocity was observed at an angle of 20°, measuring 0.00251 m/s. Conversely, the lowest average total velocity was recorded at an angle of 0°, measuring 0.00178 m/s. Similarly, at a depth of 35cm, the highest average total velocity was observed at an angle of 25°, measuring 0.00357 m/s, while the lowest value was recorded at an angle of 15°, measuring 0.00268 m/s. The data indicated that the average total velocity of soil particles can vary depending on the angle and depth of the subsoiler. The standard deviation of the total velocity in the clay simulation was higher than the sand soil simulation. However, when considering the combination of 25cm and 35cm depths, no significant differences were found among the different angles tested at 0.05 level.

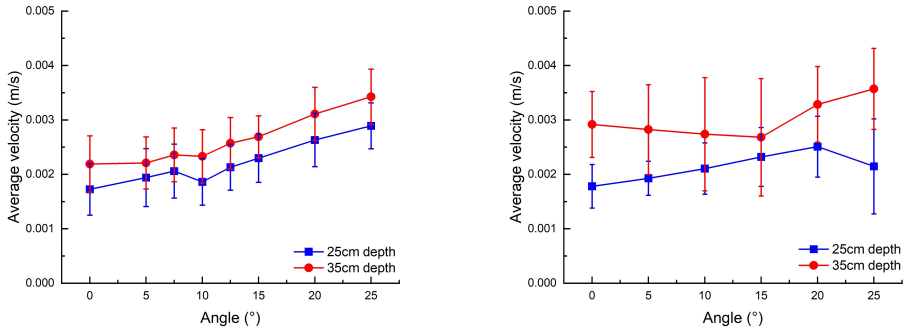

Figure 4.3.7 Average total velocity of the sand soil(left) and clay soil(right) particle

Field experiment results

Soil cone index

The soil cone index results revealed a significant difference between the values before (NT) and after tillage (T) in both sand and clay soil across the depth range of 0 to 60 cm at a 0.05 significant level. Below are more detailed comparisons between different angles and tillage depth conditions:

The soil cone index of clay soil was analysed at the same angle (10° or 20°) and different tillage depths (25 cm or 35 cm), as shown in Figure 4.3.8. The results from the left figure indicate that after tillage, the soil cone index of the 25 cm tillage depth had lower values than the 35 cm tillage depth from 0 to 10 cm depth. Although the soil cone index in the clay-10-NT condition was higher than that in the Clay-10-35-NT from 14 to 24cm depth, the soil cone index was similar after tillage in two tillage depth conditions. For the 20° condition, as shown in the right figure, the trend is similar, where the 25 cm tillage depth reduced the soil cone index more than the 35 cm tillage depth. Although the soil cone index in the field of 25 cm tillage depth is higher than the field of 35 cm tillage depth in all depths except the 17 cm position, 25 cm tillage depth has a lower value of the soil cone index after the tillage compared with the 35cm tillage depth from 5 to 18cm depth. Based on the average soil cone index measured at depths of 0 to 40 cm, no significant difference was found when comparing the same angle at different tillage depths, whether it was in the 10-degree or 20-degree conditions, at a significance level of 0.05.

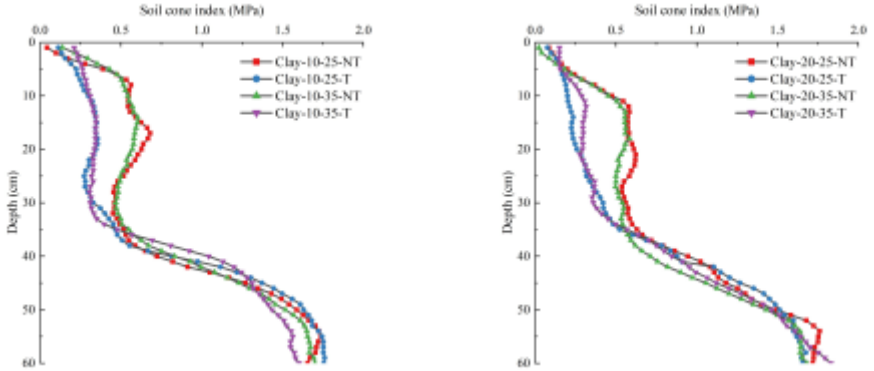

Figure 4.3.8 Soil cone index of clay soil at the same angle and different tillage depth

The soil cone index of clay soil was analysed at different angles (10° and 20°) and the same tillage depths (25 cm and 35 cm), as shown in Figure 4.3.9. The results indicate that the soil cone index was reduced after tillage in all conditions. At the 25cm depth condition, as shown in the left figure, the 20° angle resulted in a lower soil cone index in the 0-21 cm range, while the 10° angle had a lower soil cone index from 22 to 39 cm, followed by the 20° angle again. However, it should be noted that the original soil cone index values were also different. For the 35 cm depth, as shown in the right figure, the trend was similar to the 20° angle resulting in a lower soil cone index compared to the 10° after tillage, although the soil cone index values before tillage were still significantly different in the depth of 0 to 18 cm depth. Based on the average soil cone index measured at 0 to 40 cm depths, a significant difference was observed when comparing the same tillage depth at different angles of the subsoiler in the 35 cm condition. The soil cone index was significantly lower in the 20-degree angle condition than the 10-degree angle condition. However, no significant difference was found in the 25 cm condition at a significance level of 0.05.

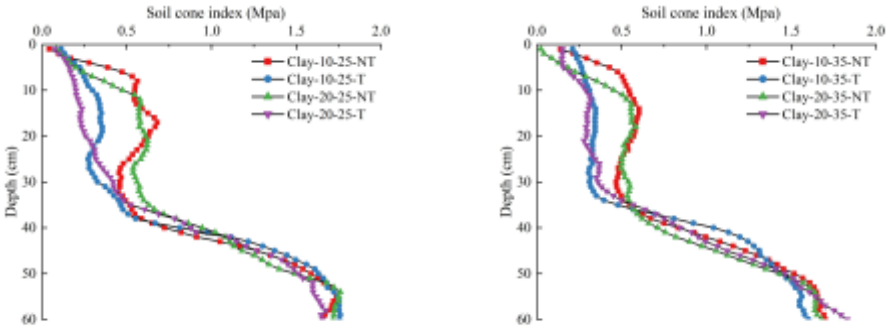

Figure 4.3.9 Soil cone index of clay soil in same tillage depth and different angle

The soil cone index of sandy soil was analysed at the same angles (10° and 20°) and different tillage depths (25 cm and 35 cm), as shown in Figure 4.3.10. It is worth noting that the soil cone index exceeds 2.5MPa when the depth is greater than 50 cm. Data at these locations were not the focus of our study. The results showed a reduction in soil cone index after the tillage in all conditions. The left figure indicated that the original field of 35-NT had a higher soil cone index than the original field of 25-NT. The right figure showed that 35cm tillage reduced more soil cone index than the 25 cm tillage. The changes in values during subsoiling will be reported in the next part of the paper. Based on the average soil cone index measured at 0 to 40 cm depths, significant differences were observed when comparing the same angle at different tillage depths in both the 10-degree and 20-degree conditions, at a significance level of 0.05. Specifically, the soil cone index at a tillage depth of 25 cm was significantly lower than at a tillage depth of 35 cm when the subsoiler angle was 10 degrees.

Conversely, the soil cone index at a tillage depth of 35 cm was significantly lower than at a tillage depth of 25 cm when the subsoiler angle was 20 degrees.

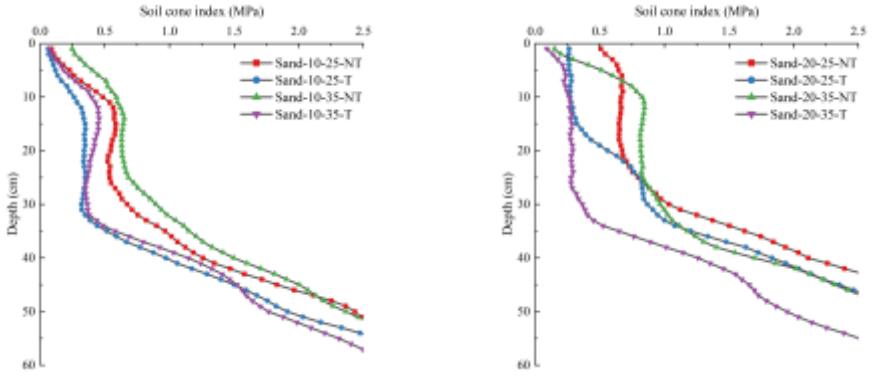

Figure 4.3.10 Soil cone index of sand soil in the same angle and different tillage depth

The soil cone index of sandy soil was analysed at different angles (10° and 20°) and the same tillage depths (25 cm and 35 cm), as shown in Figure 4.3.11. The findings revealed a reduction in soil cone index across all conditions after tillage, but with varying trends. Specifically, at an angle of 10° and tillage depth of 25 cm, the soil cone index decreased across the depth range of 0 to 60 cm. Conversely, at an angle of 20° and the 25 cm tillage depth, the reduction in soil cone index was mainly observed from 0 to 25 cm. The right figure showed that the angle of 20° resulted in higher soil cone index reduction before and after tillage compared to 10°. Our results showed that 20° angle produces a greater reduction in soil cone index in sandy soil compared to 10°. Based on the average soil cone index measured at depths of 0 to 60 cm, a significant difference was observed when comparing the different angles of the subsoiler at a tillage depth of 35 cm, with a significance level of 0.05. Based on the average soil cone index measured at 0 to 40 cm depths, a significant difference was observed when comparing the same tillage depth at different angles of the subsoiler in the 35 cm condition. The soil cone index was significantly lower in the 20-degree angle condition than the 10-degree angle condition. However, no significant difference was found in the 25 cm condition at a significance level of 0.05.

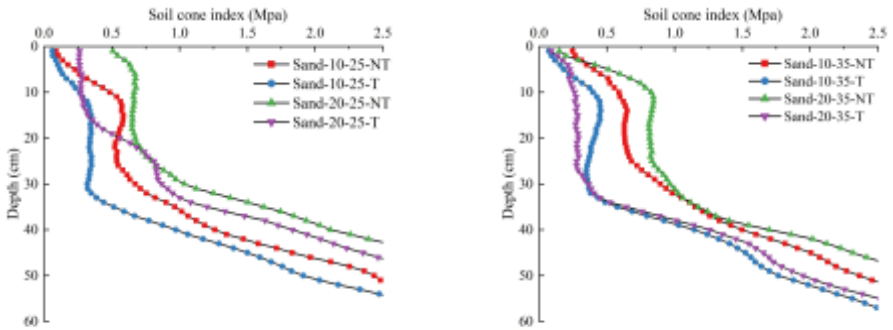

Figure 4.3.11 Soil cone index of sand soil in same tillage depth and different angle

Here is the Average soil cone index from 0 to 40 cm depth in different angles and tillage

depth, as shown in Table 4.3.1 Lowercase letters (abc) indicate the comparison under different tillage depth conditions within the same angle. Capital letters (ABC) indicate the comparison under different angles within the same tillage depth. The result is similar to the figure but displayed in the table with numbers about the average soil cone index from 0 to 40 cm depth in different angles and tillage depth conditions.

Table 4.3.1 Average soil cone index from 0 to 40 cm depth in different angles and tillage depth

Soil	Angle	Tillage depth	Before tillage	After tillage
Sand	10	25	0.5207±0.2853Bb	0.4394±0.2792Ab
	10	35	0.7041±0.2995Aa	0.5628±0.3461Aa
	20	25	0.7086±0.2959Aa	0.4311±0.2743Aa
	20	35	0.6660±0.3147Aa	0.3251±0.2084Bb
Clay	10	25	0.5032±0.1508Ba	0.3145±0.1204Aa
	10	35	0.5162±0.1393Aa	0.3046±0.1023Ba
	20	25	0.5820±0.1885Aa	0.3092±0.1647Aa
	20	35	0.5395±0.1448Aa	0.3376±0.1332Aa

The cone index measures the extent of soil compaction reduction, from 0 to 40 cm, before and after tillage. Figure 4.3.12 shows the percentage reduction in soil compaction, as measured by the cone index, before and after tillage at two different depths (25 cm and 35 cm) for four different soil conditions (Sand 10°, Sand 20°, Clay 10°, and Clay 20°). For example, for Sand 10° soil at a depth of 25 cm, there was a 40.83% reduction in soil cone index after tillage compared to before tillage. At a depth of 35 cm for the same soil condition, there was a slightly higher reduction of 42.66%. Similarly, for Sand 20° soil at a depth of 25 cm, the reduction in soil cone index after tillage was 27.41%, but at a depth of 35 cm, the reduction increased to 55.97%. The results for clay soil also indicated a reduction in cone index after tillage at both 25 cm and 35 cm depths. At an angle of 10 degrees, the cone index was reduced by 31.19% at a depth of 25 cm and 25.75% at a depth of 35 cm. At a slope angle of 20 degrees, the cone index was reduced by 35.21% at a depth of 25cm and 22.23% at a depth of 35 cm. However, the soil cone index's percentage reduction was lower than the sandy soils. Overall, the result shows that the reduction in soil compaction after tillage varied depending on the soil type, slope angle, and measurement depth.

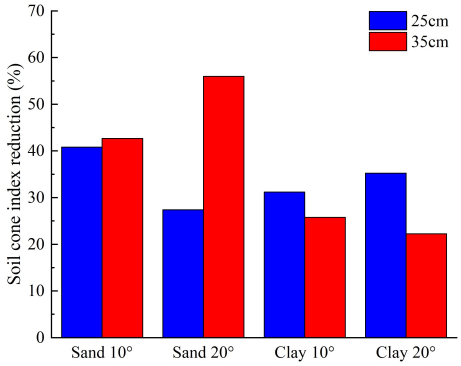

Figure 4.3.12 Soil cone index reduction (%) after the tillage

Soil surface flatness

Here is the standard deviation of the zero value length at different angles, and tillage depth represents the soil surface flatness, as shown in Table 4.3.1 Lowercase letters (abc) indicate the comparison under different tillage depth conditions within the same angle. Capital letters (ABC) indicate the comparison under different angle conditions within the same tillage depth. Before the tillage process, a significant difference was observed between sand and clay soil, indicating that the sand soil exhibited a more uneven surface than the clay soil. After the tillage process, in most angle and tillage depth conditions, the soil surface displayed a lower standard deviation (indicating increased flatness) than the measurements taken before tillage. However, these differences were not statistically significant for both sand and clay soil. When comparing different angles, angle 20 generally resulted in a higher standard deviation (indicating a less flat surface) than angle 10 after the tillage, regardless of the tillage depth (25cm or 35cm). However, it is essential to note that a statistically significant difference at the 0.05 level was only observed in the comparison between angle 20 and angle 10 at a tillage depth of 35 cm in clay soil. Regarding tillage depth, the tillage depth of 35 cm generally exhibited a lower standard deviation (indicating increased flatness) compared to the tillage depth of 25 cm within the same angle condition for both sand and clay soil after the tillage. However, a statistically significant difference at the 0.05 level was only observed in the comparison between the 25cm and 35cm tillage depths at an angle of 10 degrees in clay soil.

Table 4.3.1 Soil surface flatness (sd) before and after tillage at different angles of subsoiler and tillage depth conditions in sand and clay soil

Soil	Angle	Tillage depth	Before tillage	After tillage
Sand	10	25	1.5412±0.0116Aa	1.5644±0.4689Aa
	10	35	1.1155±0.1452Ab	1.2880±0.1364Aa
	20	25	2.0830±0.5383Aa	1.8304±0.0690Aa
	20	35	1.9347±0.6593Aa	1.5972±0.4922Aa
Clay	10	25	1.3901±0.0416Ba	1.3505±0.0487Aa
	10	35	1.4477±0.0904Ba	1.0893±0.0393Bb
	20	25	1.6649±0.1298Aa	1.7035±0.3090Aa
	20	35	1.6744±0.2010Aa	1.4950±0.1465Aa

Fuel consumption

According to Figure 4.3.13, fuel consumption is higher for the same soil type and depth when the subsoiling angle is inclined by 10° compared to 20°. In sandy soil, at a depth of 35 cm, fuel consumption with a 10° inclination is 34.26 l/h and 31.07 l/h with a 20° inclination, and at a depth of 25 cm, the values are 26.11 l/h and 22.48 l/h, respectively. In clayey soil, the effect of inclination is smaller, with consumption values of 38.70 l/h at 10° and 37.84 l/h at 20° at a depth of 35 cm, and 30.26 l/h at 10° and 29.30 l/h at 20° at a depth of 25 cm. The analysis revealed a significant difference in fuel consumption between sandy and clay soils. Specifically, fuel consumption was significantly higher in clay soil than in sandy soil at a significance level of 0.05.

Additionally, a significant increase in fuel consumption was observed as the working depth increased from 25 cm to 35 cm in both clayey and sandy soils at a significance level of 0.05. In the case of sandy soil, there was a significant decrease in fuel consumption at a significance level of 0.05 as the blade inclination angle changed from 10° to 20° at both 25 cm and 35 cm depths. However, no significant difference in fuel consumption was found when the blade inclination angle changed from 10° to 20° in clayey soil at 25 cm and 35 cm depths.

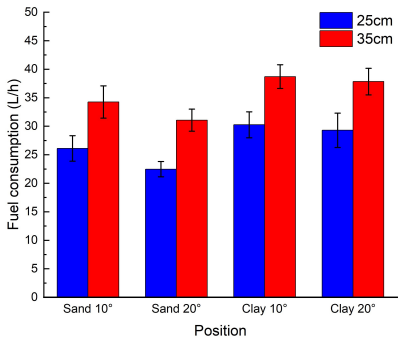

Figure 4.3.13 Fuel consumption in different soil, angle, and depth conditions

Traction force analysis

Figure 4.3.14 presents the traction force values for different working conditions,

highlighting the relationship between depth, angle, and traction force. The result showed that working at greater depths generally requires higher traction forces. In sandy soil, when working at a depth of 25 cm, the tractor needs 48.03 kN of traction force at a 10° inclination and 43.99 kN at a 20° inclination. However, at a depth of 35 cm, the required traction force increases to 58.04 kN at a 10° inclination and 67.06 kN at a 20° inclination. For clay soil, at a depth of 25 cm, the tractor necessitates 52.10 kN of traction force at a 10° inclination and 53.33 kN at a 20° inclination. At a depth of 35 cm, the required traction force is 65.34 kN at a 10° inclination and 65.89 kN at a 20° inclination. Notably, in sandy soil at a depth of 25 cm, there is a significant decrease in traction force when the angle changes from 10° to 20°. In contrast, at a depth of 35 cm, there is a significant increase in traction force when the angle changes from 10° to 20°. However, no significant differences in traction forces were observed in clay soil at a significance level of 0.05, regardless of the angle or depth.

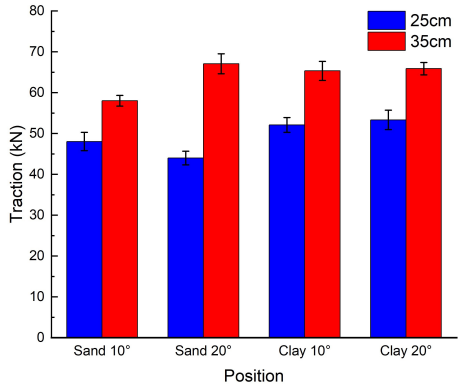

Figure 4.3.14 Traction force (kN) in different soil, angle, and depth conditions

Slip rate

The slip rate result showed higher percentages in working conditions at greater depths and with a 10° inclination of the wings of the subsoilers for both sandy and clayey soil as shown in Figure 4.3.15. Sandy soil values are influenced by both working depth and inclination, while clayey soil values are mainly influenced by inclination. At a depth of 25 cm in sandy soil, slip is 9.86% at 10° inclination and 5.92% at 20° inclination, while at a depth of 35 cm, slip is 14.74% at 10° inclination and 12.46% at 20° inclination. In clayey soil, slip is 11.61% at 10° and 10.74% at 20° inclination at a depth of 25 cm, and 19.66% at 10° and 18.32% at 20° inclination at a depth of 35 cm.

The analysis revealed a significant difference between the two soil types at a significance level of 0.05. Furthermore, significant differences were observed between the different working depths, with the 35 cm depth consistently showing a higher slip rate than the 25 cm depth in both soil types. Regarding the angle of the subsoiler, there was a significant difference in slip rates between 10° and 20°angles in sandy soil at both depths, with lower slip

rates observed for the 20° angle. However, in clayey soil, the difference in slip rates between 10° and 20° angles was not statistically significant at 0.05 level.

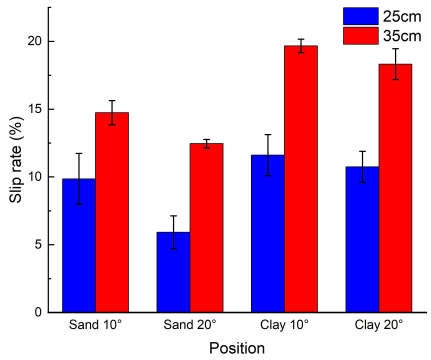

Figure 4.3.15 Slip rate (%) in different soil, angle, and depth conditions

Comparison between simulation and field experiment result

Figure 4.3.16 shows the correlation between field experiment traction with both simulation horizontal traction (left) and total traction (right). The Pearson correlation coefficient value is 0.817 and 0.752, respectively. The p-value is 0.013 and 0.031, which are both lower than 0.05. Although the simulation result is lower than the field experiment results both in sand and clay soil condition, the result showed that both simulation horizontal traction and simulation total traction showed a significant correlation with the field experiment traction at 0.05 level.

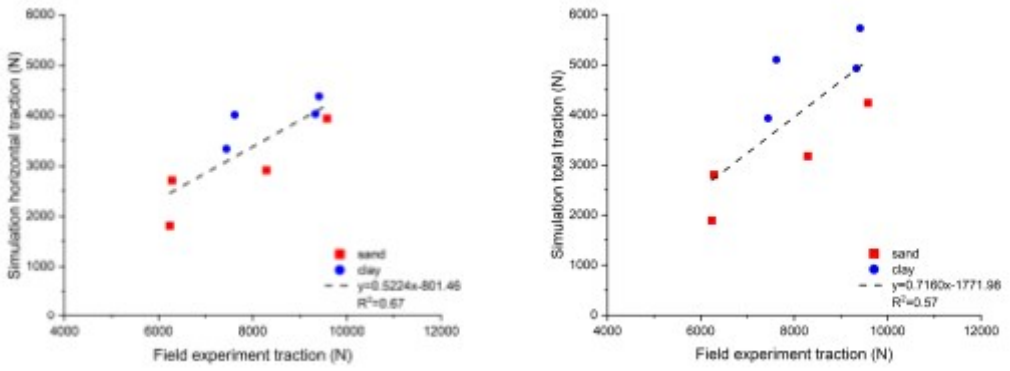

Figure 4.3.16 Correlation between field experiment traction with simulation horizontal traction (left) and field experiment traction with simulation total traction (right)

Figure 4.3.17 showed the Correlation between simulation total traction and simulation soil particles total energy. The Pearson correlation coefficient value is 0.834. The p-value is 0.010. The result showed a significant correlation between the simulation soil particles' total energy and the simulation total traction at 0.05 level. However, no significant correlation was found between the simulation soil particles' total energy and field experiment traction at 0.05 level. The Pearson correlation coefficient value is 0.542 and the p-value is 0.165.

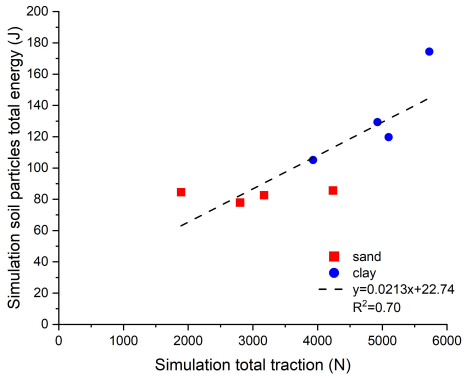

Figure 4.3.17 Correlation between simulation total traction and simulation soil particles total energy

Figure 4.3.18 showed the Correlation between field experiment traction with fuel consumption (left) and field experiment traction with slip rate (right). The Pearson correlation coefficient value is 0.858 and 0.825, respectively. The p-value is 0.006 and 0.012, which are both lower than 0.05. The result showed that fuel consumption and slip rate significantly correlated with the field experiment traction at 0.05 level.

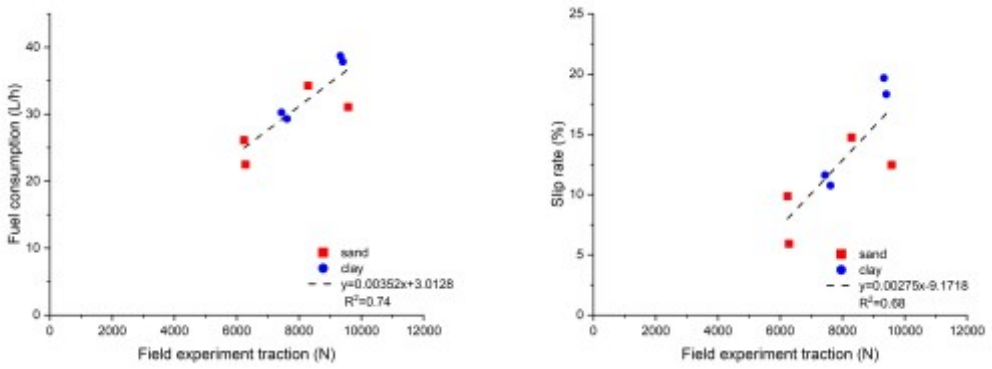

Figure 4.3.18 Correlation between field experiment traction with fuel consumption (left) and field experiment traction with slip rate (right)

4.4 Discussion

Simulation Results

Our study investigated the traction resistance of the subsoiler, energy and velocity of the soil particle in two simulated soil environments. The aim was to determine how the angle and depth of subsoiling affect the horizontal and vertical forces required for soil penetration, as well as the total energy required for tillage and the average velocity of soil particles in the horizontal and vertical directions.

The results of the study indicated that the traction resistance experienced by the subsoiler was affected by both the depth of tillage and the angle of the subsoiler. Specifically, our result demonstrated that the 35cm depth had higher resistance than the 25 cm depth for all inclination conditions of the subsoiler both in clay and soil condition. For the sand soil

simulation, when the angle was set to 10 degrees, the lowest horizontal traction resistance was observed for both 25cm and 35cm tillage depths. Moreover, the results revealed that a decrease in resistance was observed as the angle increased from less than 10 degrees, while an increase in resistance was observed as the angle exceeded 10 degrees. The vertical traction resistance of the subsoiler showed that the resistance decreased as the angle increased. At an angle of 10 degrees, the resistance was higher compared to nearby angles of 7.5 and 12.5 degrees. Furthermore, the total traction resistance of the subsoiler demonstrated that the trend of the total resistance followed that of the horizontal direction. The results indicated that the lowest total resistance was obtained when the angle was 10 degrees. When the angle was below 10 degrees, the resistance decreased as the angle increased, while it increased when the angle was greater than 10 degrees. However, The 10 degrees show no highest or lowest traction among other angles for the clay soil simulation. The horizontal and vertical traction resistance increased with the angle increase from 0 to 25 degrees.

The performance of the subsoilers is affected by the angle of the subsoiler (Li et al., 2018). For example, in a previous study, a pair of wings with 10° and 20° bend angles was developed and attached to the subsoiler foot. Among all the wings, the 10° forward bent wing showed the best performance based on the highest values of horizontal force, soil loosening area, soil upheaving area, lowest specific draft, bulk density and soil cone index compared to the other angle of the wings (Askari et al., 2016). And also, the same researcher found that the highest draft, disturbed area and remaining residue plus the lowest specific draft and mean weight diameter were obtained when applying the 10° forward bent-winged tines (Askari et al., 2019). However, different subsoil types may perform best in different angles and soil conditions (Raper, 1996; Wang et al., 2020; Zhang et al., 2022).

The total energy of soil particles, comprising translational and rotational kinetic energy, was analysed in our study. The findings revealed that a subsoiler angle of 10 degrees exhibited the highest total energy at a tillage depth of 25cm, while the lowest total energy was observed at a tillage depth of 35cm in sand soil simulation. However, no significant differences in total energy were found among different angles at 25cm or 35cm tillage depths in sand soil conditions. But in the clay simulation, 20 degree showed significant differences compared to 10, 0, and 5 degree angles at 0.05 level. Lower total energy indicates lower energy consumption during tillage, as demonstrated by previous studies (Wang et al., 2020; Zhang et al., 2022). Therefore, our result showed that the subsoiler set at a higher degree angle consumes more energy in 25cm and 35cm depth conditions in clay soil.

Our study analysed the average velocity of soil particles in horizontal and vertical directions. The results revealed that the average horizontal velocity of soil particles increased

as the angle of the subsoiler increased in sand soil. However, the increasing trend in clay soil is not clear. Although the average velocity of soil particles in the vertical direction showed a slight increase with an increase in the subsoiler angle, no significant differences were observed in the average vertical velocities of soil particles for different angles at a significance level of 0.05 in sand and clay soil. Furthermore, the results indicated that as the subsoiler angle increased, the average velocity of soil particles also increased in sand soil. However, at an angle of 10 degrees, the average velocity was smaller compared to neighbouring angles in sand soil. Moreover, in clay soil simulation, the average velocity increases first and then decrease at 20 degree in 25 cm depth. Controversy, the average velocity reduce first and then increase at 15 degree in 35 cm depth. However, when considering the combination of 25 cm and 35 cm depths, no significant differences were found among the different angles of the average velocity in clay soil at 0.05 level. It is worth noting that while some studies have described the velocity contours of soil particles, quantitative analysis of soil particle velocity to measure soil disturbance was not calculated in those studies (Chen et al., 2013; Li et al., 2018, 2016; Zhang et al., 2022).

Field Experiment Results

Our study investigated the soil cone index before and after the tillage, soil surface flatness, fuel consumption, traction force and slip rate in the field experiment. Our aim was to determine how the angle and depth of the subsoiler affect the soil structure and tillage, as well as the energy required for tillage and the working efficiency.

The soil cone index results showed that after tillage, the soil cone index was reduced in all conditions. The results showed varying reductions in soil cone index after tillage depending on the soil type, angle of the subsoiler, and tillage depth. Based on the information provided in the summary, the reduction in soil cone index after tillage was generally higher for sand soils than clay soils.

The analysis of the soil cone index after tillage revealed variations that depend on the subsoiler's angle and tillage depth. Our findings indicate that at a tillage depth of 35 cm, there is a significant difference in the soil cone index after tillage between the 10° and 20° angles of the subsoiler. This suggests that the angle of the subsoiler has a noticeable impact on the soil structure at this depth. In contrast, when the tillage depth is 25 cm, no significant difference in the soil cone index is observed between the subsoiler's 10° and 20° angles. This indicates that the angle of the subsoiler has less influence on the soil structure at this shallower depth. Furthermore, our results highlight that sand soil is more sensitive to the subsoiler's angle than clay soil. In both the 25 cm and 35 cm tillage depth conditions, there is a significant difference in the soil cone index between the 10° and 20° angles of the subsoiler in sand soil.

However, no significant difference was found in clay soil when comparing the 10° and 20° angles at the same tillage depth. However, the reduction also varied depending on the angle of the subsoiler and the tillage depth. Varying soil structures can be observed due to different subsoiling tillage methods. Hence, the selection of an appropriate tillage depth is critical, not only for economic advantages but also for agronomic benefits (Sun et al., 2023).

The results of soil surface flatness indicate that sand soil initially had a more uneven surface than clay soil. After the tillage process, the surface became flatter, but no significant differences were observed in the comparison between before and after tillage for both soil types. Angle 20 generally resulted in a less flat surface compared to angle 10, and a tillage depth of 35 cm generally produced a flatter surface compared to 25 cm. However, significant differences at the 0.05 level were only observed in specific comparisons, as mentioned above. As for the fuel consumption result, our study showed that fuel consumption is higher when the tillage depth is 35 cm compared to the 25 cm depth. In the case of sandy soil, there was a significant decrease in fuel consumption at a significance level of 0.05 as the blade inclination angle changed from 10° to 20° at both 25 cm and 35 cm depths. However, no significant difference in fuel consumption was found when the blade inclination angle changed from 10° to 20° in clayey soil at 25 cm and 35 cm depths. The disparity between the lower traction observed in the sand soil simulation at a 10-degree angle and the higher fuel consumption observed in the field experiment is intriguing. This inconsistency can be attributed to various factors, such as the design of shanks specifically tailored for certain depths, which may result in excessive traction resistence when utilised at different depths. However, recording instantaneous fuel consumption is difficult during the experiment, and repeated experiments can be added in future experiments to verify the results. Moreover, the performance of tillage equipment can vary based on the specific depth and soil type conditions encountered (Raper, 1996).

The traction resistance result showed that the traction increased as the tillage depth increased from 25 cm to 35 cm. It suggests that deeper tillage requires more force to pull the tillage implemented through the soil, affecting fuel consumption and productivity. The simulation result also proved that the clay has more traction resistance than the sand soil. Generally, clay soils require more traction resistance than sandy soils, likely due to their higher clay content and increased soil density. Research has demonstrated that different subsoilers exhibit varying levels of traction resistance depending on the soil type. For instance, studies involving angled shank and curved shank subsoilers in Norfolk sandy loam and Decatur clay loam soil have revealed distinct differences in traction resistance (Raper, 1996). These findings highlight the importance of considering both the subsoiler design and the

specific soil characteristics to optimise traction and tillage performance. And also, data suggest that the effect of the angle of the wings on traction resistance may depend on the soil type. In sandy soil, a subsoiler angle of 20° resulted in higher traction resistance than an angle 10° at a depth of 35 cm, but this trend was so clear in clayey soil. This could be due to differences in soil structure and composition and how the subsoiler interacts with the soil. Overall, these findings highlight the importance of considering soil type, depth, and subsoiler angle when designing and implementing tillage operations. Farmers and agricultural professionals can make more informed decisions about tillage practices and equipment by understanding the factors that influence traction resistance, potentially improving efficiency and reducing costs.

The result of the slip rate showed that deeper tillage has higher slip rates in sandy and clay soil. Regarding the angle of the subsoiler, there was a significant difference in slip rates between 10° and 20°angles in sandy soil at both depths, with lower slip rates observed for the 20° angle. However, in clayey soil, the difference in slip rates between 10° and 20° angles was not statistically significant at 0.05 level. It suggests that the angle of the subsoiler has a more significant impact on slip rates in sandy soils than in clayey soils. Overall, slip rates were higher in clayey soils than in sandy soils, which is likely since clay soils have a higher water-holding capacity and tend to be more cohesive, making them more difficult to tillage. These findings suggest that slip rates are affected by a combination of soil type, depth of tillage, and blade inclination angle and should be considered when selecting appropriate tillage practices for different soil types and conditions.

In summary, this study study demonstrated that the angle and depth of subsoiler tillage significantly impact the soil cone index, soil surface flatness, fuel consumption, traction force, and slip rate. The results suggest that the reduction in soil cone index after tillage was generally higher for sand soils than clay soils, but the reduction varied depending on the angle of the subsoiler and tillage depth. Traction resistance increased as the tillage depth increased from 25 cm to 35 cm, and clay soils require more traction resistance than sandy soils. Slip rates were influenced by soil type, tillage depth, and blade inclination angle, with higher slip rates observed in clayey soils than sandy soils. Deeper tillage has a higher slip rate, and there was a significant decrease in fuel consumption as the subsoiler angle changed from 10 to 20° in sandy soil. Overall, these findings highlight the importance of considering soil type, depth, and subsoiler angle when designing and implementing tillage operations to improve efficiency and reduce costs.

4.5 Conclusion

The result of this study showed that the reduction in soil cone index was influenced by

both the angle and depth of subsoiler tillage. Traction resistance increased with greater tillage depth and varies based on soil type and subsoiler angle. Furthermore, the chosen tillage depth and subsoiler angle significantly affect fuel consumption during subsoiling operations, presenting an opportunity for optimising fuel efficiency through appropriate selection. The analysis also reveals that slip rate, which reflects the effectiveness of tillage, is influenced by soil type, tillage depth, and subsoiler angle. No significant difference in soil surface flatness was observed across most tillage depths and working angles after the tillage operation. Significant correlations were observed between simulation traction with field experiment traction, simulation soil particle energy with simulation traction, and fuel consumption with field experiment traction, all at a significance level of 0.05.

These findings have practical implications for farmers and agricultural professionals. They can make informed decisions to improve efficiency, reduce costs, and enhance soil structure by considering soil type, tillage depth, and subsoiler angle. Furthermore, the study suggests avenues for future research to expand our understanding of these factors in different soil types and tillage conditions. Overall, this study contributes to the knowledge base surrounding subsoiler tillage and provides valuable insights for optimising tillage practices in agriculture. By incorporating these findings into their operations, farmers can strive for increased productivity and sustainability in their farming practices.

5. Conclusion

The first objective, centered on the intricate relationship between soil compaction and varying levels of traction resistance during agricultural operations, yields profound insights into the dynamic nature of this phenomenon. Through an exhaustive field experiment, we meticulously quantified an array of soil parameters, including soil stress, bulk density, moisture content, cone index, soil surface disturbance, rolling resistance, and slip rate, under diverse traction conditions and varying pass frequencies. Our research brings to the forefront the undeniable impact of traction resistance on soil dynamics.

Significantly, the results underscore the pronounced increase in soil stress and physical property alterations, including heightened soil bulk density, moisture content, and cone index, as traction and the number of passes intensify. It is noteworthy, however, that despite the variation in traction conditions, no significant differences were observed for the number of passes. This underscores the need to consider the dynamic factors of traction and rolling resistance alongside static weight when addressing soil compaction.

Moreover, our study underscores the pivotal role played by the permanent traffic lane, which consistently exhibited superior performance in terms of slip rate and energy

consumption across different traction conditions. Notably, the permanent traffic lane exhibited remarkable fuel savings, emphasizing its potential in not only mitigating the adverse effects of soil compaction stemming from random traffic but also enhancing operational efficiency and energy conservation. These findings resonate with a paradigm shift in soil compaction research, urging us to consider dynamic aspects, such as traction and rolling resistance, alongside traditional static weight metrics. We propose the adoption of controlled traffic farming (CTF) systems and more frequent tractor usage on permanent traffic lanes as practical measures to amplify efficiency and curtail energy consumption in agricultural practices.

Objective two delved into the intriguing realm of field variability and its implications for crop yield. By meticulously scrutinizing yield maps and Vegetation Indices (VIs) derived through Google Earth Engine (GEE), we dissected the yield differences across headlands, field edges, and the fertile field center. Notably, field size, clay content, and sand content played pivotal roles in shaping these disparities.

Our findings resoundingly validate that headlands and field edges consistently produce lower crop yields in comparison to the fecund field center. The quantitative data paints a clear picture, with yield maps indicating a reduction of 12.20% and 2.49% in headlands and field edges, respectively, compared to the bountiful field center. Concurrently, VIs underscored these discrepancies, revealing reductions of 4.27% and 2.70% (NDVI), 4.17% and 2.67% (GNDVI), and 5.87% and 3.59% (NDRE) in headlands and field edges across different metrics.

Furthermore, our investigation highlighted a critical facet of this field variability – the amplification of differences with increasing clay content and their mitigation with higher sand content. This crucial insight underscores the need for future studies to consider additional factors like soil organic content and crop type, to paint a more comprehensive picture of field variability. Moreover, our findings strongly advocate strategic machine traffic planning to mitigate yield losses in headlands and field edges, and thus boost overall agricultural productivity.

The third objective is rooted in the realm of subsoiler tillage, where we explored the nuanced relationship between subsoiler parameters, namely depth and angle, soil compaction, and fuel consumption. Our findings illuminate the intricate dynamics of subsoiler tillage, holding significant implications for optimizing fuel efficiency and enhancing soil structure.

A pivotal discovery emanates from our investigation's revelation that soil cone index reduction is profoundly influenced by the combined effects of subsoiler angle and depth. This finding underscores the need for precision in selecting subsoiler parameters to effectively combat soil compaction.

Additionally, we unveil a noteworthy observation: traction resistance escalates with increased tillage depth, albeit with variations that are contingent on soil type and subsoiler angle. This crucial insight opens the door to optimizing fuel efficiency by prudent parameter selection in subsoiler operations.

Simultaneously, our study delves into the compelling realm of slip rate, which serves as an indicator of tillage effectiveness. It demonstrates that slip rate is a multifaceted parameter influenced by diverse factors such as soil type, tillage depth, and subsoiler angle. Importantly, we discerned no significant differences in soil surface flatness across most tillage depths and angles after the tillage operation.

Practically speaking, our findings offer invaluable guidance for farmers and agricultural professionals. They empower decision-makers to make informed choices that enhance operational efficiency, curtail costs, and foster improved soil structure. The study also paves the way for promising avenues of future research, inviting further exploration of these factors in diverse soil types and tillage conditions, thus expanding the boundaries of our knowledge. By incorporating these research-driven insights into their daily operations, farmers stand poised to enhance productivity and sustainability in their agricultural endeavors.

Collectively, these three objectives provide a comprehensive understanding of the intricate interplay between soil compaction, machinery performance, and their far-reaching consequences for agricultural sustainability and productivity.

Our research underscores the imperative of encompassing dynamic elements such as traction, rolling resistance, and subsoiler parameters, transcending traditional static weight metrics in addressing soil compaction. Thoughtful management of these factors holds significant promise in alleviating soil compaction, fostering soil vitality, and curtailing energy consumption, all of which ultimately contribute to bolstering agricultural sustainability.

Moreover, our findings illuminate the pivotal role of field variability, emphasizing that crop yield is far from uniform across the expanse of a field. The identification of reduced yields in headlands and field edges, correlated with specific soil properties, underscores the pivotal role of judicious machine traffic planning in optimizing crop yields and minimizing losses.

Lastly, our exploration of subsoiler tillage adds an additional layer of depth by shedding light on the pivotal influence of subsoiler parameters in mitigating soil compaction and enhancing fuel efficiency. This nuanced comprehension of tillage dynamics empowers farmers with practical insights to enhance operational efficiency and trim costs.

In summary, this doctoral research represents a substantive contribution to the body of knowledge surrounding soil compaction, machinery performance, and tillage practices. Its real-world implications extend to both agricultural practitioners and professionals, offering

pathways to amplify productivity, diminish environmental impact, and foster a sustainable future for agriculture. As we navigate the ever-evolving terrain of modern agriculture, harnessing these insights becomes imperative to maximize the potential of our agricultural systems while minimizing their ecological footprint.

6. Bibliography

A website for precision farming service Https://onesoil.ai/en/ (accessed 17.1.23) [WWW Document], n.d.

Abebe, A.T., Tanaka, T., Yamazaki, M., 1989. Soil compaction by multiple passes of a rigid wheel relevant for optimization of traffic. J. Terramechanics 26, 139–148. https://doi.org/10.1016/0022-4898(89)90003-7

Abu-Hamdeh, N.H., Reeder, R.C., 2003. Measuring and predicting Stress Distribution under Tractive Devices in Undisturbed Soils. Biosyst. Eng. 85, 493–502. https://doi.org/10.1016/s1537-5110(03)00069-2

Aikins, K.A., Antille, D.L., Ucgul, M., Barr, J.B., Jensen, T.A., Desbiolles, J.M.A., 2021. Analysis of effects of operating speed and depth on bentleg opener performance in cohesive soil using the discrete element method. Comput. Electron. Agric. 187, 106236. https://doi.org/10.1016/j.compag.2021.106236

Al-Gaadi, K.A., Hassaballa, A.A., Tola, E., Kayad, A.G., Madugundu, R., Alblewi, B., Assiri, F., 2016. Prediction of potato crop yield using precision agriculture techniques. PLoS One 11, 1–16. https://doi.org/10.1371/journal.pone.0162219

Alaoui, A., Rogger, M., Peth, S., Blöschl, G., 2018. Does soil compaction increase floods? A review. J. Hydrol. 557, 631–642. https://doi.org/10.1016/j.jhydrol.2017.12.052

Ani, O.A., Uzoejinwa, B.B., Ezeama, A.O., Onwualu, A.P., Ugwu, S.N., Ohagwu, C.J., 2018. Overview of soil-machine interaction studies in soil bins. Soil Tillage Res. 175, 13–27. https://doi.org/10.1016/j.still.2017.08.002

Anken, T., Holpp, M., 2011. Controlled traffic farming In Canada. Encycl. Earth Sci. Ser. Part 4, 153–155. https://doi.org/10.1007/978-90-481-3585-1_32

Ankeny, M.D., Kaspar, T.C., Horton, R., 1990. Characterization of Tillage and Traffic Effects on Unconfined Infiltration Measurements. Soil Sci. Soc. Am. J. 54, 837–840. https://doi.org/10.2136/sssaj1990.03615995005400030037x

Antille, D.L., Bennett, J.M.L., Jensen, T.A., 2016. Soil compaction and controlled traffic considerations in Australian cotton-farming systems. Crop Pasture Sci. 67, 1–28.

https://doi.org/10.1071/CP15097

Antille, D.L., Chamen, W.C.T.T., Tullberg, J.N., Lal, R., 2015. The potential of controlled traffic farming to mitigate greenhouse gas emissions and enhance carbon sequestration in arable land: A critical review. Trans. ASABE 58, 707–731. https://doi.org/10.13031/trans.58.11049

Arvidsson, J., 2001. Subsoil compaction caused by heavy sugarbeet harvesters in southern Sweden I. Soil physical properties and crop yield in six field experiments. Soil Tillage Res. 60, 67–78. https://doi.org/10.1016/S0167-1987(01)00169-6

Arvidsson, J., Andersson, S., 1997. Determination of soil displacement by measuring the pressure of a column of liquid. Bibl. Fragm. Agron. 2.

Arvidsson, J., Håkansson, I., 2014. Response of different crops to soil compaction-Short-term effects in Swedish field experiments. Soil Tillage Res. 138, 56–63. https://doi.org/10.1016/j.still.2013.12.006

Arvidsson, J., Keller, T., 2007. Soil stress as affected by wheel load and tyre inflation pressure. Soil Tillage Res. 96, 284–291. https://doi.org/10.1016/j.still.2007.06.012

Arvidsson, J., Ristic, S., 1996. Soil stress and compaction effects for four tractor tyres. J. Terramechanics 33, 223–232. https://doi.org/10.1016/S0022-4898(97)00006-2

Arvidsson, J., Trautner, A., Van Den Akker, J.J.H., Schjønning, P., 2001. Subsoil compaction caused by heavy sugarbeet harvesters in southern Sweden II. Soil displacement during wheeling and model computations of compaction. Soil Tillage Res. 60, 79–89. https://doi.org/10.1016/S0167-1987(01)00168-4

Arvidsson, J., Westlin, H., Keller, T., Gilbertsson, M., 2011. Rubber track systems for conventional tractors - Effects on soil compaction and traction. Soil Tillage Res. 117, 103–109. https://doi.org/10.1016/j.still.2011.09.004

ASAE Standards, 1999. Soil cone penetrometer S 313.3. Am. Soc. Agric. Eng. 3–5.

Askari, M., Shahgholi, G., Abbaspour-Gilandeh, Y., 2019. New wings on the interaction between conventional subsoiler and paraplow tines with the soil: effects on the draft and the properties of soil. Arch. Agron. Soil Sci. 65, 88–100. https://doi.org/10.1080/03650340.2018.1486030

Askari, M., Shahgholi, G., Abbaspour-Gilandeh, Y., Tash-Shamsabadi, H., 2016. The effect of new wings on subsoiler performance. Appl. Eng. Agric. 32, 353–362. https://doi.org/10.13031/aea.32.11500

Asrar, G., Kanemasu, E.T., Yoshida, M., 1985. Estimates of Leaf Area Index from Spectral Reflectance of Wheat Under Different Cultural Practices and Solar Angle. Remote Sens. Environ. 17, 1–11.

Azevedo, R.P., Corinto, L.M., Peixoto, D.S., De Figueiredo, T., Silveira, G.C.D., Peche, P.M., Pio, L.A.S., Pagliari, P.H., Curi, N., Silva, B.M., 2022. Deep Tillage Strategies in Perennial Crop Installation: Structural Changes in Contrasting Soil Classes. Plants 11, 1–21. https://doi.org/10.3390/plants11172255

Badalikova, B., Hrub\`y, J., 2006. Influence of minimum soil tillage on development of soil structure. Soil Manag. Sustain. Adv. Geoecology 38, 430–435.

Báez-González, A.D., Chen, P.Y., Tiscareño-López, M., Srinivasan, R., 2002. Using satellite and field data with crop growth modeling to monitor and estimate corn yield in Mexico. Crop Sci. 42, 1943–1949. https://doi.org/10.2135/cropsci2002.1943

Bailey, A.C., Nichols, T.A., Johnson, C.E., 1988. Soil Stress State Determination Under Wheel Loads. Trans. ASAE 31, 1309–1314. https://doi.org/10.13031/2013.30862

Bakker, D.M., Harris, H.D., Wong, K.Y., 1995. Measurement of Stress Paths under Agricultural Vehicles and their Interpretation in Critical State Space. J. Agric. Eng. Res. 61, 247–260. https://doi.org/10.1006/jaer.1995.1052

Ball, B.C., 2013. Soil structure and greenhouse gas emissions: A synthesis of 20 years of experimentation. Eur. J. Soil Sci. 64, 357–373. https://doi.org/10.1111/EJSS.12013

Barać, S., Petrović, D., Radojević, R., Vuković, A., Biberdžić, M., others, Saša, B., Dragan, P., Rade, R., Aleksandar, V., Milan, B., 2015. Influence of soil compaction on soil changes and yield of barley and rye at the headlands and inner part of plot., in: Second International Symposium on Agricultural Engineering, ISAE-2015, 9th-10th October 2015, Belgrade-Zemun, Serbia. Proceedings. pp. 27–34.

Barbour, P.J., Martin, S.W., Burger, W., 2007. Estimating Economic Impact of Conservation Field Borders on Farm Revenue. Crop Manag. 6, 1–11. https://doi.org/10.1094/cm-2007-0614-01-rs

BASHFORD, C.Jenane.L.L., 1995. Field tractive performance comparisons between a tractor operated in the 2WD and 4WD mode 15, 47–54.

Battiato, A., 2014. SOIL-TYRE INTERACTION ANALYSIS FOR AGRICULTURAL TRACTORS: MODELLING OF TRACTION PERFORMANCE AND SOIL DAMAGE.

Battiato, A., Alaoui, A., Diserens, E., 2015. Impact of Normal and Shear Stresses Due to Wheel Slip on Hydrological Properties of an Agricultural Clay Loam: Experimental and New Computerized Approach. J. Agric. Sci. 7, 1–19. https://doi.org/10.5539/jas.v7n4p1

Battiato, A., Diserens, E., 2017. Tractor traction performance simulation on differently textured soils and validation: A basic study to make traction and energy requirements accessible to the practice. Soil Tillage Res. 166, 18–32. https://doi.org/10.1016/j.still.2016.09.005

Battiato, A., Diserens, E., 2013. Influence of Tyre Inflation Pressure and Wheel Load on the Traction Performance of a 65 kW MFWD Tractor on a Cohesive Soil. J. Agric. Sci. 5, 197–215. https://doi.org/10.5539/jas.v5n8p197

Bengough, A.G., Bransby, M.F., Hans, J., McKenna, S.J., Roberts, T.J., Valentine, T.A., 2006. Root responses to soil physical conditions; growth dynamics from field to cell, Journal of Experimental Botany. https://doi.org/10.1093/JXB/ERJ003

Berli, M., Eggers, C.G., Accorsi, M.L., Or, D., 2006. Theoretical Analysis of Fluid Inclusions for In Situ Soil Stress and Deformation Measurements. Soil Sci. Soc. Am. J. 70, 1441–1452. https://doi.org/10.2136/sssaj2005.0171

Berli, M., Kirby, J.M., Springman, S.M., Schulin, R., 2003. Modelling compaction of agricultural subsoils by tracked heavy construction machinery under various moisture conditions in Switzerland. Soil Tillage Res. 73, 57–66. https://doi.org/10.1016/S0167-1987(03)00099-0

Beylich, A., Oberholzer, H.-R., Schrader, S., Höper, H., Wilke, B.-M., 2010. Evaluation of soil compaction effects on soil biota and soil biological processes in soils. Soil Tillage Res. 109, 133–143. https://doi.org/10.1016/j.still.2010.05.010

Blanco-Canqui, H., Claassen, M.M., Stone, L.R., 2010. Controlled Traffic Impacts on Physical and Hydraulic Properties in an Intensively Cropped No-Till Soil. Soil Sci. Soc. Am. J. 74, 2142–2150. https://doi.org/10.2136/sssaj2010.0061

Bluett, C., Tullberg, J.N., McPhee, J.E., Antille, D.L., 2019. Soil and Tillage Research: Why still focus on soil compaction? Soil Tillage Res. 194, 104282. https://doi.org/10.1016/j.still.2019.05.028

Blunden, B.G., Mcbride, R.A., Daniel, H., Blackwell, P.S., 1994. Compaction of an earthy sand by rubber tracked and tired vehicles. Soil Res. 32, 1095. https://doi.org/10.1071/sr9941095

Boatman, N.D., 1994. Field margins: integrating agriculture and conservation. Proceedings of a symposium held at Coventry, UK, 18-20 April 1994.

Boatman, N.D., 1992. Effects of herbicide use, fungicide use and position in the field on the yield and yield components of spring barley. J. Agric. Sci. 118, 17–28. https://doi.org/10.1017/S0021859600067964

Boatman, N.D., Sotherton, N.W., 1988. Agronomic consequences and costs of managing field margins for game and wildlife conservation. Conf. Environ. Asp. Appl. Biol. 19-21, 1988, Univ. York, England. Incl. Ref.

Bochtis, D.D., Vougioukas, S.G., 2008. Minimising the non-working distance travelled by machines operating in a headland field pattern. Biosyst. Eng. 101, 1–12.

https://doi.org/10.1016/j.biosystemseng.2008.06.008

Bodria, L., Pellizzi, G., Piccarolo, P., 2013. Meccanica e meccanizzazione agricola.

Boguzas, V., Håkansson, I., others, 2001. Barley yield losses simulation under Lithuanian conditions using the Swedish soil compaction model., in: Proceedings of the International Conference on Sustainable Agriculture in Baltic States, Tartu, Estonia, 28-30 June, 2001. pp. 24–28.

Bolling, I., 1987. Bodenverdichtung und Triebkraftverhalten bei Reifen-Neue Meß-und Rechenmethoden. Lehrstuhl für Landmaschinen, Techn. Univ.

Botta, G.F., Jorajuria, D., Rosatto, H., Ferrero, C., 2006. Light tractor traffic frequency on soil compaction in the Rolling Pampa region of Argentina. Soil Tillage Res. 86, 9–14. https://doi.org/10.1016/j.still.2005.01.014

Boussinesq, J., 1885. Application des potentiels à l'étude de l'équilibre et du mouvement des solides élastiques: principalement au calcul des déformations et des pressions que produisent, dans ces solides, des efforts quelconques exercés sur une petite partie de leur surface . Gauthier-Villars.

Bouwman, L.A., Arts, W.B.M., 2000. Effects of soil compaction on the relationships between nematodes, grass production and soil physical properties. Appl. Soil Ecol. 14, 213–222. https://doi.org/10.1016/S0929-1393(00)00055-X

Braunack, M. V, Johnston, D.B., 2014. Changes in soil cone resistance due to cotton picker traffic during harvest on Australian cotton soils. Soil Tillage Res. 140, 29–39. https://doi.org/10.1016/j.still.2014.02.007

Brunotte, Joachim, Nolting, K., Fröba, N., Ortmeier, B., 2012. Bodenschtuz beim Pflügen: Wie hoch ist die Radlast am Furchenrad? Die Landtechnik 67, 265 – 269.

Brunotte, J, Nolting, K., Fröba, N., Ortmeier, B., 2012. Bodenschtuz beim Pflügen: Wie hoch ist die Radlast am Furchenrad? Die Landtechnik 67, 265 – 269.

Brus, D.J., Van Den Akker, J.J.H., 2018. How serious a problem is subsoil compaction in the Netherlands? A survey based on probability sampling. SOIL 4, 37–45. https://doi.org/10.5194/SOIL-4-37-2018

Bu, H., Sharma, L.K., Denton, A., Franzen, D.W., 2017. Comparison of satellite imagery and ground-based active optical sensors as yield predictors in sugar beet, spring wheat, corn, and sunflower. Agron. J. 109, 299–308. https://doi.org/10.2134/agronj2016.03.0150

Buck, C., Langmaack, M., Schrader, S., 2000. Influence of mulch and soil compaction on earthworm cast properties. Appl. Soil Ecol. 14, 223–229. https://doi.org/10.1016/S0929-1393(00)00054-8

Bukowiecki, J., Rose, T., Kage, H., 2021. Sentinel-2 data for precision agriculture?—a uav-

based assessment. Sensors 21. https://doi.org/10.3390/s21082861

Bulgakov, V., Olt, J., Kuvachov, V., Smolinskyi, S., 2020. A theoretical and experimental study of the traction properties of agricultural gantry systems. Agraarteadus 31, 10–16. https://doi.org/10.15159/jas.20.08

Bulinski, J., Sergiel, L., 2014. Effect of moisture content on soil density - compaction relation during soil compacting in the soil bin. Ann. Warsaw Univ. Life Sci. - SGGW. Agric. 64, 5–13.

Busscher, W.J., 1990. Adjustment of flat-tipped penetrometer resistance data to a common water content. Trans. ASAE 33, 519–524.

Cambi, M., Certini, G., Fabiano, F., Foderi, C., Laschi, A., Picchio, R., 2016. Impact of wheeled and tracked tractors on soil physical properties in a mixed conifer stand. iForest - Biogeosciences For. 9, 89–94. https://doi.org/10.3832/ifor1382-008

Campos, I., González-Gómez, L., Villodre, J., Calera, M., Campoy, J., Jiménez, N., Plaza, C., Sánchez-Prieto, S., Calera, A., 2019. Mapping within-field variability in wheat yield and biomass using remote sensing vegetation indices. Precis. Agric. 20, 214–236. https://doi.org/10.1007/s11119-018-9596-z

Celik, A., Raper, R.L., 2016. Comparison of various coulter-type ground-driven rotary subsoilers in terms of energy consumption and soil disruption. Soil Use Manag. 32, 250–259. https://doi.org/10.1111/sum.12256

Celik, A., Raper, R.L., 2012. Design and evaluation of ground-driven rotary subsoilers. Soil Tillage Res. 124, 203–210. https://doi.org/10.1016/j.still.2012.06.010

Chamen, T., 2015. Controlled Traffic Farming – From Worldwide Research To Adoption In Europe And Its Future Prospects. Acta Technol. Agric. 18, 64–73. https://doi.org/10.1515/ata-2015-0014

Chaney, K., Wilcox, A., Perry, N.H., Boatman, N.D., 1999. The economics of establishing field margins and buffer zones of different widths in cereal fields. Asp. Appl. Biol. 54, 79–84.

Chaudhary, M.R., Khera, R., Singh, C.J., 1991. Tillage and irrigation effects on root growth, soil water depletion and yield of wheat following rice. J. Agric. Sci. 116, 9–16. https://doi.org/10.1017/s0021859600076097

Chen, Y., Munkholm, L.J., Nyord, T., 2013. A discrete element model for soil–sweep interaction in three different soils. Soil Tillage Res. 126, 34–41. https://doi.org/10.1016/j.still.2012.08.008

Cid, P., Carmona, I., Murillo, J.M., Gómez-Macpherson, H., 2014. No-tillage permanent bed planting and controlled traffic in a maize-cotton irrigated system under Mediterranean

conditions: Effects on soil compaction, crop performance and carbon sequestration. Eur. J. Agron. 61, 24–34. https://doi.org/10.1016/j.eja.2014.08.002

Cohrs, C.W., Cook, R.L., Gray, J.M., Albaugh, T.J., 2020. Sentinel-2 leaf area index estimation for pine plantations in the southeastern United States. Remote Sens. 12. https://doi.org/10.3390/RS12091406

Colombi, T., Keller, T., 2019. Developing strategies to recover crop productivity after soil compaction—A plant eco-physiological perspective. Soil Tillage Res. 191, 156–161. https://doi.org/10.1016/j.still.2019.04.008

Colombi, T., Torres, L.C., Walter, A., Keller, T., 2018. Feedbacks between soil penetration resistance, root architecture and water uptake limit water accessibility and crop growth – A vicious circle. Sci. Total Environ. 626, 1026–1035. https://doi.org/10.1016/j.scitotenv.2018.01.129

Cook, S.K., Ingle, S., 1997. The effect of boundary features at the field margins on yields of winter wheat. Asp. Appl. Biol. 50, 459–466.

Cui, K., Défossez, P., Richard, G., 2007. A new approach for modelling vertical stress distribution at the soil/tyre interface to predict the compaction of cultivated soils by using the PLAXIS code. Soil Tillage Res. 95, 277–287. https://doi.org/10.1016/j.still.2007.01.010

Czarnecki, J., Brennensthul, M., Białczyk, W., Ptak, W., Gil, Ł., 2019. Analysis of Traction Properties and Power of Wheels Used on Various Agricultural Soils. Agric. Eng. 23, 13–23. https://doi.org/10.1515/agriceng-2019-0002

d'Andrimont, Raphaël; Verhegghen, Astrid; Lemoine, Guido; Kempeneers, Pieter; Meroni, Michele; van der Velde, Marijn European Commission, J.R.C. (JRC), 2021. EUCROPMAP 2018 [WWW Document].

d'Andrimont, R., Verhegghen, A., Lemoine, G., Kempeneers, P., Meroni, M., van der Velde, M., 2021. From parcel to continental scale – A first European crop type map based on Sentinel-1 and LUCAS Copernicus in-situ observations. Remote Sens. Environ. 266. https://doi.org/10.1016/j.rse.2021.112708

DAVIES, D.B., FINNEY, J.B., RICHARDSON, S.J., 1973. RELATIVE EFFECTS OF TRACTOR WEIGHT AND WHEEL-SLIP IN CAUSING SOIL COMPACTION. J. Soil Sci. 24, 399–409. https://doi.org/10.1111/j.1365-2389.1973.tb00775.x

de Lima, R.P., Keller, T., 2021. Soil stress measurement by load cell probes as influenced by probe design, probe position, and soil mechanical behaviour. Soil Tillage Res. 205, 104796. https://doi.org/10.1016/j.still.2020.104796

de Lima, R.P., Keller, T., 2019. Impact of sample dimensions, soil-cylinder wall friction and

elastic properties of soil on stress field and bulk density in uniaxial compression tests. Soil Tillage Res. 189, 15–24. https://doi.org/10.1016/j.still.2018.12.021

De Pue, J., Cornelis, W.M., 2019. DEM simulation of stress transmission under agricultural traffic Part 1: Comparison with continuum model and parametric study. Soil Tillage Res. 195, 104408. https://doi.org/10.1016/j.still.2019.104408

De Snoo, G.R., 1994. Cost-benefits of unsprayed crop edges in winter wheat, sugar beet and potatoes. Unsprayed F. margins Implic. Environ. Biodivers. Agric. Pract. 167.

DeArmond, D., Emmert, F., Lima, A.J.N., Higuchi, N., 2019. Impacts of soil compaction persist 30 years after logging operations in the Amazon Basin. Soil Tillage Res. 189, 207–216. https://doi.org/10.1016/j.still.2019.01.010

Défossez, P., Richard, G., Boizard, H., O'Sullivan, M.F., 2003. Modeling change in soil compaction due to agricultural traffic as function of soil water content. Geoderma 116, 89–105. https://doi.org/10.1016/S0016-7061(03)00096-X

Delenne, J.Y., El Youssoufi, M.S., Cherblanc, F., Bénet, J.C., 2004. Mechanical behaviour and failure of cohesive granular materials. Int. J. Numer. Anal. Methods Geomech. 28, 1577–1594. https://doi.org/10.1002/nag.401

Dexter, A.R., 1987. Compression of soil around roots. Plant Soil 97, 401–406. https://doi.org/10.1007/bf02383230

Di Renzo, A., Di Maio, F.P., 2004. Comparison of contact-force models for the simulation of collisions in DEM-based granular flow codes. Chem. Eng. Sci. 59, 525–541.

Diserens, E., 2009. Calculating the contact area of trailer tyres in the field. Soil Tillage Res. 103, 302–309. https://doi.org/10.1016/j.still.2008.10.020

Drusch, M., Del Bello, U., Carlier, S., Colin, O., Fernandez, V., Gascon, F., Hoersch, B., Isola, C., Laberinti, P., Martimort, P., Meygret, A., Spoto, F., Sy, O., Marchese, F., Bargellini, P., 2012. Sentinel-2: ESA's Optical High-Resolution Mission for GMES Operational Services. Remote Sens. Environ. 120, 25–36. https://doi.org/10.1016/j.rse.2011.11.026

Dürr, C., Aubertot, J.-N.N., 2000. Emergence of seedlings of sugar beet (Beta vulgaris L.) as affected by the size, roughness and position of aggregates in the seedbed 219, 211–220. https://doi.org/10.1023/A:1004723901989

Duttmann, R., Brunotte, J., Bach, M., 2013. Spatial analyses of field traffic intensity and modeling of changes in wheel load and ground contact pressure in individual fields during a silage maize harvest. Soil Tillage Res. 126, 100–111. https://doi.org/10.1016/j.still.2012.09.001

Duttmann, R., Schwanebeck, M., Nolde, M., Horn, R., 2014. Predicting Soil Compaction Risks Related to Field Traffic during Silage Maize Harvest. Soil Sci. Soc. Am. J. 78,

408–421. https://doi.org/10.2136/sssaj2013.05.0198

EDEM, 2018. EDEM 2018 [WWW Document]. URL https://altair.com/edem

EDEM 2018 [WWW Document], n.d. URL https://www.altair.com/edem/

Edwards, L.M., 2013. The effects of soil freeze-thaw on soil aggregate breakdown and concomitant sediment flow in Prince Edward Island: A review. Can. J. Soil Sci. 93, 459–472. https://doi.org/10.4141/CJSS2012-059

Ekinci, Ş., Çarman, K., Kahramanli, H., 2015. Investigation and modeling of the tractive performance of radial tires using off-road vehicles. Energy 93, 1953–1963. https://doi.org/10.1016/j.energy.2015.10.070

Eriksson, J., Hakansson, I., Danfors, B., 1974. Jordpackning--markstruktur--groda. Medd Jordbruktek Inst.

EUROSTAT 2019, 2019. European statistics on agriculture, forestry and fisheries [WWW Document] [WWW Document]. URL https://ec.europa.eu/eurostat/data/database (accessed 17.1.23)

Febo, P., Lucarelli, F., Pessina, D., others, 2000. Soil-tyre interaction parameters influencing soil compaction: a study of contact area prediction models. Adv. Geoecology 191–201.

Fendt. Fendt 826 Vario [WWW Document], n.d. https://doi.org/[online] Available at:https://www.fendt.com/it/trattori/800-vario-elementi-di-rilievo [Accessed 24 Mar 2023]

Fleige, H., Horn, R., others, 2000. Field experiments on the effect of soil compaction on soil properties, runoff, interflow and erosion. Adv. Geoecology 258–268.

Fouli, Y., Cade-Menun, B.J., Cutforth, H.W., 2013. Freeze-thaw cycles and soil water content effects on infiltration rate of three Saskatchewan soils. Can. J. Soil Sci. 93, 485–496. https://doi.org/10.4141/CJSS2012-060

Frölich, O.K., 1934. Druckverteilung im Baugrunde: mit besonderer Berücksichtung der plastischen Erscheinungen. J. Springer.

G.D. Vermeulen, J.N. Tullberg, and W.C.T.C. 8. ., 2010. Controlled Traffic Farming.

Gao, F., Anderson, M., Daughtry, C., Johnson, D., 2018. Assessing the variability of corn and soybean yields in central Iowa using high spatiotemporal resolution multi-satellite imagery. Remote Sens. 10. https://doi.org/10.3390/rs10091489

Gaženja, U., 2019. THE DECREASE OF WHEAT YIELD ON THE PLOT EDGES – HEADLANDS DUE TO SOIL COMPACTION. Proc. 47th Int. Symp. Actual Tasks Agric. Eng. 5 - 7 March 2019, Opatija, Croat. 2019 pp.97-106 ref.18 97–106.

Gerard, C.J., Sexton, P., Shaw, G., 1982. Physical Factors Influencing Soil Strength and Root Growth 1. Agron. J. 74, 875–879.

Gitelson, A.A., Kaufman, Y.J., Merzlyak, M.N., 1996. Use of a green channel in remote sensing of global vegetation from EOS- MODIS. Remote Sens. Environ. 58, 289–298. https://doi.org/10.1016/S0034-4257(96)00072-7

Gliński, J., Lipiec, J., 2000. Soil physical conditions and plant roots. CRC press.

Godwin, R.J., Miller, P.C.H., 2003. A review of the technologies for mapping within-field variability. Biosyst. Eng. 84, 393–407. https://doi.org/10.1016/S1537-5110(02)00283-0

Graves, A.R., Morris, J., Deeks, L.K., Rickson, R.J., Kibblewhite, M.G., Harris, J.A., Farewell, T.S., Truckle, I., 2015. The total costs of soil degradation in England and Wales. Ecol. Econ. 119, 399–413. https://doi.org/10.1016/j.ecolecon.2015.07.026

Gregorich, E.G., McLaughlin, N.B., Lapen, D.R., Ma, B.L., Rochette, P., 2014. Soil Compaction, Both an Environmental and Agronomic Culprit: Increased Nitrous Oxide Emissions and Reduced Plant Nitrogen Uptake. Soil Sci. Soc. Am. J. 78, 1913–1923. https://doi.org/10.2136/sssaj2014.03.0117

Grosch, K.A., 1996. The rolling resistance, wear and traction properties of tread compounds. Rubber Chem. Technol. https://doi.org/10.5254/1.3538383

Gysi, M., 2001. Compaction of a Eutric Cambisol under heavy wheel traffic in Switzerland: Field data and a critical state soil mechanics model approach. Soil Tillage Res. 61, 133–142. https://doi.org/10.1016/S0167-1987(01)00161-1

Gysi, M., Klubertanz, G., Vulliet, L., 2000. Compaction of an Eutric Cambisol under heavy wheel traffic in Switzerland - Field data and modelling. Soil Tillage Res. 56, 117–129. https://doi.org/10.1016/S0167-1987(00)00132-X

Gysi Taenikon, M A Fluehler, H., n.d. Influence of single passes with high wheel load on a structured, unploughed sandy loam soil. Soil Tillage Res.

Haas, C., Holthusen, D., Mordhorst, A., Lipiec, J., Horn, R., 2016. Elastic and plastic soil deformation and its influence on emission of greenhouse gases. Int. Agrophysics 30, 173–184. https://doi.org/10.1515/INTAG-2015-0088

Håkansson, I., Reeder, R.C., 1994. Subsoil compaction by vehicles with high axle load-extent, persistence and crop response. Soil Tillage Res. 29, 277–304. https://doi.org/10.1016/0167-1987(94)90065-5

Hallonborg, U., 1996. Super ellipse as tyre-ground contact area. J. Terramechanics 33, 125–132. https://doi.org/10.1016/S0022-4898(96)00013-4

Hamza, M.A., Anderson, W.K., 2005. Soil compaction in cropping systems: A review of the nature, causes and possible solutions. Soil Tillage Res. 82, 121–145. https://doi.org/10.1016/j.still.2004.08.009

Hang, C., Gao, X., Yuan, M., Huang, Y., Zhu, R., 2018. Discrete element simulations and

experiments of soil disturbance as affected by the tine spacing of subsoiler. Biosyst. Eng. 168, 73–82. https://doi.org/10.1016/j.biosystemseng.2017.03.008

Harris, H.D., Bakker, D.M., 1994. A soil stress transducer for measuring in situ soil stresses. Soil Tillage Res. 29, 35–48. https://doi.org/10.1016/0167-1987(94)90100-7

He, T., Ding, Q., Li, Y., He, R., Xue, J., Qiu, W., 2017. Stress transmission coefficient: A soil stress transmission property for a loading process. Soil Tillage Res. 166, 179–184. https://doi.org/10.1016/j.still.2016.09.013

Hengl, T., 2018. Sand content in % (kg / kg) at 6 standard depths (0, 10, 30, 60, 100 and 200 cm) at 250 m resolution (Version v02) [Data set]. [WWW Document]. URL 10.5281/zenodo.1476854

Henry, H.A.L., 2007. Soil freeze-thaw cycle experiments: Trends, methodological weaknesses and suggested improvements. Soil Biol. Biochem. 39, 977–986.

Horn, R., 2004. Time Dependence of Soil Mechanical Properties and Pore Functions for Arable Soils. Soil Sci. Soc. Am. J. 68, 1131–1137. https://doi.org/10.2136/SSSAJ2004.1131

Horn, R., Domzzał, H., Słowińska-Jurkiewicz, A., van Ouwerkerk, C., 1995. Soil compaction processes and their effects on the structure of arable soils and the environment. Soil Tillage Res. 35, 23–36. https://doi.org/10.1016/0167-1987(95)00479-C

Horn, R., Fleige, H., 2003. A method for assessing the impact of load on mechanical stability and on physical properties of soils, Soil and Tillage Research. Elsevier. https://doi.org/10.1016/S0167-1987(03)00102-8

Horn, R., Holthusen, D., Dörner, J., Mordhorst, A., Fleige, H., 2019. Scale-dependent soil strengthening processes – What do we need to know and where to head for a sustainable environment? Soil Tillage Res. 195. https://doi.org/10.1016/j.still.2019.104388

Horn, R., Richards, B.G., Gräsle, W., Baumgartl, T., Wiermann, C., 1998. Theoretical principles for modelling soil strength and wheeling effects - A review. J. Plant Nutr. Soil Sci. 161, 333–346. https://doi.org/10.1002/jpln.1998.3581610402

Horn, R., Way, T., Rostek, J., 2003. Effect of repeated tractor wheeling on stress/strain properties and consequences on physical properties in structured arable soils. Soil Tillage Res. 73, 101–106. https://doi.org/10.1016/s0167-1987(03)00103-x

Https://www.google.it/earth/about/versions/, n.d. Google earth pro [WWW Document].

Huber, S., Prokop, G., Arrouays, D., Banko, G., Bispo, A., Jones, R.J.A., Kibblewhite, M.G., Lexer, W., Möller, A., Rickson, R.J., Shishkov, T., Stephens, M., Toth, G., Akker, J.J.H. Van den, Varallyay, G., Verheijen, F.G.A., Jones, A.R., 2008. Environmental assessment of soil for monitoring: volume I indicators and criteria, Office for the Official

Publications of the European Communities. https://doi.org/10.2788/93515

Hussein, M.A., Antille, D.L., Kodur, S., Chen, G., Tullberg, J.N., 2021. Controlled traffic farming effects on productivity of grain sorghum, rainfall and fertiliser nitrogen use efficiency. J. Agric. Food Res. 3, 100111. https://doi.org/10.1016/j.jafr.2021.100111

IBM Corp. Released 2019. IBM SPSS Statistics for Windows, Version 26.0. Armonk, N.I.C., n.d. SPSS.

Institute for European Environmental Policy, Soares, C.D., Ecologic, Intravital microscopic techniques, 2012. Environmentally Harmful Subsidies: Identification and Assessment Annex 5 : Subsidy level indicators for the case studies. Eur. Comm. DG Environ. 1–26.

J. Jin, L. Tang, 2010. Optimal Coverage Path Planning for Arable Farming on 2D Surfaces. Trans. ASABE 53, 283–295. https://doi.org/10.13031/2013.29488

Jabro, J.D., Iversen, W.M., Evans, R.G., Allen, B.L., Stevens, W.B., 2014. Repeated Freeze-Thaw Cycle Effects on Soil Compaction in a Clay Loam in Northeastern Montana. Soil Sci. Soc. Am. J. 78, 737–744. https://doi.org/10.2136/SSSAJ2013.07.0280

Jabro, J.D., Stevens, W.B., Iversen, W.M., Sainju, U.M., Allen, B.L., 2021. Soil cone index and bulk density of a sandy loam under no-till and conventional tillage in a corn-soybean rotation. Soil Tillage Res. 206. https://doi.org/10.1016/j.still.2020.104842

Jarvis, N.J., 2007. A review of non-equilibrium water flow and solute transport in soil macropores: Principles, controlling factors and consequences for water quality, European Journal of Soil Science. https://doi.org/10.1111/J.1365-2389.2007.00915.X

Jia, M., Liu, B., Xue, J., Ma, G., 2021. Coupled three-dimensional discrete element–finite difference simulation of dynamic compaction. Acta Geotech. 16, 731–747. https://doi.org/10.1007/s11440-020-01055-y

Johnson, C.E., Burt, E.C., 1990. Method of predicting soil stress state under tires. Trans. Am. Soc. Agric. Eng. 33, 713–717. https://doi.org/10.13031/2013.31390

Jordan, D., Ponder, F., Hubbard, V.C., 2003. Effects of soil compaction, forest leaf litter and nitrogen fertilizer on two oak species and microbial activity. Appl. Soil Ecol. 23, 33–41. https://doi.org/10.1016/S0929-1393(03)00003-9

Jun, H.G., Way, T.R., Löfgren, B., Landström, M., Bailey, A.C., Burt, E.C., McDonald, T.P., 2004. Dynamic load and inflation pressure effects on contact pressures of a forestry forwarder tire. J. Terramechanics 41, 209–222. https://doi.org/10.1016/j.jterra.2004.03.002

Kaczorowska–Dolowy, M., Godwin, R.J., Dickin, E., White, D.R., Misiewicz, P.A., 2019. Controlled traffic farming delivers better crop yield of winter bean as a result of improved root development. Agron. Res. 17, 725–740.

https://doi.org/10.15159/AR.19.136

Kayad, A., Sozzi, M., Gatto, S., Marinello, F., Pirotti, F., 2019. Monitoring within-field variability of corn yield using sentinel-2 and machine learning techniques. Remote Sens. 11. https://doi.org/10.3390/rs11232873

Kayad, A., Sozzi, M., Gatto, S., Whelan, B., Sartori, L., Marinello, F., 2021. Ten years of corn yield dynamics at field scale under digital agriculture solutions: A case study from North Italy. Comput. Electron. Agric. 185, 106126. https://doi.org/10.1016/j.compag.2021.106126

Kayad, A.G., Al-Gaadi, K.A., Tola, E., Madugundu, R., Zeyada, A.M., Kalaitzidis, C., 2016. Assessing the spatial variability of alfalfa yield using satellite imagery and ground-based data. PLoS One 11, 1–15. https://doi.org/10.1371/journal.pone.0157166

Keller, T., 2018. APPROACHES TOWARDS UNDERSTANDING SOIL COMPACTION.

Keller, T., 2005. A Model for the prediction of the contact area and the distribution of vertical stress below agricultural tyres from readily available tyre parameters. Biosyst. Eng. 92, 85–96. https://doi.org/10.1016/j.biosystemseng.2005.05.012

Keller, T., Arvidsson, J., 2016. A model for prediction of vertical stress distribution near the soil surface below rubber-tracked undercarriage systems fitted on agricultural vehicles. Soil Tillage Res. 155, 116–123. https://doi.org/10.1016/j.still.2015.07.014

Keller, T., Arvidsson, J., 2004. Technical solutions to reduce the risk of subsoil compaction: Effects of dual wheels, tandem wheels and tyre inflation pressure on stress propagation in soil. Soil Tillage Res. 79, 191–205. https://doi.org/10.1016/j.still.2004.07.008

Keller, T., Arvidsson, J., Dexter, A.R., 2007a. Soil structures produced by tillage as affected by soil water content and the physical quality of soil. Soil Tillage Res. 92, 45–52. https://doi.org/10.1016/j.still.2006.01.001

Keller, T., Berli, M., Ruiz, S., Lamandé, M., Arvidsson, J., Schjønning, P., Selvadurai, A.P.S.S., 2014. Transmission of vertical soil stress under agricultural tyres: Comparing measurements with simulations. Soil Tillage Res. 140, 106–117. https://doi.org/10.1016/j.still.2014.03.001

Keller, T., Défossez, P., Weisskopf, P., Arvidsson, J., Richard, G., 2007b. SoilFlex: A model for prediction of soil stresses and soil compaction due to agricultural field traffic including a synthesis of analytical approaches. Soil Tillage Res. 93, 391–411. https://doi.org/10.1016/j.still.2006.05.012

Keller, T., Dexter, A.R., 2012. Plastic limits of agricultural soils as functions of soil texture and organic matter content. Soil Res. 50, 7–17. https://doi.org/10.1071/SR11174

Keller, T., Håkansson, I., 2010. Estimation of reference bulk density from soil particle size

distribution and soil organic matter content. Geoderma 154, 398–406. https://doi.org/10.1016/j.geoderma.2009.11.013

Keller, T., Lamandé, M., 2010. Challenges in the development of analytical soil compaction models. Soil Tillage Res. 111, 54–64. https://doi.org/10.1016/j.still.2010.08.004

Keller, T., Ruiz, S., Stettler, M., Berli, M., 2016. Determining Soil Stress beneath a Tire: Measurements and Simulations. Soil Sci. Soc. Am. J. 80, 541–553. https://doi.org/10.2136/sssaj2015.07.0252

Keller, T., Sandin, M., Colombi, T., Horn, R., Or, D., 2019. Historical increase in agricultural machinery weights enhanced soil stress levels and adversely affected soil functioning. Soil Tillage Res. 194, 104293. https://doi.org/10.1016/j.still.2019.104293

Keller, T., Trautner, A., Arvidsson, J., 2002. Stress distribution and soil displacement under a rubber-tracked and a wheeled tractor during ploughing, both on-land and within furrows. Soil Tillage Res. 68, 39–47. https://doi.org/10.1016/S0167-1987(02)00082-X

Khafizov, C., Khafizov, R., Nurmiev, A., Galiev, I., 2020. OPTIMIZATION OF MAIN PARAMETERS OF TRACTOR AND UNIT FOR PLOWING SOIL, TAKING INTO ACCOUNT THEIR INFLUENCE ON YIELD OF GRAIN CROPS, in: Malinovska, L., Osadcuks, V. (Eds.), 19TH INTERNATIONAL SCIENTIFIC CONFERENCE ENGINEERING FOR RURAL DEVELOPMENT, Engineering for Rural Development. pp. 585–590. https://doi.org/10.22616/ERDev.2020.19.TF131

Kingwell, R., Fuchsbichler, A., 2011. The whole-farm benefits of controlled traffic farming: An Australian appraisal. Agric. Syst. 104, 513–521. https://doi.org/10.1016/j.agsy.2011.04.001

Kirby, J.M., 1999a. Soil stress measurement: Part I. Transducer in a uniform stress field. J. Agric. Eng. Res. 72, 151–160.

Kirby, J.M., 1999b. Soil Stress Measurement. Part 2: Transducer beneath a Circular Loaded Area. J. Agric. Eng. Res. 73, 141–149. https://doi.org/10.1006/jaer.1998.0400

Kirby, J.M., 1991. Strength and deformation of agricultural soil: measurement and practical significance. Soil Use Manag. 7, 223–229. https://doi.org/10.1111/j.1475-2743.1991.tb00878.x

Kirby, J.M., Bengough, A.G., 2002. Influence of soil strength on root growth: Experiments and analysis using a critical-state model. Eur. J. Soil Sci. 53, 119–127. https://doi.org/10.1046/J.1365-2389.2002.00429.X

Kirby, J.M., Blunden, B.G., Trein, C.R., 1997. Simulating soil deformation using a critical-state model: II. Soil compaction beneath tyres and tracks. Eur. J. Soil Sci. 48, 59–70. https://doi.org/10.1111/j.1365-2389.1997.tb00185.x

Kretzschmar, A., 1991. Burrowing ability of the earthworm Aporrectodea longa limited by soil compaction and water potential. Biol. Fertil. Soils 11, 48–51. https://doi.org/10.1007/bf00335834

Kriging method in ArcGIS pro, n.d. . https://pro.arcgis.com/en/pro-app/latest/tool-reference/spatial-analyst/kriging.htm.

Kristoffersen, A.Ø., Riley, H., 2005. Effects of Soil Compaction and Moisture Regime on the Root and Shoot Growth and Phosphorus Uptake of Barley Plants Growing on Soils with Varying Phosphorus Status. Nutr. Cycl. Agroecosystems 72, 135–146. https://doi.org/10.1007/s10705-005-0240-8

Kross, A., McNairn, H., Lapen, D., Sunohara, M., Champagne, C., 2015. Assessment of RapidEye vegetation indices for estimation of leaf area index and biomass in corn and soybean crops. Int. J. Appl. Earth Obs. Geoinf. 34, 235–248. https://doi.org/10.1016/j.jag.2014.08.002

Kuemmel, B., 2003. Theoretical investigation of the effects of field margin and hedges on crop yields. Agric. Ecosyst. Environ. 95, 387–392. https://doi.org/10.1016/S0167-8809(02)00086-5

Kuht, J., Research, E.R.-A., 2004, undefined, 2004. Soil compaction effect on soil physical properties and the content of nutrients in spring barley (Hordeum vulgare L.) and spring wheat (Triticum aestivum L.). researchgate.net 2, 187–194.

Lamandé, M., Keller, T., Berisso, F., Stettler, M., Schjønning, P., 2015. Accuracy of soil stress measurements as affected by transducer dimensions and shape. Soil Tillage Res. 145, 72–77. https://doi.org/10.1016/j.still.2014.08.011

Lamandé, M., Schjønning, P., 2018. Soil mechanical stresses in high wheel load agricultural field traffic: A case study. Soil Res. 56, 129–135. https://doi.org/10.1071/SR17117

Lamandé, M., Schjønning, P., 2011a. Transmission of vertical stress in a real soil profile. Part I: Site description, evaluation of the Söhne model, and the effect of topsoil tillage. Soil Tillage Res. 114, 57–70. https://doi.org/10.1016/j.still.2011.05.004

Lamandé, M., Schjønning, P., 2011b. Transmission of vertical stress in a real soil profile. Part III: Effect of soil water content. Soil Tillage Res. 114, 78–85. https://doi.org/10.1016/j.still.2010.10.001

Lamandé, M., Schjønning, P., 2008. The ability of agricultural tyres to distribute the wheel load at the soil-tyre interface. J. Terramechanics 45, 109–120. https://doi.org/10.1016/j.jterra.2008.09.004

Lamandé, M., Schjønning, P., Tøgersen, F.A., 2007. Mechanical behaviour of an undisturbed soil subjected to loadings: Effects of load and contact area. Soil Tillage Res. 97, 91–106.

https://doi.org/10.1016/j.still.2007.09.002

Larsen, T., Schjønning, P., Axelsen, J., 2004. The impact of soil compaction on euedaphic Collembola. Appl. Soil Ecol. 26, 273–281. https://doi.org/10.1016/j.apsoil.2003.12.006

Lassen, P., Lamandé, M., Stettler, M., Keller, T., Jørgensen, M.S., Lilja, H., 2013. Terranimo ® - A Soil Compaction Model with internationally compatible input options. EFITA-WCCA -CIGR Conf. "Sustainable Agric. through ICT Innov. 24–27.

Latsch, A., Anken, T., 2019. Soil and crop responses to a "light" version of Controlled Traffic Farming in Switzerland. Soil Tillage Res. 194, 104310. https://doi.org/10.1016/j.still.2019.104310

Lee, W.S., Alchanatis, V., Yang, C., Hirafuji, M., Moshou, D., Li, C., 2010. Sensing technologies for precision specialty crop production. Comput. Electron. Agric. 74, 2–33. https://doi.org/10.1016/j.compag.2010.08.005

Li, B., Chen, Y., Chen, J., 2018. Comparison of two subsoiler designs using the discrete element method (DEM). Trans. ASABE 61, 1529–1537. https://doi.org/10.13031/trans.12629

Li, B., Chen, Y., Chen, J., 2016. Modeling of soil-claw interaction using the discrete element method (DEM). Soil Tillage Res. 158, 177–185. https://doi.org/10.1016/j.still.2015.12.010

Li, Y.X., Tullberg, J.N., Freebairn, D.M., 2007. Wheel traffic and tillage effects on runoff and crop yield. Soil Tillage Res. 97, 282–292. https://doi.org/10.1016/j.still.2005.10.001

Lipiec, J., St e pniewski, W., e pniewski, W.S., St e pniewski, W., 1995. Effects of soil compaction and tillage systems on uptake and losses of nutrients. Soil Tillage Res. 35, 37–52. https://doi.org/10.1016/0167-1987(95)00474-7

Liu, D., Gong, Y., Zhang, Xuejun, Yu, Q., Zhang, Xiao, Chen, X., Wang, Y., 2022. EDEM Simulation Study on the Performance of a Mechanized Ditching Device for Codonopsis Planting. Agriculture 12, 1238. https://doi.org/10.3390/agriculture12081238

Liu, K., Benetti, M., Sozzi, M., Gasparini, F., Sartori, L., 2022. Soil Compaction under Different Traction Resistance Conditions—A Case Study in North Italy. Agriculture 12, 1–23. https://doi.org/10.3390/agriculture12111954

Lu, Xingli, Lu, Xingneng, 2017. Tillage and crop residue effects on the energy consumption, input–output costs and greenhouse gas emissions of maize crops. Nutr. Cycl. Agroecosystems 108, 323–337. https://doi.org/10.1007/s10705-017-9859-5

Maestrini, B., Basso, B., 2018. Predicting spatial patterns of within-field crop yield variability. F. Crop. Res. 219, 106–112. https://doi.org/10.1016/j.fcr.2018.01.028

Marshall, E.J.P., Arnold, G.M., 1995. Factors affecting field weed and field margin flora on a

farm in Essex, UK. Landsc. Urban Plan. 31, 205–216. https://doi.org/10.1016/0169-2046(94)01047-C

Materechera, S.A., Alston, A.M., Kirby, J.M., Dexter, A.R., 1992. Influence of root diameter on the penetration of seminal roots into a compacted subsoil. Plant Soil 144, 297–303. https://doi.org/10.1007/BF00012888

McHugh, A.D., Tullberg, J.N., Freebairn, D.M., 2009. Controlled traffic farming restores soil structure. Soil Tillage Res. 104, 164–172. https://doi.org/10.1016/j.still.2008.10.010

McPhee, J.E., Aird, P.L., Hardie, M.A., Corkrey, S.R., 2015. The effect of controlled traffic on soil physical properties and tillage requirements for vegetable production. Soil Tillage Res. 149, 33–45. https://doi.org/10.1016/j.still.2014.12.018

McPhee, J.E., Antille, D.L., Tullberg, J.N., Doyle, R.B., Boersma, M., 2020. Managing soil compaction – A choice of low-mass autonomous vehicles or controlled traffic? Biosyst. Eng. 195, 227–241. https://doi.org/10.1016/j.biosystemseng.2020.05.006

Md-Tahir, H., Zhang, J., Xia, J., Zhang, C., Zhou, H., Zhu, Y., 2019. Rigid lugged wheel for conventional agricultural wheeled tractors - Optimising traction performance and wheel-soil interaction in field operations. Biosyst. Eng. 188, 14–23. https://doi.org/10.1016/j.biosystemseng.2019.10.001

Miriti, M., 2013. The effects of tillage systems on soil physical properties and water conservation in a sandy loam soil in Eastern Kenya. J. Soil Sci. Environ. Manag. 4, 146–154. https://doi.org/10.5897/jssem2013.0395

Mohawesh, O., Ishida, T., Fukumura, K., Yoshino, K., 2008. Assessment of spatial variability of penetration resistance and hardpan characteristics in a cassava field. Aust. J. Soil Res. 46, 210–218. https://doi.org/10.1071/SR07118

Moreno, R.G., Álvarez, M.C.D., Alonso, A.T., Barrington, S., Requejo, A.S., 2008. Tillage and soil type effects on soil surface roughness at semiarid climatic conditions. Soil Tillage Res. 98, 35–44. https://doi.org/10.1016/j.still.2007.10.006

Mossadeghi-Björklund, M., Arvidsson, J., Keller, T., Koestel, J., Lamandé, M., Larsbo, M., Jarvis, N., 2016. Effects of subsoil compaction on hydraulic properties and preferential flow in a Swedish clay soil. Soil Tillage Res. 156, 91–98. https://doi.org/10.1016/j.still.2015.09.013

Munkholm, L.J., Schjønning, P., 2004. Structural vulnerability of a sandy loam exposed to intensive tillage and traffic in wet conditions. Soil Tillage Res. 79, 79–85. https://doi.org/10.1016/j.still.2004.03.012

N.V. Halpin, T.C. and P.F.R., 2012. Economic Evaluation of Precision Controlled Traffic Farming in the Australian Sugar Industry: - A case study of an early adopter., DEEDI

eResearch Archive (eRA).

Naderi-Boldaji, M., Alimardani, R., Hemmat, A., Sharifi, A., Keyhani, A., Tekeste, M.Z., Keller, T., 2014. 3D finite element simulation of a single-tip horizontal penetrometer-soil interaction. Part II: Soil bin verification of the model in a clay-loam soil. Soil Tillage Res. 144, 211–219. https://doi.org/10.1016/j.still.2014.03.008

Nadykto, V., Arak, M., Olt, J., 2015. Theoretical research into the frictional slipping of wheel-type undercarriage taking into account the limitation of their impact on the soil. Agron. Res. 13, 148–157.

Nichols, T.A., Bailey, A.C., Johnson, C.E., Grisso, R.D., 1987. Stress State Transducer for Soil. Trans. Am. Soc. Agric. Eng. 30, 1237–1241. https://doi.org/10.13031/2013.30551

Nurmiev, A., Khafizov, C., Khafizov, R., Ziganshin, B., 2018. OPTIMIZATION OF MAIN PARAMETERS OF TRACTOR WORKING WITH SOIL-PROCESSING IMPLEMENT, in: Malinovska, L., Osadcuks, V. (Eds.), 17TH INTERNATIONAL SCIENTIFIC CONFERENCE: ENGINEERING FOR RURAL DEVELOPMENT, Engineering for Rural Development. pp. 161–167. https://doi.org/10.22616/ERDev2018.17.N191

O'Sullivan, M.F., Henshall, J.K., Dickson, J.W., 1999. A simplified method for estimating soil compaction. Soil Tillage Res. 49, 325–335. https://doi.org/10.1016/S0167-1987(98)00187-1

Obour, P.B., Kolberg, D., Lamandé, M., Børresen, T., Edwards, G., Sørensen, C.G., Munkholm, L.J., 2018. Compaction and sowing date change soil physical properties and crop yield in a loamy temperate soil. Soil Tillage Res. 184, 153–163. https://doi.org/10.1016/j.still.2018.07.014

Obour, P.B., Schjønning, P., Peng, Y., Munkholm, L.J., 2017. Subsoil compaction assessed by visual evaluation and laboratory methods. Soil Tillage Res. 173, 4–14. https://doi.org/10.1016/j.still.2016.08.015

Oldeman, L.R., Hakkeling, R.T.A., Sombroek, W.G., others, 1990. World map of the status of human-induced soil degradation: an explanatory note. International Soil Reference and Information Centre.

Olsen, H.J., 1994. Calculation of subsoil stresses. Soil Tillage Res. 29, 111–123. https://doi.org/10.1016/0167-1987(94)90047-7

Panda, S.S., Ames, D.P., Panigrahi, S., 2010. Application of vegetation indices for agricultural crop yield prediction using neural network techniques. Remote Sens. 2, 673–696. https://doi.org/10.3390/rs2030673

Patel, M.S., Singh, N.T., 1981. Changes in bulk density and water intake rate of a coarse

textured soil in relation to different levels of compaction. J. Indian Soc. Soil Sci. 29, 110–112.

Patel, N.K., Patnaik, C., Dutta, S., Shekh, A.M., Dave, A.J., 2001. Study of crop growth parameters using Airborne Imaging Spectrometer data. Int. J. Remote Sens. 22, 2401–2411. https://doi.org/10.1080/01431160117383

Peigné, J., Vian, J.F., Cannavacciuolo, M., Lefevre, V., Gautronneau, Y., Boizard, H., 2013. Assessment of soil structure in the transition layer between topsoil and subsoil using the profil cultural method. Soil Tillage Res. 127, 13–25. https://doi.org/10.1016/J.STILL.2012.05.014

Peth, S., Horn, R., Fazekas, O., Richards, B.G., 2006. Heavy soil loading and its consequence for soil structure, strength, and deformation of arable soils. J. Plant Nutr. Soil Sci. 169, 775–783. https://doi.org/10.1002/jpln.200620112

Piccoli, I., Sartori, F., Polese, R., Berti, A., 2020. Crop yield after 5 decades of contrasting residue management. Nutr. Cycl. Agroecosystems 117, 231–241. https://doi.org/10.1007/s10705-020-10067-9

Pichlmaier, B., Honzek, R., 2011. Traktion Management for Large Tractors (in German With English Summary) 84–94.

Poodt, M.P., Koolen, A.J., Van Der Linden, J.P., 2003. FEM analysis of subsoil reaction on heavy wheel loads with emphasis on soil preconsolidation stress and cohesion. Soil Tillage Res. 73, 67–76. https://doi.org/10.1016/S0167-1987(03)00100-4

Prasuhn, V., 2011. Soil erosion in the Swiss midlands: Results of a 10-year field survey. Geomorphology 126, 32–41.

Pulido-Moncada, M., Katuwal, S., Kristensen, J.B., Munkholm, L.J., 2021. Effects of bio-subsoilers on subsoil pore-system functionality: Case study with intact soil columns. Geoderma 385, 114897. https://doi.org/10.1016/j.geoderma.2020.114897

Pytka, J., Dabrowski, J., 2001. Determination of the stress-strain relationship for sandy soil in field experiments. J. Terramechanics 38, 185–200. https://doi.org/10.1016/S0022-4898(00)00020-3

Pytka, J., Dabrowski, J., Zajac, M., Tarkowski, P., 2006. Effects of reduced inflation pressure and vehicle loading on off-road traction and soil stress and deformation state. J. Terramechanics 43, 469–485. https://doi.org/10.1016/j.jterra.2005.06.001

R. L. Raper, D. W. Reeves, 2007. In-Row Subsoiling and Controlled Traffic Effects on Coastal Plain Soils. Trans. ASABE 50, 1109–1115. https://doi.org/10.13031/2013.23619

R. L. Raper, F. J. Arriaga, 2007. Comparing Peak and Residual Soil Pressures Measured by Pressure Bulbs and Stress-State Transducers. Trans. ASABE 50, 339–344.

https://doi.org/10.13031/2013.22624

R19075P, P.N., 2020. Evaluation of Emission Reductions and Cost Savings in Sectional Control Air Seeders, Drills, and Sowing Equipment across the Canadian Prairies. Can. Agric. Partnersh. Dec, 23–26.

Radford, B.J., Bridge, B.J., Davis, R.J., McGarry, D., Pillai, U.P., Rickman, J.F., Walsh, P.A., Yule, D.F., 2000. Changes in the properties of a Vertisol and responses of wheat after compaction with harvester traffic. Soil Tillage Res. 54, 155–170. https://doi.org/10.1016/s0167-1987(00)00091-x

Radford, B.J., Wilson-Rummenie, A.C., Simpson, G.B., Bell, K.L., Ferguson, M.A., 2001. Compacted soil affects soil macrofauna populations in a semi-arid environment in central Queensland. Soil Biol. Biochem. 33, 1869–1872. https://doi.org/10.1016/s0038-0717(01)00104-3

Raghavan, G.S.V., McKyes, E., Chassé, M., 1977. Effect of wheel slip on soil compaction. J. Agric. Eng. Res. 22, 79–83. https://doi.org/10.1016/0021-8634(77)90095-6

Raper, R.L., 1996. SUBSOILER SHAPES FOR SITE−SPECIFIC TILLAGE 93, 195–219.

Raper, R.L., Bailey, A.C., Burt, E.C., Way, T.R., Liberati, P., 1995. The effects of reduced inflation pressure on soil-tire interface stresses and soil strength. J. Terramechanics 32, 43–51. https://doi.org/10.1016/0022-4898(95)00002-I

Raper, R.L., Reeves, D.W., Burt, E.C., 1998. Using in-row subsoiling to minimize soil compaction caused by traffic. J. Cotton Sci. 2, 130–135.

Raper, R.L., Schwab, E.B., 2008. Development of an In-row subsoiler attachment to reduce smearing. Am. Soc. Agric. Biol. Eng. Annu. Int. Meet. 2008, ASABE 2008 7, 4295–4308. https://doi.org/10.13031/2013.27462

Rauws, G., Auzet, A.V., 1989. Laboratory experiments on the effects of simulated tractor wheelings on linear soil erosion. Soil Tillage Res. 13, 75–81.

Richards, B.., 1992. Modelling interactive load-deformation and flow processes in soils, including unsaturated and swelling soils. Int. J. Rock Mech. Min. Sci. Geomech. Abstr. 29, 215. https://doi.org/10.1016/0148-9062(92)90596-r

Ridge, R.E., 2001. Trends in sugar cane mechanization. Int. Sugar J. 103, 150–154.

Rodrigues, C.K., Da Silva Lopes, E., M'ller, M.M.L., Genú, A.M., 2015. Variabilidade espacial da compactação de um solo submetido ao tráfego de harvester e forwarder. Sci. For. Sci. 43, 387–394.

Rogger, M., Blöschl, G., Rogger, M., Blöschl, G., 2017. The impact of soil compaction on runoff. EGUGA 19, 4841.

Rosolem, C.A., Foloni, J.S.S., Tiritan, C.S., 2002. Root growth and nutrient accumulation in

cover crops as affected by soil compaction. Soil Tillage Res. 65, 109–115. https://doi.org/10.1016/s0167-1987(01)00286-0

Ruiz, S., Or, D., Schymanski, S.J., 2015. Soil penetration by earthworms and plant roots - Mechanical energetics of bioturbation of compacted soils. PLoS One 10. https://doi.org/10.1371/JOURNAL.PONE.0128914

Sahin, U., Angin, I., Kiziloglu, F.M., 2008. Effect of freezing and thawing processes on some physical properties of saline-sodic soils mixed with sewage sludge or fly ash. Soil Tillage Res. 99, 254–260.

Salem, H.M., Valero, C., Muñoz, M.Á., Rodríguez, M.G., Silva, L.L., 2015. Short-term effects of four tillage practices on soil physical properties, soil water potential, and maize yield. Geoderma 237–238, 60–70. https://doi.org/10.1016/j.geoderma.2014.08.014

SANDERS, S., MOSIMANN, T., 2005. Erosionsschutz durch Intervallbegrünung in Fahrgassen: Ergebnisse aus Versuchen im Winterweizen. Wasser und Abfall 34–38.

Sartori, L., Basso, B., Bertocco, M., Oliviero, G., 2005. Energy use and economic evaluation of a three year crop rotation for conservation and organic farming in NE Italy. Biosyst. Eng. 91, 245–256. https://doi.org/10.1016/j.biosystemseng.2005.03.010

Schjønning, P., Lamandé, M., 2018. Models for prediction of soil precompression stress from readily available soil properties. Geoderma 320, 115–125. https://doi.org/10.1016/j.geoderma.2018.01.028

Schjønning, P., Lamandé, M., Keller, T., Labouriau, R., 2020. Subsoil shear strength – Measurements and prediction models based on readily available soil properties. Soil Tillage Res. 200, 104638. https://doi.org/10.1016/j.still.2020.104638

Schjønning, P., Lamandé, M., Lassen, P., 2016. An Introduction to Terranimo. Unpubl. note, Aarhus Univ. Dept. Agroecol. 17.

Schjønning, P., Lamandé, M., Tøgersen, F.A., Arvidsson, J., Keller, T., 2008. Modelling effects of tyre inflation pressure on the stress distribution near the soil-tyre interface. Biosyst. Eng. 99, 119–133. https://doi.org/10.1016/j.biosystemseng.2007.08.005

Schjønning, P., Lamandé, M., Tøgersen, F.A., Pedersen, J., Hansen, P.O.M., 2006. Minimering af jordpakning. Størrelse og fordeling af stress i trædefladen mellem hjul og jord. DJF-Rapport Markbrug 127, Danmarks JordbrugsForskning, Tjele.

Schjonning, P., Munkholm, L.J., Lamande, M., 2022. Soil characteristics and root growth in a catena across and outside the wheel tracks for different slurry application systems. SOIL \& TILLAGE Res. 221. https://doi.org/10.1016/j.still.2022.105422

Schjønning, P., Stettler, M., Keller, T., Lassen, P., Lamandé, M., 2015a. Predicted tyre-soil interface area and vertical stress distribution based on loading characteristics. Soil

Tillage Res. 152, 52–66. https://doi.org/10.1016/j.still.2015.03.002

Schjønning, P., van den Akker, J.J.H., Keller, T., Greve, M.H., Lamandé, M., Simojoki, A., Stettler, M., Arvidsson, J., Breuning-Madsen, H., 2015b. Driver-Pressure-State-Impact-Response (DPSIR) analysis and risk assessment for soil compaction-A European perspective, Advances in Agronomy. Elsevier Ltd. https://doi.org/10.1016/bs.agron.2015.06.001

Schneider, F., Don, A., Hennings, I., Schmittmann, O., Seidel, S.J., 2017. The effect of deep tillage on crop yield – What do we really know? Soil Tillage Res. 174, 193–204. https://doi.org/10.1016/j.still.2017.07.005

Schreiber, M., Kutzbach, H.D., 2008. Influence of soil and tire parameters on traction. Res. Agric. Eng. 54, 43–49. https://doi.org/10.17221/3105-rae

Scott, D.I., Tams, A.R., Berry, P.M., Mooney, S.J., 2005. The effects of wheel-induced soil compaction on anchorage strength and resistance to root lodging of winter barley (Hordeum vulgare L.). Soil Tillage Res. 82, 147–160. https://doi.org/10.1016/j.still.2004.06.008

Serrano, J.M., Peca, J.O., Silva, J.R., Marquez, L., 2009. The effect of liquid ballast and tyre inflation pressure on tractor performance. Biosyst. Eng. 102, 51–62. https://doi.org/10.1016/j.biosystemseng.2008.10.001

Sharma, A.K., Pandey, K.P., 1996. A review on contact area measurement of pneumatic tyre on rigid and deformable surfaces. J. Terramechanics 33, 253–264. https://doi.org/10.1016/S0022-4898(97)00008-6

Shestak, C.J., Busse, M.D., 2005. Compaction Alters Physical but Not Biological Indices of Soil Health. Soil Sci. Soc. Am. J. 69, 236. https://doi.org/10.2136/sssaj2005.0236

Sibley, A.M., Grassini, P., Thomas, N.E., Cassman, K.G., Lobell, D.B., 2014. Testing remote sensing approaches for assessing yield variability among maize fields. Agron. J. 106, 24–32. https://doi.org/10.2134/agronj2013.0314

Silva, R.P., Rolim, M.M., Gomes, I.F., Pedrosa, E.M.R., Tavares, U.E., Santos, A.N., 2018. Numerical modeling of soil compaction in a sugarcane crop using the finite element method. Soil Tillage Res. 181, 1–10. https://doi.org/10.1016/j.still.2018.03.019

Simojoki, A., Fazekas-Becker, O., Horn, R., 2008. Macro-and microscale gaseous diffusion in a Stagnic Luvisol as affected by compaction and reduced tillage. Agric. food Sci. 17, 252–264.

Sivarajan, S., Maharlooei, M., Bajwa, S.G., Nowatzki, J., 2018. Impact of soil compaction due to wheel traffic on corn and soybean growth, development and yield. Soil Tillage Res. 175, 234–243. https://doi.org/10.1016/j.still.2017.09.001

Smith, R., Ellies, A., Horn, R., 2000. Modified Boussinesq's equations for nonuniform tire loading. J. Terramechanics 37, 207–222. https://doi.org/10.1016/S0022-4898(00)00007-0

Sohne, W., 1958. Fundamentals of pressure distribution and soil compaction under tractor tires. Agric. Eng. 39, 290.

Söhne, W., 1953. Druckverteilung im boden und bodenverformung unter schlepperreifen. Grundlagen der Landtechnik-Konstrukteurhefte.

Song, W., Jiang, X., Li, L., Ren, L., Tong, J., 2022. Increasing the width of disturbance of plough pan with bionic inspired subsoilers. Soil Tillage Res. 220, 105356. https://doi.org/10.1016/j.still.2022.105356

Sparkes, D.L., Jaggard, K.W., Ramsden, S.J., Scott, R.K., 1998a. The effect of field margins on the yield of sugar beet and cereal crops. Ann. Appl. Biol. 132, 129–142. https://doi.org/10.1111/j.1744-7348.1998.tb05190.x

Sparkes, D.L., Ramsden, S.J., Jaggard, K.W., Scott, R.K., 1998b. The case for headland set-aside: Consideration of whole-farm gross margins and grain production on two farms with contrasting rotations. Ann. Appl. Biol. 133, 245–256.

Spekken, M., de Bruin, S., 2013. Optimized routing on agricultural fields by minimizing maneuvering and servicing time. Precis. Agric. 14, 224–244. https://doi.org/10.1007/s11119-012-9290-5

Speller, C.S., Cleal, R.A.E., Runham, S.R., 1992. A comparison of winter wheat yields from headlands with other positions in five fen peat fields. Monogr. Crop Prot. Counc. 47.

Stepniewski, W., Gliński, J., Ball, B.C., 1994. Effects of Compaction on Soil Aeration Properties, Developments in Agricultural Engineering. https://doi.org/10.1016/B978-0-444-88286-8.50016-7

Stettler, M., Keller, T., Weisskopf, P., Lamandé, M., Lassen, P., Schjønning, P., 2014. Terranimo® - a web-based tool for evaluating soil compaction. Landtechnik 69, 132–138.

Sun, Q., Sun, W., Zhao, Z., Jiang, W., Zhang, P., Sun, X., Xue, Q., 2023. Soil Compaction and Maize Root Distribution under Subsoiling Tillage in a Wheat–Maize Double Cropping System. Agronomy 13, 1–12. https://doi.org/10.3390/agronomy13020394

Sunoj, S., Kharel, D., Kharel, T., Cho, J., Czymmek, K.J., Ketterings, Q.M., 2021. Impact of headland area on whole field and farm corn silage and grain yield. Agron. J. 113, 147–158. https://doi.org/10.1002/agj2.20489

Szatanik-Kloc, A., Horn, R., Lipiec, J., Siczek, A., Boguta, P., 2019. Initial growth and root surface properties of dicotyledonous plants in structurally intact field soil and compacted headland soil. Soil Tillage Res. 195, 104387. https://doi.org/10.1016/j.still.2019.104387

Tamás, K., Jóri, I.J., Mouazen, A.M., 2013. Modelling soil-sweep interaction with discrete element method. Soil Tillage Res. 134, 223–231. https://doi.org/10.1016/j.still.2013.09.001

Taylor, J.H., 1983. Benefits of permanent traffic lanes in a controlled traffic crop production system. Soil Tillage Res. https://doi.org/10.1016/0167-1987(83)90040-5

Tekeste, M.Z., Raper, R.L., Schwab, E.B., 2008. Soil Drying Effects on Soil Strength and Depth of Hardpan Layers as Determined from Cone Index Data. Agric. Eng. Int. CIGR J. X, 1–17.

ten Damme, L., Schjønning, P., J. Munkholm, L., Green, O., K. Nielsen, S., Lamandé, M., 2021a. Soil structure response to field traffic: Effects of traction and repeated wheeling. Soil Tillage Res. 213. https://doi.org/10.1016/j.still.2021.105128

ten Damme, L., Schjønning, P., J. Munkholm, L., Green, O., K. Nielsen, S., Lamandé, M., 2021b. Traction and repeated wheeling – effects on contact area characteristics and stresses in the upper subsoil. Soil Tillage Res. 211. https://doi.org/10.1016/j.still.2021.105020

ten Damme, L., Stettler, M., Pinet, F., Vervaet, P., Keller, T., Munkholm, L.J., Lamandé, M., 2020. Construction of modern wide, low-inflation pressure tyres per se does not affect soil stress. Soil Tillage Res. 204, 104708. https://doi.org/10.1016/j.still.2020.104708

Tijink, F.G.J., 1994. Quantification of vehicle running gear, in: Developments in Agricultural Engineering. Elsevier, pp. 391–415.

Toscano, P., Castrignanò, A., Filippo, S., Gennaro, D., Vittorio Vonella, A., Ventrella, D., Matese, A., 2019. A Precision Agriculture Approach for Durum Wheat Yield Assessment Using Remote Sensing Data and Yield Mapping. https://doi.org/10.3390/agronomy9080437

Tucker, C.J., 1979. Red and photographic infrared linear combinations for monitoring vegetation. Remote Sens. Environ. 8, 127–150. https://doi.org/10.1016/0034-4257(79)90013-0

Tucker, C.J., Holben, B.N., Elgin, J.H., McMurtrey, J.E., 1981. Remote sensing of total dry-matter accumulation in winter wheat. Remote Sens. Environ. 11, 171–189. https://doi.org/10.1016/0034-4257(81)90018-3

Tullberg, J., 2010. Tillage, traffic and sustainability-A challenge for ISTRO. Soil Tillage Res. 111, 26–32. https://doi.org/10.1016/j.still.2010.08.008

Tullberg, J., Antille, D.L., Bluett, C., Eberhard, J., Scheer, C., 2018. Controlled traffic farming effects on soil emissions of nitrous oxide and methane. Soil Tillage Res. 176, 18–25. https://doi.org/10.1016/j.still.2017.09.014

Tullberg, J.N., Yule, D.F., McGarry, D., 2007. Controlled traffic farming-From research to adoption in Australia. Soil Tillage Res. 97, 272–281. https://doi.org/10.1016/j.still.2007.09.007

Tuzzin de Moraes, M., Debiasi, H., Carlesso, R., Cezar Franchini, J., Rodrigues da Silva, V., Bonini da Luz, F., 2016. Soil physical quality on tillage and cropping systems after two decades in the subtropical region of Brazil. Soil Tillage Res. 155, 351–362. https://doi.org/10.1016/j.still.2015.07.015

Ucgul, M., Fielke, J.M., Saunders, C., 2015. Three-dimensional discrete element modelling (DEM) of tillage: Accounting for soil cohesion and adhesion. Biosyst. Eng. 129, 298–306. https://doi.org/10.1016/j.biosystemseng.2014.11.006

Ucgul, M., Fielke, J.M., Saunders, C., 2014. 3D DEM tillage simulation: Validation of a hysteretic spring (plastic) contact model for a sweep tool operating in a cohesionless soil. Soil Tillage Res. 144, 220–227. https://doi.org/10.1016/j.still.2013.10.003

Unger, P.W., 1991. Overwinter Changes in Physical Properties of No-Tillage Soil. Soil Sci. Soc. Am. J. 55, 778–782. https://doi.org/10.2136/SSSAJ1991.03615995005500030024X

Upadhyaya, S.K., Wulfsohn, D., 1990. and 2-D Tire Contact Area 33.

Uteau, D., Pagenkemper, S.K., Peth, S., Horn, R., 2013. Root and time dependent soil structure formation and its influence on gas transport in the subsoil. Soil Tillage Res. 132, 69–76. https://doi.org/10.1016/j.still.2013.05.001

Uzun, B., Yol, E., Furat, Ş., Topakçi, M., Çanakçi, M., Karayel, D., 2012. The effects of different tillage methods on the post-wheat second crop sesame: Seed yield, energy budget, and economic return. Turkish J. Agric. For. 36, 399–407. https://doi.org/10.3906/tar-1011-1505

Van Den Akker, J.J.H., 2004. SOCOMO: A soil compaction model to calculate soil stresses and the subsoil carrying capacity. Soil Tillage Res. 79, 113–127. https://doi.org/10.1016/j.still.2004.03.021

Vaz, C.M.P., Manieri, J.M., de Maria, I.C., Tuller, M., 2011. Modeling and correction of soil penetration resistance for varying soil water content. Geoderma 166, 92–101. https://doi.org/10.1016/j.geoderma.2011.07.016

VDI, 2014. Machine operation with regard to the trafficability of soils used for agriculture, VDI-Richtlinien 6101.

Vega, A., Córdoba, M., Castro-Franco, M., Balzarini, M., 2019. Protocol for automating error removal from yield maps. Precis. Agric. 20, 1030–1044. https://doi.org/10.1007/s11119-018-09632-8

Voorhees, W.B., 1983. Relative Effectiveness of Tillage and Natural Forces in Alleviating

Wheel-Induced Soil Compaction. Soil Sci. Soc. Am. J. 47, 129–133. https://doi.org/10.2136/SSSAJ1983.03615995004700010026X

Walton, O.R., 1983. Particle-dynamics calculations of shear flow. Stud. Appl. Mech. https://doi.org/10.1016/B978-0-444-42192-0.50033-5

WANG, F., HUANG, J., TANG, Y., WANG, X., 2007. New Vegetation Index and Its Application in Estimating Leaf Area Index of Rice. Rice Sci. 14, 195–203. https://doi.org/10.1016/s1672-6308(07)60027-4

Wang, X., Hu, H., Wang, Q., Li, H., He, J., Chen, W., 2017. Calibration Method of Soil Contact Characteristic Parameters Based on DEM Theory. Nongye Jixie Xuebao/Transactions Chinese Soc. Agric. Mach. 48, 78–85. https://doi.org/10.6041/j.issn.1000-1298.2017.12.009

Wang, Y., Li, N., Ma, Y., Tong, J., Pfleging, W., Sun, J., 2020. Field experiments evaluating a biomimetic shark-inspired (BioS) subsoiler for tillage resistance reduction. Soil Tillage Res. 196. https://doi.org/10.1016/j.still.2019.104432

Ward, M., Forristal, P.D., McDonnell, K., 2020. Impact of field headlands on wheat and barley performance in a cool Atlantic climate as assessed in 40 Irish tillage fields. Irish J. Agric. Food Res. 59, 85–97. https://doi.org/10.15212/ijafr-2020-0113

Way, T.R., Bailey, A.C., Raper, R.L., Burt, E.C., 1995. Tire Lug Height Effect on Soil Stresses and Bulk Density. Trans. ASAE 38, 669–674. https://doi.org/10.13031/2013.27879

Way, T.R., Kishimoto, T., 2004. Interface pressures of a tractor drive tyre on structured and loose soils. Biosyst. Eng. 87, 375–386.

Welch, R.Y., Behnke, G.D., Davis, A.S., Masiunas, J., Villamil, M.B., 2016. Using cover crops in headlands of organic grain farms: Effects on soil properties, weeds and crop yields. Agric. Ecosyst. Environ. 216, 322–332. https://doi.org/10.1016/j.agee.2015.10.014

Wells, L.G., Stombaugh, T.S., Shearer, S.A., 2005. Crop yield response to precision deep tillage. Trans. Am. Soc. Agric. Eng. 48, 895–901. https://doi.org/10.13031/2013.18493

Wiermann, C., Way, T.R., Horn, R., Bailey, A.C., Burt, E.C., 1999. Effect of various dynamic loads on stress and strain behavior of a Norfolk sandy loam. Soil Tillage Res. 50, 127–135. https://doi.org/10.1016/S0167-1987(98)00199-8

Wilcox, A., Perry, N.H., Boatman, N.D., Chaney, K., 2000. Factors affecting the yield of winter cereals in crop margins. J. Agric. Sci. 135, 335–346. https://doi.org/10.1017/S002185969900828X

Wollny, E., 1898. Untersuchungen über den Einflußder mechanischen Bearbeitung auf die

Fruchtbarkeit des Bodens. Forschungen auf dem Gebiet der Agrik. 20, 231–290.

Wulfsohn, D., Upadhyaya, S.K., 1992. Determination of dynamic three-dimensional soil-tyre contact profile. J. Terramechanics 29, 433–464. https://doi.org/10.1016/0022-4898(92)90046-M

Xue, J., Su, B., 2017. Significant remote sensing vegetation indices: A review of developments and applications. J. Sensors 2017. https://doi.org/10.1155/2017/1353691

Yao, F., Tang, Y., Wang, P., Zhang, J., 2015. Estimation of maize yield by using a process-based model and remote sensing data in the Northeast China Plain. Phys. Chem. Earth 87–88, 142–152. https://doi.org/10.1016/j.pce.2015.08.010

Zhang, L., Zhai, Y., Chen, J., Zhang, Z., Huang, S., 2022. Optimization design and performance study of a subsoiler underlying the tea garden subsoiling mechanism based on bionics and EDEM. Soil Tillage Res. 220, 105375. https://doi.org/10.1016/j.still.2022.105375

Zhang, R., Li, J., 2006. Simulation on mechanical behavior of cohesive soil by Distinct Element Method. J. Terramechanics 43, 303–316. https://doi.org/10.1016/j.jterra.2005.05.006

Zheng, K., He, J., Li, H., Diao, P., Wang, Q., Zhao, H., 2016. Research on polyline soil-breaking blade subsoiler based on subsoiling soil model using discrete element method. Nongye Jixie Xuebao/Transactions Chinese Soc. Agric. Mach. 47, 62–72. https://doi.org/10.6041/j.issn.1000-1298.2016.09.010

Zhou, J. wei, Du, C. long, Liu, S. yong, Liu, Y., 2016. Comparison of three types of swirling generators in coarse particle pneumatic conveying using CFD-DEM simulation. Powder Technol. 301, 1309–1320.

Zink, A., Fleige, H., Horn, R., 2010. Load Risks of Subsoil Compaction and Depths of Stress Propagation in Arable Luvisols. Soil Sci. Soc. Am. J. 74, 1733–1742. https://doi.org/10.2136/SSSAJ2009.0336

Zoz, F.M., Grisso, R., 2003a. Traction and Tractor Performance. Agric. Equip. Technol. Conf. 1–47.

Zoz, F.M., Grisso, R.D., 2003b. ASAE DISTINGUISHED LECTURE SERIES Traction and Tractor Performance.